Development of tough ion gel membranes composed of CO_2-philic ionic liquids and semi-crystalline polymer network

何, 勝男

(Degree)
博士（学術）

(Date of Degree)
2024-09-25

(Date of Publication)
2025-09-01

(Resource Type)
doctoral thesis

(Report Number)
甲第9026号

(URL)
https://hdl.handle.net/20.500.14094/0100492535

Doctoral Dissertation

Development of tough ion gel membranes composed of CO_2-philic ionic liquids and semi-crystalline polymer network

(高 CO_2 親和性イオン液体と半結晶性高分子から構成される高強度イオンゲル膜の創製)

Jul 2024

Graduate School of Engineering

Kobe University

HE SHENGNAN

何 勝男

Acknowledgment

As I sit down to write this dissertation and look back on the past few years of my academic journey, I am struck by the realization that my time as a student is coming to an end. This period of learning has been incredibly memorable. None of this would have been achievable without the unwavering support and guidance generously provided by my supervisors and colleagues. Their encouragement and assistance have been invaluable throughout, and as I reach this milestone, I am profoundly grateful for everything they have done for me.

First and foremost, I want to express my heartfelt gratitude to Prof. Matsuyama. His invaluable supervision played a pivotal role in the successful completion of this dissertation. I deeply appreciate Prof. Matsuyama's guidance and advice throughout my research journey. Additionally, I extend my sincere thanks to Prof. Kamio, whose assistance was instrumental in various aspects such as topic selection, research methods, data analysis, and writing. I am particularly grateful for Prof. Kamio's meticulous feedback and unwavering support during the paper revision process. The professors' meticulousness and rigorous academic approach serve as inspirations for my future endeavors. I extend my heartfelt gratitude to Prof. Matsuyama and Prof. Kamio, wishing them continued success and fulfillment in both their professional and personal lives.

Secondly, I would like to express my sincere gratitude to Mr. Ogino and Mr. Mori for their significant contributions to this doctoral thesis. Their valuable feedback and suggestions during my research and defense were instrumental in my success. I also extend my thanks to Mr. Kumagai sensei, Ms. Miyake, Ms. Kamio, and Ms. Ono from the Membrane Center for their strong support and assistance. Their dedication greatly facilitated the smooth progression of my scientific research. My appreciation extends to

the Membrane Center for funding the experimental platform and to the China Scholarship Council for providing financial support. These resources allowed me to focus wholeheartedly on my research. I wish everyone all the best in their future endeavors. Thank you all for your support.

Finally, I want to extend my heartfelt thanks to my family and friends. Their care and support enabled me to pursue my studies without worry, providing me with the confidence to complete my degree. I also wish my partners and colleagues all the best in their research endeavors and hope that everything goes smoothly for them. Thank you for your companionship and support throughout this journey.

HE SHENGNAN

Graduate School of Engineering

Kobe University, Japan

July 01, 2024

Table of contents

Chapter 1

General introduction

1.1 Carbon dioxide (CO_2) emissions

According to the Global Carbon Budget 2023 report, global carbon dioxide emissions from burning coal, crude oil, and natural gas will reach record highs in 2023 [1]. This trend increases the concentration of greenhouse gases in the atmosphere, worsening global warming and leading to various climate changes such as extreme weather events, melting glaciers, and rising sea levels. In response, there is a global effort to replace traditional fossil fuels with renewable energy to reduce emissions. However, renewable energy currently meets only about 13% of global energy demand. As depicted in **Fig. 1.1**, coal the fossil fuel with the highest carbon intensity—will continue to play a significant role in the energy mix for the foreseeable future. Therefore, advancing carbon capture technology is essential to mitigate the environmental impact of fossil fuel combustion.

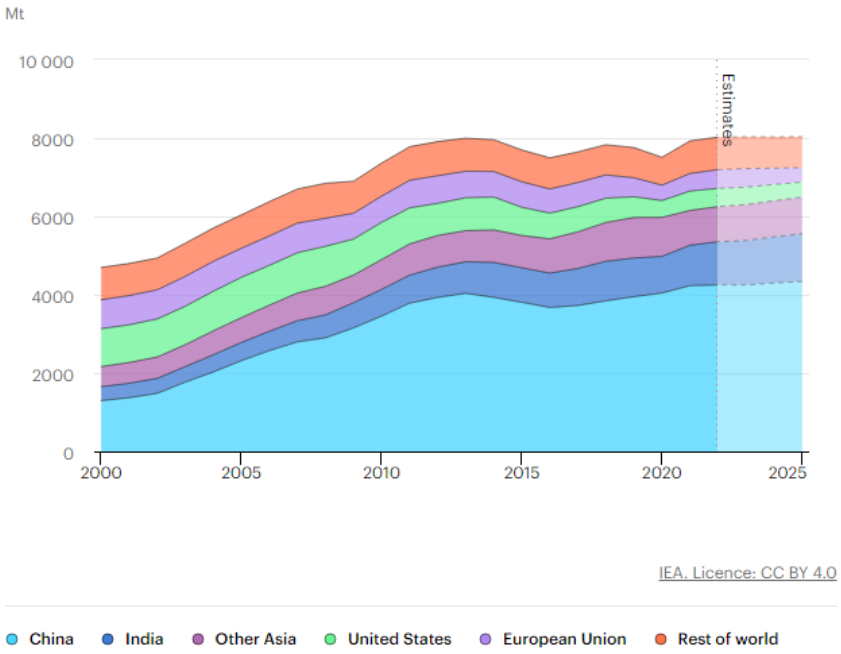

Fig. 1.1 Global coal consumption from 2000 to 2025 according to the International Energy Agency.

1.2 CO_2 capture technology

Carbon capture technology, also known as carbon capture and storage (CCS), captures CO_2 generated during industrial processes or power generation and either stores it underground or repurposes it for industrial use to prevent its release into the atmosphere. This technology encompasses three primary carbon capture methods: pre-combustion capture, oxy-combustion capture, and post-combustion capture [2-6]. **Fig. 1.2** illustrates the three carbon capture processes.

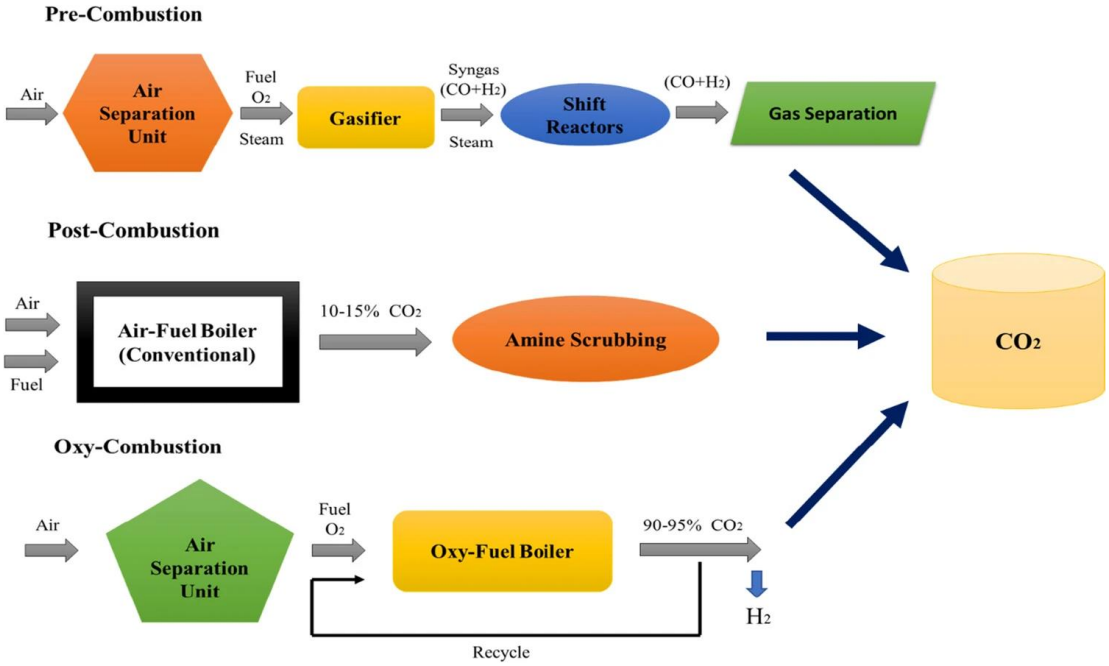

Fig. 1.2 Different technologies of CO_2 capture [6].

1.2.1 Pre-combustion capture technology

Pre-combustion capture is commonly used in integrated gasification combined cycle (IGCC) systems (**Fig. 1.3**). In this process, coal is gasified at high pressure with oxygen to produce syngas. The resulting syngas is then converted to CO_2 and H_2. This process increases gas pressure and CO_2 concentration, making it easier to capture the CO_2. The H_2 and syngas produced can also be reused as alternative fuels [7, 8]. Pre-combustion capture is a relatively mature technology due to its compact capture system and potential for improved efficiency and pollutant control. However, the commercial application of IGCC technology has been limited due to technical and economic challenges. It requires complex auxiliary systems and incurs significantly higher capital costs compared to conventional coal-fired power plants.

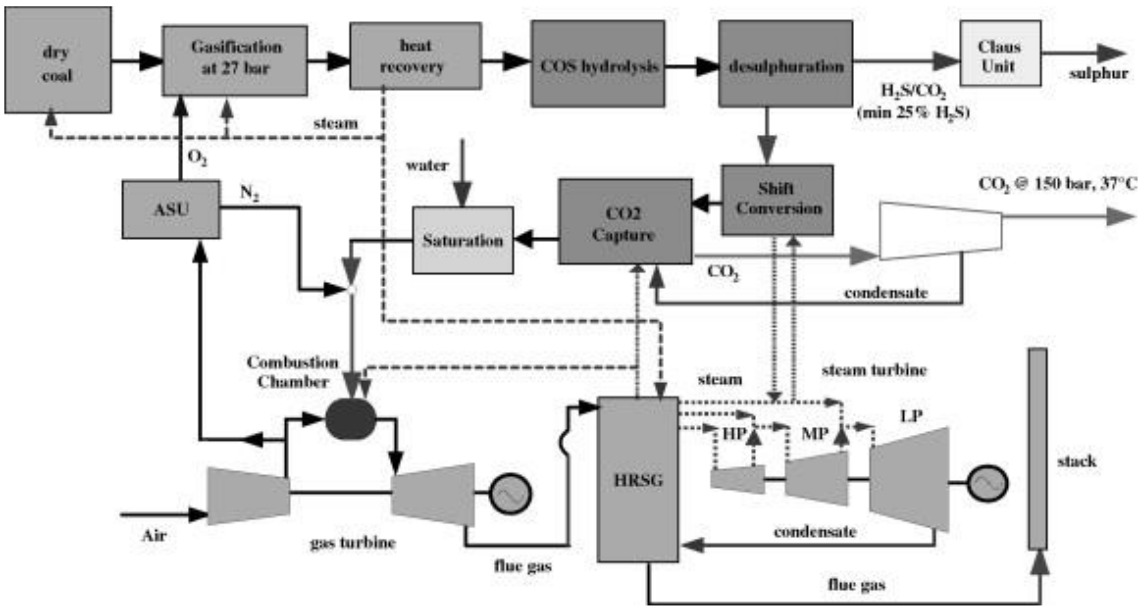

Fig. 1.3 Radiant-IGCC with capture of CO_2 [9].

1.2.2 Oxy-combustion capture

Oxy-combustion involves burning fossil fuels with pure oxygen or oxygen-enriched air. The main byproducts of this process are carbon dioxide, water, and inert gases. After condensing the water vapor, the CO_2 is purified through low-temperature flash evaporation, achieving a CO_2 concentration of 80% to 98% by volume, significantly improving the CO_2 capture rate. Oxy-combustion technology is mainly used in solid fuel boilers due to its compatibility with coal, low pollutant emissions, and straightforward operation [10, 11]. However, the technology remains niche, and there are currently no working integrated CCS plants using oxyfuel combustion [8].

1.2.3 Post-combustion capture

Post-combustion carbon capture technology is the primary method used by existing power plants to separate CO_2 from the exhaust gases of burning fossil fuels. This approach is widely applicable and can be easily integrated into existing power generation facilities

without significant modifications, thereby enhancing the overall efficiency of post-combustion carbon capture equipment. Post-combustion carbon capture technology has a high level of maturity and is widely used in commercial factories [12]. Although there are some technical challenges, it remains the most established carbon capture strategy and plays a key role in sustainability efforts [13].

1.3 Post-combustion carbon capture technologies

Post-combustion carbon capture is currently the most advanced carbon capture technology available. Based on the capture principle, it can be divided into methods such as absorption, adsorption, cryogenic distillation, and membrane separation. Each method offers distinct advantages and challenges in terms of efficiency, cost, and compatibility with different industrial processes. For instance, absorption uses chemical solvents to capture CO_2, while adsorption relies on solid materials like activated carbon to trap the gas. Cryogenic distillation uses low temperatures to separate CO_2 from other gases, and membrane separation employs selective membranes to isolate CO_2. In the following sections, we will detail the key features of each carbon capture technology.

1.3.1 Absorption method

Amine chemical absorption is one of the most advanced CO_2 capture technologies among absorption methods and is widely used in industries worldwide. This technology relies on the chemical reaction between solvents and CO_2 molecules, allowing for the efficient absorption and separation of carbon dioxide by choosing suitable solvents. Commonly used solvents include various alcohol amines in aqueous solutions, such as monoethanolamine (MEA), diethanolamine (DEA), and methyl diethanolamine (MDEA). These alcohol amines exhibit a strong affinity for CO_2 in chemical reactions, making them

ideal choices in capture technology [14, 15]. **Fig. 1.4** presents the process flow diagram for the absorption of CO_2 using ethanolamine. However, amine chemical absorption faces several challenges in practical applications. First, the regeneration process of the solvent typically consumes a significant amount of energy, especially at high temperatures, due to the high heat energy required for the separation of the solvent and CO_2. This poses challenges to energy efficiency in industrial applications. Additionally, amine solvents are prone to thermal degradation at high temperatures, resulting in solvent loss and potential by-products that can pose hazards to equipment and the environment. Given these limitations, it is crucial to develop new solvents and enhance existing solvent systems to improve the performance and sustainability of CO_2 capture technology. Exploring mixed solvent solutions is a promising direction [7, 12, 16-20]. By combining different types of solvents, it may be possible to achieve better CO_2 capture performance while also reducing solvent energy consumption and losses. In summary, although amine chemical absorption has shown good performance in CO_2 capture, its energy consumption and solvent stability are still areas of concern.

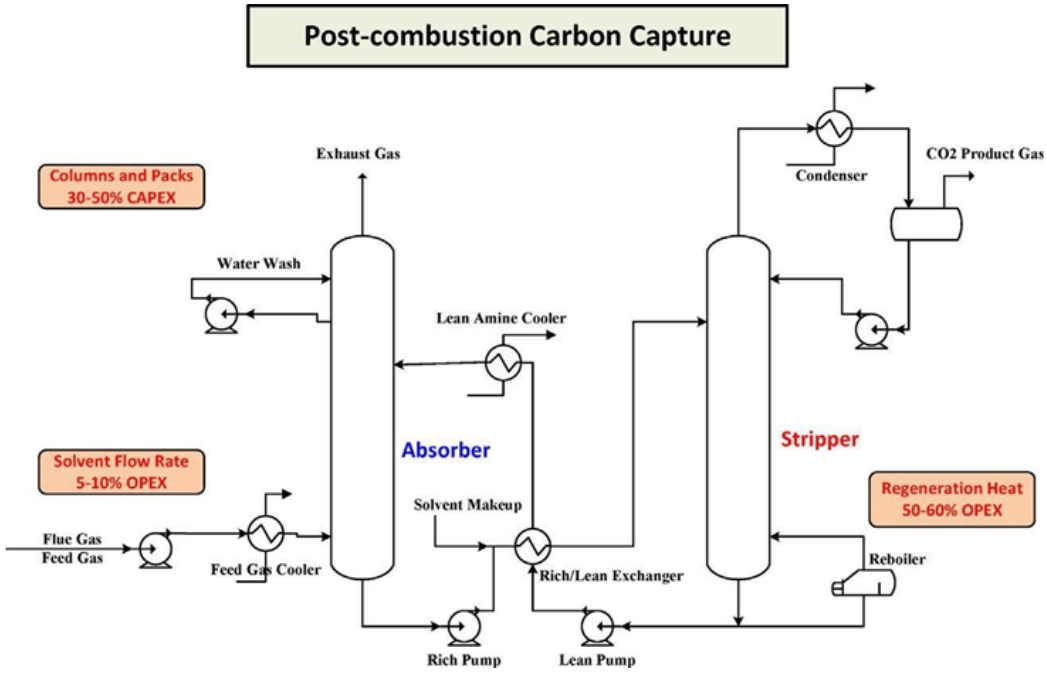

Fig. 1.4 Schematic representation of amine-solvent-based chemical absorption system for separation of CO_2 from flue gas [21].

1.3.2 Adsorption method

Adsorption is a cost-effective separation process in post-combustion carbon capture technology. This technology involves capturing CO_2 by passing the flue gas through an adsorbent. The choice of adsorbent is crucial for the process, and the adsorbents are classified as either physical or chemical based on the adsorption mechanism [7]. Physical adsorbents bind to CO_2 through van der Waals forces, while chemical adsorbents bind to the gas by forming covalent bonds. For efficient CO_2 capture using adsorption methods, the adsorbent should have high selectivity and high adsorption capacity, as well as mechanical and thermal stability over multiple adsorption and desorption cycles. Common physical adsorbents include porous materials such as activated carbon, alumina, and zeolites. The porous structure of these materials provides excellent adsorption properties and allows for efficient CO_2 capture. However, these materials have some

limitations, such as sensitivity to water vapor and low binding energy, which can impact their performance. To improve adsorption efficiency, researchers are exploring other adsorbents such as amine-functionalized adsorbents, metal-organic frameworks (MOFs), and alkali metal oxide adsorbents [22-25]. These new adsorbents generally offer higher CO_2 adsorption capacity and selectivity. However, they also present challenges such as high cost and instability at high temperatures and various pH levels, which hinder their widespread application. Nonetheless, with further research and optimization, these adsorbents have the potential to become more effective and reliable CO_2 capture solutions in the future [26-30].

1.3.3 Low-temperature carbon capture technology

Low-temperature carbon capture technology is an innovative method for capturing CO_2 by utilizing the cold energy of liquefied natural gas (LNG). This technology efficiently captures carbon by cooling flue gas to liquefy and separate CO_2. The separation process involves compression, cooling, and expansion stages, leveraging cryogenic principles to extract CO_2 from the flue gas [32]. **Fig. 1.5** shows a schematic diagram of cryogenic distillation, a commonly used method in cryogenic separation. Cryogenic methods can achieve up to 99% carbon dioxide recovery and purity levels without the use of organic solvents or adsorbents [33, 34]. This high level of efficiency and purity makes cryogenic carbon capture technology appealing for practical applications. However, the temperature difference between the cryogenic system and the environment can lead to heat loss, reducing the overall efficiency. Additionally, water can freeze at low temperatures, potentially causing pipeline blockages and posing challenges to the operation and reliability of the system. Despite these challenges, cryogenic technology is

the most viable option when low-cost cold energy such as LNG is readily available.

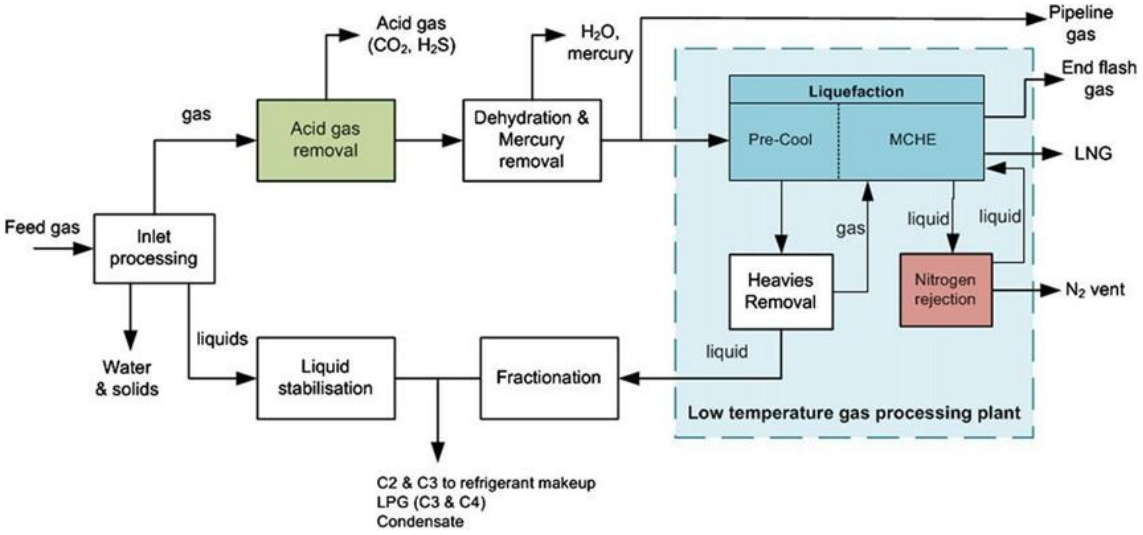

Fig. 1.5 Schematic diagram of the cryogenic distillation process [35].

1.3.4 Membrane separation technology

Membrane separation technology is a novel separation method that has garnered widespread attention for its low energy consumption, simple process, and low investment requirements. This technology was introduced in the natural gas industry in the 1980s and demonstrated its commercial feasibility in CO_2 separation. As the global focus on reducing carbon emissions intensifies, the US Department of Energy (DOE) has set a goal of capturing 90% of CO_2 emissions while limiting the increase in the cost of electricity (COE) to 35%. This establishes a clear direction and standard for the application of membrane separation technology in CO_2 capture. **Fig. 1.6** illustrates a multi-step membrane process developed by Membrane Technology and Research (MTR, USA). This process showcases the significant potential of membrane technology in CO_2 capture. Compared to other CO_2 capture technologies, membranes with high CO_2 permeability and a CO_2/N_2 selectivity ratio of 50 are closer to meeting the DOE's target. This combination of high selectivity and high permeability makes membrane separation

technology stand out in CO_2 capture. Membrane separation technology holds great promise as an environmentally friendly and sustainable solution for CO_2 capture. Its high efficiency makes it a potential alternative, especially in scenarios requiring rapid and large-scale separation of CO_2. With further research and development, membrane separation technology is expected to become one of the leading technologies in the field of CO_2 capture in the future [36, 37].

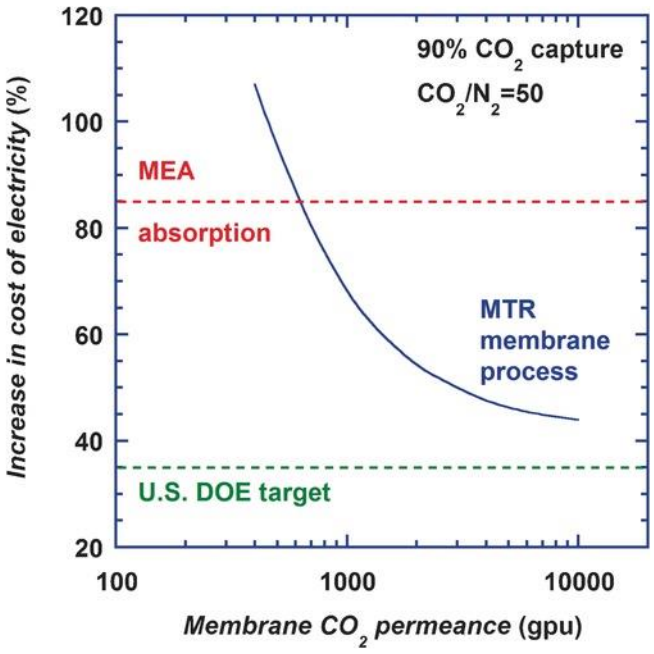

Fig. 1.6 The potential of membrane technology for CO_2 capture from flue gas derived from coal-fired power plants to meet the U.S. DOE target in terms of the increase in the cost of electricity (COE) [38].

1.4 CO_2 separation membrane

Compared with other separation technologies, membrane separation has demonstrated significant engineering and economic benefits in CO_2 capture. These advantages include low energy consumption, simple operation, a small footprint, and low investment requirements. As a result, membrane separation technology is gaining

increasing attention for capturing CO_2 from flue gas produced by coal-fired power plants and other fossil fuel sources. Researchers are exploring different types of CO_2 separation membranes to address diverse application needs and challenges. These membranes can be categorized into polymer membranes, inorganic membranes, and polymer-inorganic hybrid membranes based on their material composition. Polymer membranes are popular due to their lightweight nature, flexibility, and low cost, making them suitable for a widely applications. Inorganic membranes typically exhibit higher thermal stability and mechanical strength, making them ideal for high-temperature and harsh environment applications. However, their manufacturing costs are relatively high, which limits their widespread adoption. Polymer-inorganic hybrid membranes combine the benefits of both materials, offering the flexibility of polymers and the heat and chemical resistance of inorganic materials. This makes hybrid membranes a promising solution that balances performance and cost control. Currently, researchers are extensively studying these different types of membranes to optimize their performance by improving selectivity and permeability, reducing costs, enhancing durability, and expanding their application scope. Through continuous innovation and improvement, membrane separation technology is expected to play an increasingly important role in the field of CO_2 capture and contribute significantly to more efficient and cost-effective carbon emission reduction.

1.4.1 Polymer membrane

Polymer membranes are mainly made of glassy or rubbery organic polymers [39]. In 2002, they held the largest share of the gas separation membrane market. Rubber polymer membranes offer high permeability but tend to have lower selectivity due to the softness and elasticity of their polymer chains [40]. Conversely, glassy polymer

membranes are highly selective but usually have lower permeability due to their rigidity [41]. This creates a trade-off between the permeability and selectivity of polymer membranes. **Fig. 1.7** shows the relationship between selectivity and permeability in polymer membranes, adapted from Robeson's trade-off model. One strategy to overcome this trade-off is to blend two polymers with different strengths and properties to create new polymer membranes, which have been shown to significantly enhance CO_2 permeability and CO_2/N_2 selectivity [42-47]. However, one of the main challenges limiting most polymer membrane applications is their stability and plasticization at high temperatures. At high CO_2 partial pressure and temperature, plasticization of polymer membranes can reduce their long-term stability and CO_2 permeability. Thus, addressing these issues and enhancing the performance and stability of polymer membranes remain ongoing and appealing goals in materials science research.

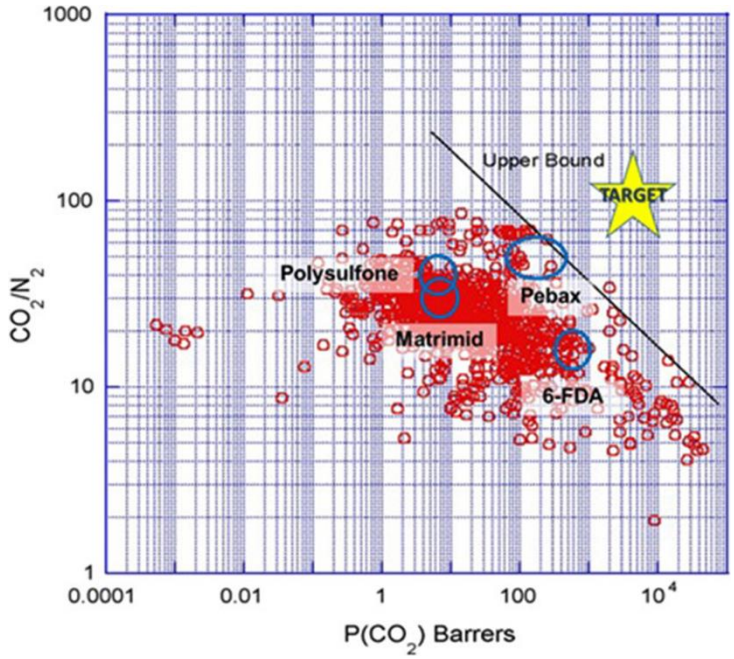

Fig. 1.7 Revisited upper bound data for CO_2 membrane separation [44].

1.4.2 Inorganic membranes

In terms of structure, inorganic membranes can be divided into two major types: porous membranes and dense membranes. Porous membranes are particularly favored in CO_2 separation applications due to their unique size selectivity, as well as their thermal and chemical stability. Inorganic membranes typically demonstrate higher CO_2 permeability, surpassing the Robeson upper bound, which makes them promising candidates for gas separation processes. However, inorganic membranes face several limitations, including high costs, brittleness, and structural defects. These challenges hinder the widespread adoption of inorganic membranes in industrial applications [48]. As a result, most research on inorganic separation membranes is confined to the laboratory stage. While these membranes exhibit excellent performance in research environments, various obstacles must be overcome to facilitate their large-scale implementation. Researchers are actively working to address the challenges associated with inorganic membranes, such as reducing production costs, improving mechanical strength and durability, and minimizing structural imperfections. Inorganic membrane development is focused on overcoming these challenges to enable the transition from laboratory research to commercial-scale implementation. By successfully addressing these obstacles, inorganic membranes could play a crucial role in future CO_2 capture technologies, contributing to more efficient and sustainable carbon reduction strategies.

1.4.3 Polymer-inorganic hybrid membranes

Mixed matrix membranes (MMMs) represent an innovative approach to gas separation by combining a polymer matrix with porous inorganic fillers. This hybrid design leverages the strengths of both materials while mitigating the inherent limitations of pure polymer and inorganic membranes, offering a compelling solution. **Fig. 1.8**

illustrates the gas separation mechanism of MMMs, which primarily relies on solution diffusion and Knudsen diffusion. As a result, MMMs combine the processability of organic materials with the exceptional gas permeability of inorganic porous materials [49-52]. MMMs exhibit strong gas separation performance, addressing challenges such as the permeability-selectivity trade-off often encountered in pure polymer membranes and the brittleness issue of inorganic membranes. These membranes are poised to offer enhanced performance and stability across various gas separation applications. Despite these advantages, fabricating defect-free thin films in MMM remains a significant challenge. Issues such as filler-induced sedimentation and pore blockage during the fabrication process present major hurdles that must be overcome to optimize MMMs [53-56]. By overcoming these obstacles, MMMs have the potential to become a leading technology in gas separation, providing more efficient and sustainable solutions for CO_2 capture and other gas purification processes.

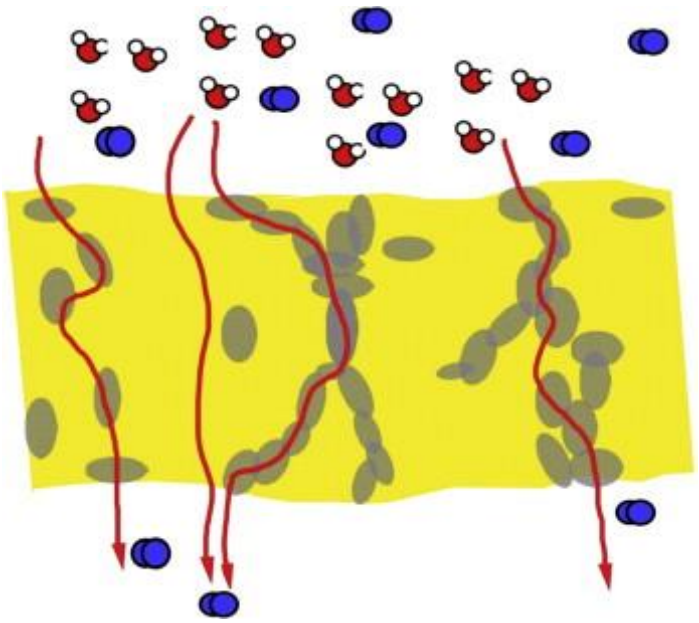

Fig. 1.8 Schematic diagram of a MMM comprised of a polymer matrix and filler (ideal contact).

1.5 Ionic liquid-based membranes

Ionic liquids (ILs) have garnered significant interest from researchers due to their unique properties, including high thermal stability and negligible volatility. These characteristics, combined with their high affinity for CO_2, make ILs attractive candidates for CO_2 capture and separation applications [57]. **Fig. 1.9** illustrates the structures of common RTIL cations and anions. In addition, Blanchard et al. reported on the gas solubility of many common ILs, showing that CO_2 exhibits excellent solubility in most ILs. The interactions between the gas and the IL's anions primarily drive this solubility, followed by interactions with the cations [58-62]. In other words, selecting the right IL can enhance the CO_2 separation performance of ionic liquid membranes. Currently, IL-based separation membranes include supported ionic liquid membranes (SILM), poly(ionic liquid) membranes (PIL), and ion gel membranes. Each type of membrane offers unique advantages and applications in CO_2 separation. SILMs, which consist of a porous support impregnated with an ionic liquid, exhibit high selectivity in gas separation. The choice of IL and support material allows for fine-tuning of the properties, resulting in optimized performance for CO_2 capture. PIL membranes, on the other hand, provide adjustable properties due to the incorporation of ionic liquid moieties within a polymer matrix. This adaptability allows researchers to tailor the membranes to specific separation requirements. Ion gel membranes, composed of ionic liquids and three-dimensional polymer networks demonstrate high mechanical stability and separation properties under harsh operating conditions. This resilience makes ion gels promising for challenging industrial applications. Overall, the integration of ionic liquids and membrane technology holds great potential for advancing CO_2 separation processes and providing

environmentally friendly, energy-efficient solutions to reduce greenhouse gas emissions [63, 64]. As research in this area continues, IL-based membranes may become a cornerstone in the quest for more sustainable and effective carbon capture methods.

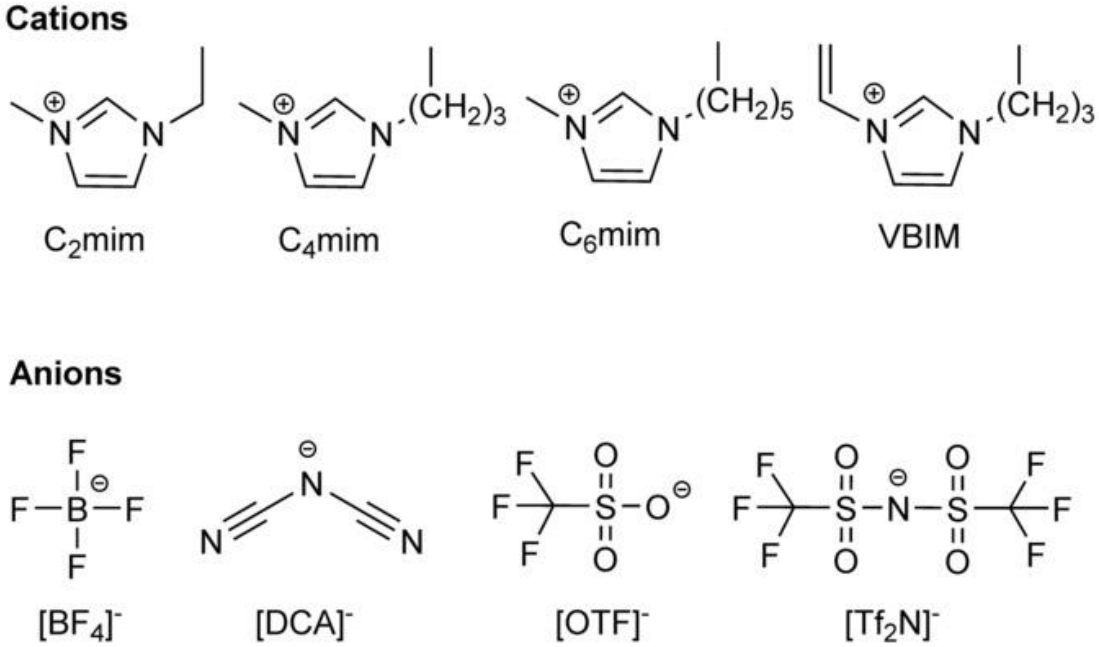

Fig. 1.9 The structures of commonly used RTIL cations and anions [38].

1.5.1 Supported ionic liquid membranes (SILMs)

In the development of combining ILs with membrane separation technology for CO_2 capture, supported ionic liquid membranes (SILMs) were one of the earliest strategies adopted [65, 66]. These membranes exploit the properties of ionic liquids to overcome the instabilities in supported liquid membranes (SLMs), thereby reducing solvent evaporation [67, 68]. In the initial implementations of SILMs, CO_2 separation relied on the solution diffusion mechanism. The CO_2 permeability and selectivity of the membrane could be predicted based on the solubility and diffusion coefficients of CO_2 in the ionic liquid [58, 69]. In recent years, functionalized ionic liquid-based SILMs have been proposed to further enhance the CO_2 separation performance of these membranes [70].

Thanks to the functionalization of ionic liquid groups, SILMs follow a facilitated transport mechanism during CO_2 separation, with the separation performance depending on the specific parameters and properties of the ionic liquid. **Fig. 1.10** presents a schematic diagram of CO_2/N_2 separation using a supported ionic liquid membrane [68]. The exceptional CO_2 separation performance of SILMs makes them a promising option for CO_2 capture. However, the stability of SILMs can be compromised if the transmembrane pressure difference exceeds the capillary forces within the porous material containing the ionic liquid. In such cases, the ionic liquid can easily be expelled from the porous support. In other words, under high transmembrane pressure differences, the separation performance of SILMs becomes unstable [69]. Researchers are actively working on strategies to address these challenges, such as enhancing the compatibility of ionic liquids with support materials and fine-tuning the functional groups in ionic liquids to improve stability and separation efficiency. Through ongoing research and development, SILMs hold great potential as a cutting-edge solution for efficient and sustainable CO_2 capture.

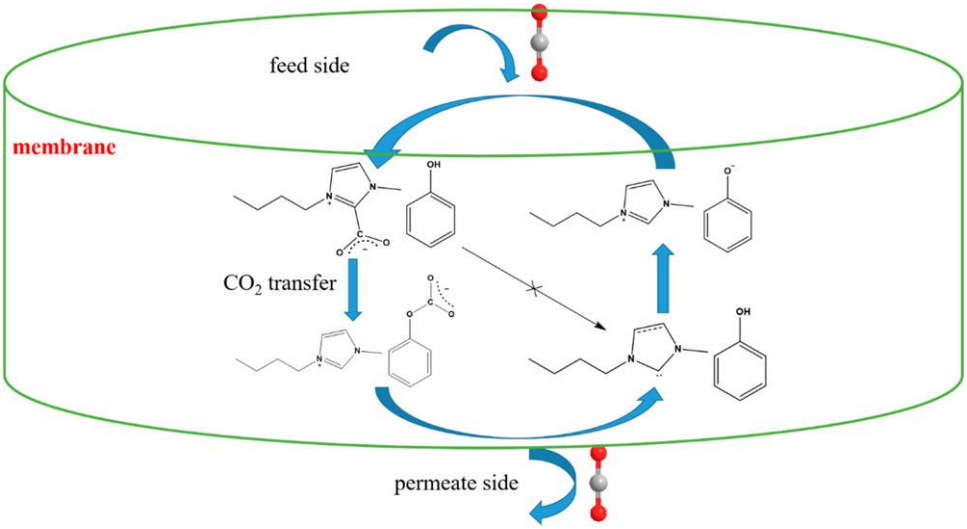

Fig. 1.10 A schematic diagram of CO_2/N_2 separation of a supported ionic liquid membrane.

1.5.2 Poly(ionic liquid) membranes

As mentioned before, ionic liquids may leak out of SILMs under high feed pressure. In contrast, PIL membranes have gained attention for their improved mechanical stability [71, 72]. However, pure PIL membranes generally exhibit lower gas diffusion and permeance because of their dense polymer chains. Achieving optimal CO_2 permeance is challenging unless the membrane thickness is sufficiently small. Therefore, Noble introduced the concept of a PIL-IL composite membrane and incorporated free ionic liquid into the PIL framework, successfully solving this problem [63, 73]. Compared to pure PIL membranes, the free ionic liquids in PIL-IL composite membranes improve the CO_2 permeability and the CO_2 permeability of the membrane increases with the ionic liquid loading. However, the plasticization of PIL-IL membranes under high pressure limits their use under extreme conditions. In summary, while the development of PIL-IL composite membranes shows promise, addressing challenges related to cost and performance under extreme conditions is essential for broader industrial applications. Through continued research and optimization, PIL-IL composite membranes have the potential to provide efficient and stable CO_2 separation solutions across various operating environments.

1.5.3 Ion gel membranes

Ionic liquids exhibit higher CO_2 solubility and diffusion coefficients than pure polymer membranes. Therefore, combining ionic liquids with polymers helps enhance the affinity of polymer for CO_2, which improves the diffusion rate that is limited by the restricted mobility of polymer chains [69]. Ion gel membrane is one of the convenient

methods to combine polymers and ionic liquids. Ion gel membranes consist of a large amount of ionic liquid and a small amount of polymer networks. The polymer network provides the mechanical strength of the ion gel, while the IL ensures the CO_2 separation performance of the membrane [74-78]. High-performance ion gel membranes with IL content exceeding 80 wt% can be prepared by selecting suitable polymer networks and ionic liquids. This high IL content allows for excellent CO_2 permeability and overcomes the pressure resistance challenges of SILM membranes and the low CO_2 permeability of PIL membranes. However, it is important to note that the presence of ionic liquids can induce plasticization, which can compromise the mechanical strength of the ion gel. **Fig. 1.11** uses a PVDF-HFP/IL ion gel membrane to illustrate the impact of IL content on Young's modulus of the ion gel and the permeability of different gases [79]. This highlights the trade-off between CO_2 permeability and mechanical strength in ion gel membranes. Therefore, breaking this trade-off is a key area of focus in the development of ion gel membranes. To advance ion gel technology, research is being conducted to optimize the composition and structure of ion gel membranes. For instance, balancing the amount of ionic liquid and polymer, or employing advanced fabrication techniques, can help enhance the overall performance of the membrane. Achieving an optimal balance between mechanical stability and CO_2 separation efficiency is crucial for the broader adoption of ion gel membranes in practical applications.

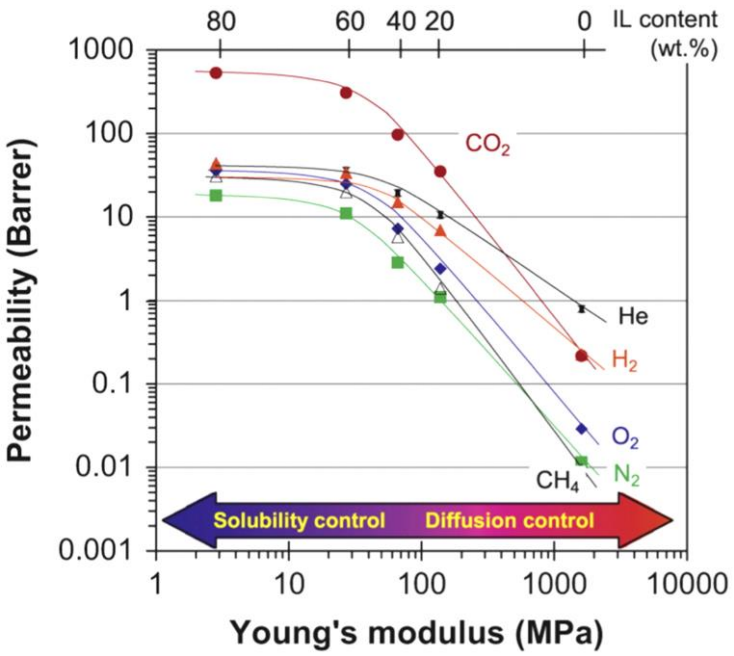

Fig. 1.11 Correlation of the gas permeability with Young's modulus of a PVDF-HFP-based polymer-IL gel membrane [79].

1.6 Challenges of ion gel membranes for CO_2 separation

The application of ionic liquids in gas separation membranes has been widely studied, and significant progress has been made in this area. Ion gel membranes show promise in surpassing the efficiency of traditional polymer membranes for CO_2/N_2 separation. The ionic liquid is a crucial factor influencing the gas separation performance of ion gels, by adjusting the ratio of ionic liquid to polymer components, the gas separation performance of the ion gel membrane can be effectively fine-tuned. As the IL content in ion gels increases, the CO_2 permeability of the membranes also increases, and the CO_2/N_2 permselectivity is unchanged. However, a higher content of ionic liquids means a reduction in polymer content, this will decrease the mechanical strength of the ion gel membrane. To address this issue, a feasible solution has been proposed in the form of developing tough ion gel membranes [80-83]. This approach aims to enhance the

mechanical properties of ion gel membranes without sacrificing their CO_2 separation performance. Additionally, the use of CO_2-philic ionic liquids for the preparation of tough ion gel membranes can further optimize the CO_2 separation efficiency of membranes.

1.7 Tough ion gels

To achieve ion gel membranes with high CO_2 permeability and CO_2/N_2 permselectivity, it is essential to optimize the polymer network structure and enhance the mechanical strength of the ion gel. Single network (SN) ion gel membranes, composed of a single polymer network and ionic liquid, often exhibit brittleness and high Young's modulus under mechanical load due to the limited energy dissipation capacity of the single network. This makes it challenging to prepare CO_2 separation membranes with high IL content [84]. To overcome these challenges, researchers have proposed various strategies for producing tough ion gels. Double network (DN) ion gels have gained significant attention for their unique polymer network structure and toughening mechanisms [85, 86]. DN ion gels are inspired by the toughening mechanisms observed in DN hydrogels, which rely on energy dissipation principles to enhance mechanical properties. The DN ion gel consists of two interpenetrating polymer networks, where the first network provides high strength and stiffness, while the second network allows for flexibility. This combination results in membranes that can accommodate higher ionic liquid content while maintaining mechanical integrity and high performance in CO_2 separation. The process of network changes during the stretching of DN gels is illustrated in **Fig. 1.12** [87]. Kamio et al. successfully developed inorganic/organic DN ion gels based on these DN principles. These DN ion gels, with high ionic liquid content, do not fracture under high compressive stress and maintain excellent CO_2 separation

performance even under high transmembrane pressure differentials [88]. This breakthrough demonstrates the potential of DN ion gels to resolve the trade-off between CO_2 permeability and mechanical strength in ion gels.

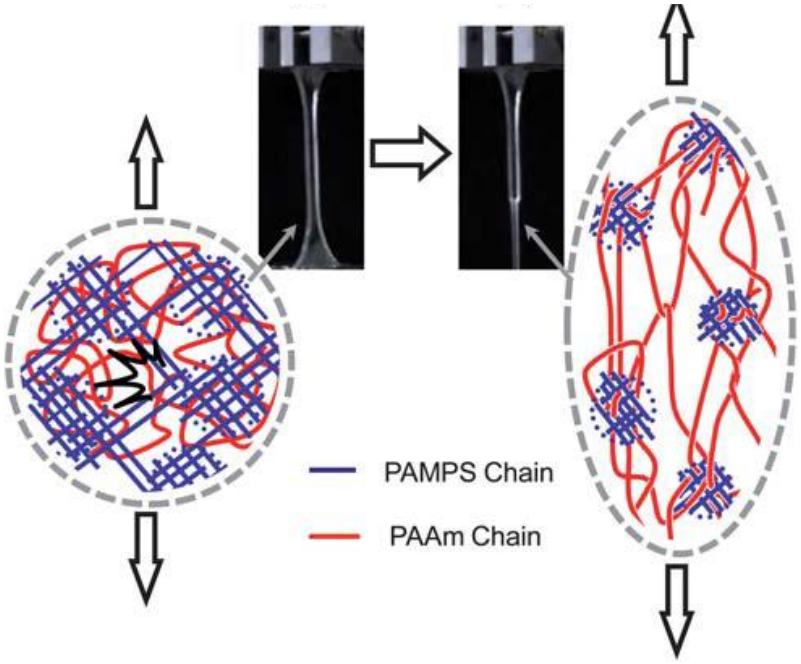

Fig. 1.12 Schematic diagram of the change process of the polymer network when the double network gel is stretched [87].

1.8 Purpose of this dissertation

Ion gel membranes hold great promise for CO_2 separation, but they face a challenge in balancing CO_2 permeability with mechanical strength. Typically, increasing the ionic liquid content in an ion gel boosts CO_2 permeability, but it also reduces the mechanical strength. To address this trade-off, developing tough ion gel membranes becomes a key strategy for enhancing CO_2 permeability while maintaining high mechanical strength. Moreover, using ionic liquids with high CO_2 affinity in these tough ion gel membranes can further improve CO_2 separation performance due to differences in the solubility and diffusion coefficients of ILs for CO_2 and N_2. The focus of this dissertation is to use ionic

liquids with high CO_2 affinity alongside suitable polymer networks to develop ion gel membranes that are both durable and highly permeable to CO_2. This approach aims to overcome the traditional trade-off between CO_2 permeability and mechanical strength in ion gel membranes, leading to the development of membranes capable of high-performance CO_2 separation while withstanding challenging operational conditions.

1.9 Scope of this thesis

This thesis includes the following 5 chapters.

Chapter 1: This chapter summarizes the development status and prospects of membrane separation technology in carbon capture technology. The advantages of CO_2 separation membranes based on ionic liquids are proposed, especially the potential and challenges of ion gel membranes for CO_2 separation. Finally, there is the research purpose and scope of this dissertation.

Chapter 2: A tough ion gel membrane composed of a semi-crystalline polymer, a cross-linkable polymer, and a CO_2-philic ionic liquid was developed. In the developed ion gel, the energy dissipation mechanism of the semi-crystalline polymer provides the ion gel with high mechanical strength, and the high compatibility of the cross-linkable polymer and IL gives good IL holding properties. Good mechanical strength and IL retention properties enable ion gels to have excellent CO_2 separation performance under variable pressure and high temperature. In addition, when the IL content of the ion gel was as high as 85 wt%, the CO_2 permeability was 2400 barrer and the CO_2/N_2 permselectivity was 40. The developed IPN ion gel membrane has the potential for carbon capture.

Chapter 3: In Chapter 2, we successfully developed tough IPN ion gels containing

CO_2-philic ionic liquid. The IL content of the ion gel was up to 85 wt%. Although the IL content of the ion gel is higher than 80 wt%, the limited mechanical strength limits the further increase of the IL content in the ion gel. Therefore, in this chapter, we aim to develop ion gel membranes with higher mechanical strength to increase the IL content of ion gels. We have successfully developed a tough IPN ion gel membrane with the DN principle. The ion gel membrane is composed of a semi-crystalline polymer, a highly stretchable tetra-arm polyethylene glycol (tetra-PEG) network, and CO_2-philic IL. The semi-crystalline polymer network forms a crystalline cross-linked structure and acts as a sacrificial bond, while the tetra-PEG network acts as a hidden length to prevent macro-destruction to the ion gel network under highly stretched conditions. The toughening effect of the DN principle improves the mechanical strength of the ion gel, and the IL content increased to 92.5 wt%. The ion gel membrane containing 92.5 wt% had a CO_2 permeability of 3100 barrer and a CO_2/N_2 permselectivity of 43. In addition, the ion gel also had a CO_2 permeability of more than 2000 barrer and a CO_2/N_2 permselectivity of 20 after 10 days of long-term stability testing under high temperature and humidity conditions. The designed IPN ion gel has the potential for CO_2 separation from coal-fired power plants.

Chapter 4: Building on the findings from Chapter 3, where the semi-crystalline polymer was successfully utilized to prepare ion gels with a double network principle, this chapter further explores the potential of semi-crystalline polymers in creating tough DN ion gels. The enhancement in mechanical properties allowed for an increased IL content of 92.5 wt% in the membrane in Chapter 3, which resulted in a high CO_2 permeability. However, the CO_2/N_2 permselectivity was limited to 43. To improve CO_2/N_2 pernselectivity, this chapter develops a DN ion gel membrane comprising a CO_2-

philic ionic liquid, a semi-crystalline polymer, and a loosely cross-linked poly(N,N'-dimethylacrylamide) (PDMAAm) network. In this DN ion gel, the physically cross-linked polyvinyl alcohol (PVA) network serves as a sacrificial bond, toughening the ion gel by dissipating energy. The entanglement of the loosely cross-linked PDMAAm network with the PVA network significantly enhances the fracture strain of the ion gel. Owing to the excellent toughness of the DN ion gel, the IL content can reach up to 93 wt%, resulting in a CO_2 permeability of 2920 barrer. The high solubility selectivity of IL for CO_2/N_2 enabled the DN ion gel to exhibit an exceptional CO_2/N_2 permselectivity of 61. Even with an IL content of 80 wt%, the CO_2 permeability remained stable under high transmembrane pressure differences. The CO_2 permeability reached 2300 barrer, while maintaining a CO_2/N_2 permselectivity of 30 at 80 °C and 80% relative humidity. The CO_2 separation performance of this DN ion gel membrane satisfies the requirements for CO_2 capture from flue gas in coal-fired power plants.

Chapter 5: A summary of this dissertation.

References

[1] G.C. Budget, Global carbon budget 2023, 2023.

[2] J.L.J. Ling, W. Yang, H.S. Park, et al., A comparative review on advanced biomass oxygen fuel combustion technologies for carbon capture and storage, Energy, 284, 2023, 128566.

[3] D. Jansen, M. Gazzani, G. Manzolini, et al., Pre-combustion CO_2 capture, International Journal of Greenhouse Gas Control, 40, 2015, 167-187.

[4] F. Wu, M.D. Argyle, P.A. Dellenback, M. Fan, Progress in O_2 separation for oxy-fuel combustion-A promising way for cost-effective CO_2 capture: A review, Progress in Energy and Combustion Science, 67, 2018, 188-205.

[5] Y. Wang, L. Zhao, A. Otto, et al., A review of post-combustion CO_2 capture technologies from coal-fired power plants, Energy Procedia, 114, 2017, 650-665.

[6] T. Patil, S. Dharaskar, M. Sinha, S.S. Jampa, Effectiveness of ionic liquid-supported membranes for carbon dioxide capture: a review, Environmental Science and Pollution Research, 29(24), 2022, 35723-35745.

[7] P. Madejski, K. Chmiel, N. Subramanian, T. Kuś, Methods and techniques for CO_2 capture: review of potential solutions and applications in modern energy technologies, Energies, 15(3), 2022, 887.

[8] W.L. Theo, J.S. Lim, H. Hashim, et al., Review of pre-combustion capture and ionic liquid in carbon capture and storage, Applied Energy, 183, 2016, 1633-1663.

[9] M. Kanniche, R. Gros Bonnivard, P. Jaud, et al., Pre-combustion, post-combustion and oxy-combustion in thermal power plant for CO_2 capture, Applied Thermal Engineering, 30(1), 2010, 53-62.

[10] V. Kindra, A. Rogalev, E. Lisin, et al., Techno-economic analysis of the oxy-fuel

combustion power cycles with near-zero emissions, Energies, 14(17), 2021, 5358.

[11] C. C. Cormos, Oxy-combustion of coal, lignite and biomass: A techno-economic analysis for a large scale carbon capture and storage (CCS) project in Romania, Fuel, 169, 2016, 50-57.

[12] C. Chao, Y. Deng, R. Dewil, et al., Post-combustion carbon capture, Renewable and Sustainable Energy Reviews, 138, 2021, 110490.

[13] M. Kárászová, B. Zach, Z. Petrusová, et al., Post-combustion carbon capture by membrane separation, Review, Separation and Purification Technology, 238, 2020, 116448.

[14] C. H. Yu, C. S. Tan, Mixed alkanolamines with low regeneration energy for CO_2 capture in a rotating packed bed, Energy Procedia, 37, 2013, 455-460.

[15] R. Maceiras, Á. Cancela, Measurement of the interfacial area during CO_2 capture with alkanolamines, Chemical Engineering Journal, 172(1), 2011, 335-340.

[16] J. Kittel, R. Idem, D. Gelowitz, et al., Corrosion in MEA units for CO_2 capture: Pilot plant studies, Energy Procedia, 1(1), 2009, 791-797.

[17] A. Ghayur, T.V. Verheyen, E. Meuleman, Biological and chemical treatment technologies for waste amines from CO_2 capture plants, Journal of Environmental Management, 241, 2019, 514-524.

[18] F.A. Tobiesen, H.F. Svendsen, Study of a modified amine-based regeneration unit, Industrial & Engineering Chemistry Research, 45(8), 2006, 2489-2496.

[19] M.R.M. Abu Zahra, L.H.J. Schneiders, J.P.M. Niederer, et al., CO_2 capture from power plants: Part I. A parametric study of the technical performance based on monoethanolamine, International Journal of Greenhouse Gas Control, 1(1), 2007, 37-46.

[20] F. Bougie, D. Pokras, X. Fan, Novel non-aqueous MEA solutions for CO_2 capture,

International Journal of Greenhouse Gas Control, 86, 2019, 34-42.

[21] Z. Liang, W. Rongwong, H. Liu, et al., Recent progress and new developments in post-combustion carbon-capture technology with amine based solvents, International Journal of Greenhouse Gas Control, 40, 2015, 26-54.

[22] M. Castro, S.J. Warrender, P.A. Wright, et al., Silicoaluminophosphate molecular sieves STA-7 and STA-14 and their structure-dependent catalytic performance in the conversion of methanol to olefins, The Journal of Physical Chemistry C, 113(35), 2009, 15731-15741.

[23] G. Férey, Hybrid porous solids: past, present, future, Chemical Society Reviews, 37(1), 2008, 191-214.

[24] K.S. Walton, M.B. Abney, M. Douglas LeVan, CO_2 adsorption in Y and X zeolites modified by alkali metal cation exchange, Microporous and Mesoporous Materials, 91(1), 2006, 78-84.

[25] M. Abe, K. Kawashima, K. Kozawa, et al., Amination of activated carbon and adsorption characteristics of its aminated surface, Langmuir, 16(11), 2000, 5059-5063.

[26] X. Hu, L. Liu, X. Luo, et al., A review of N-functionalized solid adsorbents for post-combustion CO_2 capture, Applied Energy, 260, 2020, 114244.

[27] A. Modak, S. Jana, Advancement in porous adsorbents for post-combustion CO_2 capture, Microporous and Mesoporous Materials, 276, 2019, 107-132.

[28] S. Wang, S. Yan, X. Ma, J. Gong, Recent advances in capture of carbon dioxide using alkali-metal-based oxides, Energy & Environmental Science, 4(10), 2011, 3805-3819.

[29] P.L. Llewellyn, S. Bourrelly, C. Serre, et al., High uptakes of CO_2 and CH_4 in mesoporous metal-organic frameworks MIL-100 and MIL-101, Langmuir, 24(14), 2008, 7245-7250.

[30] S. Dasgupta, N. Biswas, Aarti, et al., CO_2 recovery from mixtures with nitrogen in a vacuum swing adsorber using metal organic framework adsorbent: A comparative study, International Journal of Greenhouse Gas Control, 7, 2012, 225-229.

[31] C. Song, Q. Liu, S. Deng, et al., Cryogenic-based CO_2 capture technologies: State-of-the-art developments and current challenges, Renewable and Sustainable Energy Reviews, 101, 2019, 265-278.

[32] A. Brunetti, F. Scura, G. Barbieri, E. Drioli, Membrane technologies for CO_2 separation, Journal of Membrane Science, 359(1), 2010, 115-125.

[33] F. Fazlollahi, A. Bown, E. Ebrahimzadeh, L.L. Baxter, Transient natural gas liquefaction and its application to CCC-ES (energy storage with cryogenic carbon capture™), Energy, 103, 2016, 369-384.

[34] F. Fazlollahi, A. Bown, E. Ebrahimzadeh, L.L. Baxter, Design and analysis of the natural gas liquefaction optimization process-CCC-ES (energy storage of cryogenic carbon capture), Energy, 90, 2015, 244-257.

[35] T.E. Rufford, S. Smart, G.C.Y. Watson, et al., The removal of CO_2 and N_2 from natural gas: A review of conventional and emerging process technologies, Journal of Petroleum Science and Engineering, 94-95, 2012, 123-154.

[36] A. Tabe-Mohammadi, A review of the applications of membrane separation technology in natural gas treatment, Separation Science and Technology, 34(10), 1999, 2095-2111.

[37] B. Li, B. Qi, Z. Guo, et al., Recent developments in the application of membrane separation technology and its challenges in oil-water separation: A review, Chemosphere, 327, 2023, 138528.

[38] J. Liu, X. Hou, H.B. Park, H. Lin, High-performance polymers for membrane

CO_2/N_2 separation, Chemistry-A European Journal, 22(45), 2016, 15980-15990.

[39] F.A.H. Juber, Z.A. Jawad, B.L.F. Chin, et al., The prospect of synthesis of PES/PEG blend membranes using blend NMP/DMF for CO_2/N_2 separation, Journal of Polymer Research, 28(5), 2021, 177.

[40] S.S. Swain, L. Unnikrishnan, S. Mohanty, S.K. Nayak, Carbon nanotubes as potential candidate for separation of H_2/CO_2 gas pairs, International Journal of Hydrogen Energy, 42(49), 2017, 29283-29299.

[41] M. Farnam, H. Mukhtar, A. Mohd Shariff, A review on glassy polymeric membranes for gas separation, Applied Mechanics and Materials, 625, 2014, 701-703.

[42] D. Shekhawat, D.R. Luebke, H.W. Pennline, A review of carbon dioxide selective membranes: A topical report, United States, 2003, 1040.

[43] L.M. Robeson, Correlation of separation factor versus permeability for polymeric membranes, Journal of Membrane Science, 62(2), 1991, 165-185.

[44] L.M. Robeson, The upper bound revisited, Journal of Membrane Science, 320(1), 2008, 390-400.

[45] N. Norahim, P. Yaisanga, K. Faungnawakij, et al., Recent membrane developments for CO_2 separation and capture, Chemical Engineering & Technology, 41(2), 2018, 211-223.

[46] W. Yave, A. Car, K.V. Peinemann, et al., Gas permeability and free volume in poly(amide-b-ethylene oxide)/polyethylene glycol blend membranes, Journal of Membrane Science, 339(1), 2009, 177-183.

[47] A. Car, C. Stropnik, W. Yave, K.V. Peinemann, PEG modified poly(amide-b-ethylene oxide) membranes for CO_2 separation, Journal of Membrane Science, 307(1), 2008, 88-95.

[48] H. Li, X. Ding, Y. Zhang, J. Liu, Porous graphene nanosheets functionalized thin film nanocomposite membrane prepared by interfacial polymerization for CO_2/N_2 separation, Journal of Membrane Science, 543, 2017, 58-68.

[49] M. Chawla, H. Saulat, M. Masood Khan, et al., Membranes for CO_2/CH_4 and CO_2/N_2 gas separation, Chemical Engineering & Technology, 43(2), 2020, 184-199.

[50] T.T. Moore, R. Mahajan, D.Q. Vu, W.J. Koros, Hybrid membrane materials comprising organic polymers with rigid dispersed phases, AIChE Journal, 50(2), 2004, 311-321.

[51] S. Li, Y. Liu, D.A. Wong, J. Yang, Recent advances in polymer-inorganic mixed matrix membranes for CO_2 separation, Polymers, 13(15), 2021, 2539.

[52] M. Rezakazemi, A. Ebadi Amooghin, M.M. Montazer-Rahmati, et al., State-of-the-art membrane based CO_2 separation using mixed matrix membranes (MMMs): An overview on current status and future directions, Progress in Polymer Science, 39(5), 2014, 817-861.

[53] T. S. Chung, L.Y. Jiang, Y. Li, S. Kulprathipanja, Mixed matrix membranes (MMMs) comprising organic polymers with dispersed inorganic fillers for gas separation, Progress in Polymer Science, 32(4), 2007, 483-507.

[54] T.T. Moore, W.J. Koros, Non-ideal effects in organic-inorganic materials for gas separation membranes, Journal of Molecular Structure, 739(1), 2005, 87-98.

[55] G. Clarizia, C. Algieri, E. Drioli, Filler-polymer combination: a route to modify gas transport properties of a polymeric membrane, Polymer, 45(16), 2004, 5671-5681.

[56] Y. Li, H. M. Guan, T.S. Chung, S. Kulprathipanja, Effects of novel silane modification of zeolite surface on polymer chain rigidification and partial pore blockage in polyethersulfone (PES)-zeolite A mixed matrix membranes, Journal of Membrane

Science, 275(1), 2006, 17-28.

[57] S. C. Lu, A.L. Khan, I.F.J. Vankelecom, Polysulfone-ionic liquid based membranes for CO_2/N_2 separation with tunable porous surface features, Journal of Membrane Science, 518, 2016, 10-20.

[58] Q. Gan, Y. Zou, D. Rooney, et al., Theoretical and experimental correlations of gas dissolution, diffusion, and thermodynamic properties in determination of gas permeability and selectivity in supported ionic liquid membranes, Advances in Colloid and Interface Science, 164(1), 2011, 45-55.

[59] C.A. Ohlin, P.J. Dyson, G. Laurenczy, Carbon monoxide solubility in ionic liquids: determination, prediction and relevance to hydroformylation, Chemical Communications, (9), 2004, 1070-1071.

[60] A. Heintz, S.P. Verevkin, Thermodynamic properties of mixtures containing ionic liquids. 6. Activity coefficients at infinite dilution of hydrocarbons, alcohols, esters, and aldehydes in 1-Methyl-3-octyl-imidazolium tetrafluoroborate using gas-liquid chromatography, Journal of Chemical & Engineering Data, 50(5), 2005, 1515-1519.

[61] L.A. Blanchard, D. Hancu, E.J. Beckman, J.F. Brennecke, Green processing using ionic liquids and CO_2, Nature, 399(6731), 1999, 28-29.

[62] P.J. Dyson, G. Laurenczy, C. André Ohlin, et al., Determination of hydrogen concentration in ionic liquids and the effect (or lack of) on rates of hydrogenation, Chemical Communications, 19, 2003, 2418-2419.

[63] M.G. Cowan, D.L. Gin, R.D. Noble, Poly(ionic liquid)/ionic liquid ion-gels with high “free” ionic liquid content: Platform membrane materials for CO_2/light gas separations, Accounts of Chemical Research, 49(4), 2016, 724-732.

[64] S. Xiong, D. Yin, M.U. Javaid, et al., Ionic liquids-based membranes for carbon

dioxide separation, Israel Journal of Chemistry, 59(9), 2019, 824-831.

[65] P. Scovazzo, A.E. Visser, J.H. Davis Jr, et al., Supported ionic liquid membranes and facilitated ionic liquid membranes, ACS Symposium Series, 818, 2002, 69-87.

[66] P. Scovazzo, J. Kieft, D.A. Finan, et al., Gas separations using non-hexafluorophosphate [PF6]-anion supported ionic liquid membranes, Journal of Membrane Science, 238(1), 2004, 57-63.

[67] I.K. Swati, Q. Sohaib, S. Cao, et al., Protic/aprotic ionic liquids for effective CO_2 separation using supported ionic liquid membrane, Chemosphere, 267, 2021, 128894.

[68] X. Zhang, W. Xiong, Z. Tu, et al., Supported ionic liquid membranes with dual-site interaction mechanism for efficient separation of CO_2, ACS Sustainable Chemistry & Engineering, 7(12), 2019, 10792-10799.

[69] Z. Dai, R.D. Noble, D.L. Gin, et al., Combination of ionic liquids with membrane technology: A new approach for CO_2 separation, Journal of Membrane Science, 497, 2016, 1-20.

[70] A. Klemm, Y. Y. Lee, H. Mao, B. Gurkan, Facilitated transport membranes with ionic liquids for CO_2 separations, Frontiers in Chemistry, 8, 2020.

[71] R.M. Teodoro, L.C. Tomé, D. Mantione, et al., Mixing poly(ionic liquid)s and ionic liquids with different cyano anions: Membrane forming ability and CO_2/N_2 separation properties, Journal of Membrane Science, 552, 2018, 341-348.

[72] J. Yin, C. Zhang, Y. Yu, et al., Tuning the microstructure of crosslinked poly(ionic liquid) membranes and gels via a multicomponent reaction for improved CO_2 capture performance, Journal of Membrane Science, 593, 2020, 117405.

[73] J.E. Bara, S. Lessmann, C.J. Gabriel, et al., Synthesis and performance of polymerizable room-temperature ionic liquids as gas separation membranes, Industrial &

engineering chemistry research, 46(16), 2007, 5397-5404.

[74] S.U. Hong, D. Park, Y. Ko, I. Baek, Polymer-ionic liquid gels for enhanced gas transport, Chemical communications, (46), 2009, 7227-7229.

[75] J.C. Jansen, G. Clarizia, P. Bernardo, et al., Gas transport properties and pervaporation performance of fluoropolymer gel membranes based on pure and mixed ionic liquids, Separation and Purification Technology, 109, 2013, 87-97.

[76] J.C. Jansen, K. Friess, G. Clarizia, et al., High ionic liquid content polymeric gel membranes: Preparation and performance, Macromolecules, 44(1), 2011, 39-45.

[77] L. Liang, Q. Gan, P. Nancarrow, Composite ionic liquid and polymer membranes for gas separation at elevated temperatures, Journal of membrane science, 450, 2014, 407-417.

[78] S. Kanehashi, M. Kishida, T. Kidesaki, et al., CO_2 separation properties of a glassy aromatic polyimide composite membranes containing high-content 1-butyl-3-methylimidazolium bis (trifluoromethylsulfonyl) imide ionic liquid, Journal of membrane science, 430, 2013, 211-222.

[79] K. Friess, J.C. Jansen, F. Bazzarelli, et al., High ionic liquid content polymeric gel membranes: Correlation of membrane structure with gas and vapour transport properties, Journal of Membrane Science, 415-416, 2012, 801-809.

[80] Y. Yu, X. Yang, C. Zhang, et al., A tough double-network ion gel membrane based on poly (ionic liquid) for efficient carbon capture, Separation and Purification Technology, 331, 2024, 125591.

[81] F. Ranjbaran, E. Kamio, H. Matsuyama, Ion gel membrane with tunable inorganic/organic composite network for CO_2 separation, Industrial & Engineering Chemistry Research, 56(44), 2017, 12763-12772.

[82] F. Moghadam, E. Kamio, T. Yoshioka, H. Matsuyama, New approach for the fabrication of double-network ion gel membranes with high CO_2/N_2 separation performance based on facilitated transport, Journal of Membrane Science, 530, 2017, 166-175.

[83] J. Zhang, E. Kamio, A. Matsuoka, et al., Novel tough ion-gel-based CO_2 separation membrane with interpenetrating polymer network composed of semicrystalline and cross-linkable polymers, Industrial & Engineering Chemistry Research, 61(13), 2022, 4648-4658.

[84] S. Fuchs, K. Shariati, M. Ma, Specialty tough hydrogels and their biomedical applications, Advanced healthcare materials, 9(2), 2020, 1901396.

[85] J.P. Gong, Why are double network hydrogels so tough?, Soft Matter, 6(12), 2010, 2583-2590.

[86] J.P. Gong, Y. Katsuyama, T. Kurokawa, Y. Osada, Double-network hydrogels with extremely high mechanical strength, Advanced Materials, 15(14), 2003, 1155-1158.

[87] M.A. Haque, T. Kurokawa, J.P. Gong, Super tough double network hydrogels and their application as biomaterials, Polymer, 53(9), 2012, 1805-1822.

[88] E. Kamio, M. Kinoshita, T. Yasui, et al., Preparation of inorganic/organic double-network ion gels using a cross-linkable polymer in an open system, Macromolecules, 53(19), 2020, 8529-8538.

Chapter 2

Development of an ion gel membrane containing a CO_2-philic ionic liquid in interpenetrating semi-crystalline and cross-linkable polymer networks

2.1 Introduction

The combustion of fossil fuels is one of the primary contributors to the greenhouse gas CO_2. As these fuels continue to burn, the atmospheric concentration of CO_2 steadily increases. This upward trend in CO_2 concentration plays a direct role in the escalation of global warming and sets off a cascade of climatic shifts, including the heightened occurrence of extreme weather events, disturbances in ecosystems, and the emergence of water scarcity issues [1, 2]. Therefore, the development of separation membranes for efficient CO_2 capture holds profound practical significance in curbing and mitigating atmospheric CO_2 concentration. Among the currently reported separation membranes for CO_2 capture, glassy polymers such as polyimides, polymers of intrinsic microporosity (PIMs), and thermally rearranged (TR) polymers are widely utilized owing to their high CO_2 permeability [3, 4]. However, during long-term stability tests, the CO_2 permeability of these glassy polymer membranes tends to decrease due to physical aging [5, 6]. In contrast, rubbery polymer membranes, due to their flexible polymer chains, exhibit a stable CO_2 permeability and are unaffected by physical aging, but the polymer membrane

possesses a low CO_2/N_2 permselectivity. [7-9]

On the contrary, ionic liquid (IL) is a remarkable CO_2 separation membrane material, characterized by a CO_2 permeability coefficient that remains unaffected by physical aging, and a high diffusion coefficient surpassing that of conventional polymer membranes by an order of magnitude [10-17]. It is noteworthy that the diffusivity of CO_2 in ILs is contingent upon viscosity, which in turn is influenced by the interactions between its constituent anions and cations [18-20]. Weaker interactions between anions and cations lead to higher CO_2 diffusivity [21]. It has been reported that [Emim][$B(CN)_4$] stands out for its excellent combination of CO_2 solubility and diffusivity, making it the first choice for CO_2 separation applications [22]. SILMs designed based on [Emim][$B(CN)_4$] exhibit an impressive CO_2/N_2 permselectivity of up to 53 and a theoretical maximum CO_2 permeability of 2830 [23]. Thus, ion gel membranes prepared from [Emim][$B(CN)_4$] are expected to exhibit excellent CO_2 permeability and CO_2/N_2 permselectivity. The ion gel membrane consists of a small amount of polymer and a large amount of IL, and the high mechanical strength of the ion gel allows for a high IL content in the membrane, which in turn exhibits high CO_2 permeability [24]. In the latest advancement in tough ion gel membranes, interpenetrating polymer network (IPN) ion gels composed of semi-crystalline and cross-linkable polymers are prominent contenders due to their superior mechanical strength and CO_2 separation properties [25-32]. In IPN ion gels previously prepared by our group, it has been demonstrated that poly(vinylidene fluoride)-hexafluoropropylene copolymer (PVDF-HFP) as a semi-crystalline polymer network is capable of providing mechanical strength to ion gels [29]. Thus, PVDF-HFP is a promising candidate for the development of semi-crystalline polymer networks within tough ion gels containing [Emim][$B(CN)_4$]. The tough IPN ion gels can be achieved by

strategically designing suitable cross-linkable polymer networks.

In this study, we planned to fabricate a high mechanical strength ion gel membrane by interpenetrating the PVDF-HFP and a cross-linkable polymer. To achieve this goal, we synthesized a cross-linkable polymer with excellent compatibility with [Emim][$B(CN)_4$], allowing the designed IPN ion gel membranes to contain up to 85 wt% IL content. In addition, we evaluated the CO_2 separation performance of the developed ion gels at different transmembrane pressures and temperatures. The designed IPN ion gels remained stable for CO_2 permeability during long-term stability tests of over 200 hours.

2.2 Experimental

2.2.1 Materials

[Emim][$B(CN)_4$] was procured from Sigma-Aldrich Co., and a pellet of PVDF-HFP with a weight-averaged molecular weight of 400,000 g/mol was also obtained from the same source. To ascertain cross-linkable polymers have high compatibility with [Emim][$B(CN)_4$], we conducted compatibility tests using various commercial polymers, all of which were sourced from Sigma-Aldrich Co. Details regarding the polymers employed are outlined in **Table 2.1**. The monomers utilized for synthesizing the cross-linkable polymers were sourced from Sigma-Aldrich Co. *N*-succinimidyl acrylate (NSA), serving as the cross-linking functional group, was procured from Tokyo Chemical Industry Co., Ltd., Japan. The initiator, azobisisobutyronitrile (AIBN), was obtained from FUJIFILM Wako Pure Chemical Co. Super-dehydrated 1,4-dioxane and anhydrous toluene were employed as solvents for the synthesis of the cross-linkable polymer, both purchased from FUJIFILM Wako Pure Chemical Co. Diethylene glycol bis(3-aminopropyl)ether (DGBE) and acetone were utilized as the crosslinker and solvent,

respectively, and were procured from Tokyo Chemical Industry Co., Ltd.

Table 2.1 Used polymers and the results of the compatibility test with [Emim][B(CN)$_4$].

Name of polymers	Abbreviation	Molecular weight	Compatibility with [Emim][B(CN)$_4$]
polyacrylamide	PAm	M_n 40,000	Incompatible
polyvinylpyrrolidone	PVP	M_n 40,000	Incompatible
Polydimethylslioxane	PDMS	M_w 95,000	Incompatible
Polymethyl methacrylate	PMMA	M_w 15,000	Compatible
Polybutyl methacrylate	PBuMA	M_w 211,000	Incompatible
Polyvinyl alcohol	PVA	M_w 70,000	Incompatible
Polymethyl acrylate	PMA	M_w 40,000	Compatible
PolyN-isopropyl acrylamide	PNIPAM	M_n 5,000	Compatible
Polyacrylic acid	PAc	N.A.	Incompatible
Polystyrene	PSt	M_n 170,000	Incompatible
Polydimethylacrylamide	PDMAM	M_n 10,000	Compatible
Polyethyl acrylate	PEA	M_w 95,000	Compatible

M_n: Number average molecular weight, M_w: Weight average molecular weight, N.A.: not available.

2.2.2 Compatibility tests of polymers with [Emim][B(CN)$_4$]

Table 2.1 describes in detail the results of the compatibility tests between the commercial polymers used in this study and [Emim][B(CN)$_4$]. The following is the evaluation step for the compatibility test. The compatibility of each polymer in IL was assessed by observing the state of the polymer/IL mixture after evaporation of the organic solvent from the IL/polymer/organic solvent solution. [33] First, the polymer (0.216 g) was mixed with the organic solvent (1.92 g) for 2 h to obtain a homogeneous solution. Subsequently, IL was added to the polymer solution and stirred for 10 min until a clarified solution was obtained. The resultant mixture was then placed in an oven drying at 80 °C for 24 h to eliminate the solvent. The resulting mixture was then in and high clarity

indicated good compatibility between the polymer and IL. Conversely, precipitation or turbidity of the solution indicates poor compatibility between the polymer and IL. Based on the results in **Table 2.1**, we identified five candidate polymers suitable for incorporation into the interpenetrating polymer network.

2.2.3 Synthesis of cross-linkable polymers

Synthesis of cross-linkable polymers by free radical polymerization. The three-necked round-bottomed flask was first sealed and then purged with N_2 five times for 10 min each. Then, 18.0 g of solvent was added to the flask using a syringe. Subsequently, a mixture of 20.0 g of monomer with a solution containing NSA and AIBN dissolved in 2.0 g of solvent was injected into the flask. The proportions of NSA and AIBN were adjusted to 3.0 mol% and 0.5 mol%, respectively, based on the monomer. After adding the reagents, the solution in the flask was purged with N_2 for 30 min while stirring. It was then stirred continuously for 24 h at 333 K in an oil bath. Purification of the product was carried out by reprecipitation and repeated twice. Finally, the solid product obtained was thoroughly dried in a vacuum oven at 363 K for 48 h to obtain a cross-linkable polymer. The purity of the five cross-linkable polymers was assessed using ^{1}H-NMR spectroscopy, [34] and the proportion of actual NSA in the cross-linkable polymers is shown in **Table 2.2**.

Table 2.2 Synthesized cross-linkable polymers, the monomer and solvent to synthesize the cross-linkable polymer, and the NSA ratio of the cross-linkable polymer.

Name of polymers	Monomer	Solvent	NSA ratio (mol%)
Poly(methyl methacrylate-*co*-NSA)	Methyl methacrylate	Toluene	2.97
Poly(methyl acrylate-*co*-NSA)	Methyl acrylate	Toluene	2.86

Poly(n-isopropyl acrylamide-*co*-NSA)	N-isopropylacrylamide	1,4-Dioxane	2.98
Poly(dimethylacrylamide-*co*-NSA)	Dimethylacrylamide	Toluene	3.46
Poly(ethyl acrylate-*co*-NSA)	Ethyl acrylate	1,4-Dioxane	3.16

2.2.4 Preparation of ion gel membranes

2.2.4.1 Single-network (SN) ion gels

To prepare the SN ion gel, 0.64 g of PVDF-HFP or cross-linkable polymer was first mixed with 9.24 g of acetone and stirred for 2 h to ensure that the polymer was completely dissolved. Subsequently, 5.12 g of IL was added to the mixture. For PVDF-HFP SN ion gel, the precursor solution was poured into the open mold directly. Additionally, to prepare a cross-linkable polymer SN ion gel, a solution consisting of 0.04 g DGBE and 1.0 g acetone was added to the mixture of cross-linkable polymer and acetone precursor solution. The solution was stirred for 5 min and then sonicated for 1 min to eliminate air bubbles and poured into an open mold. The molds were heated in an oven at 50 °C for 24 h and then transferred to a hot plate at 70 °C for 24 h of drying to obtain SN ion gels. The IL content of the SN ion gel was 80 wt%. A schematic diagram of the SN ion gel preparation process is shown in **Fig. 2.1**.

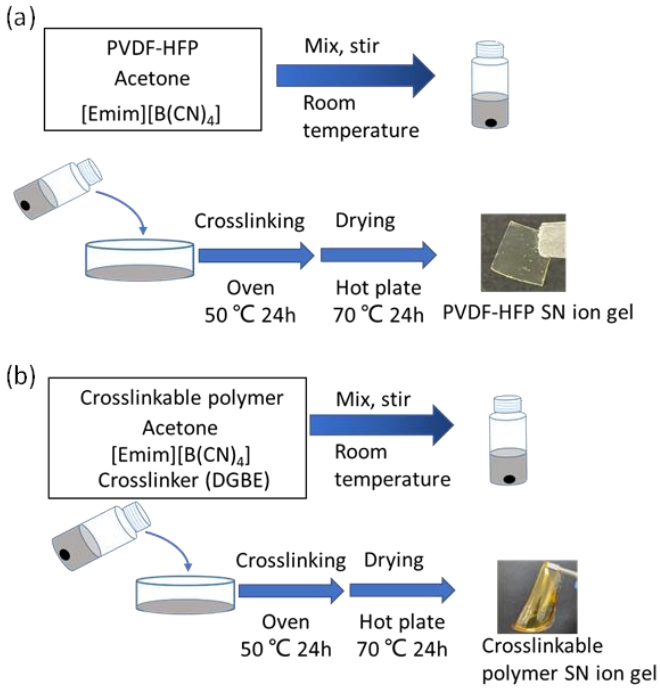

Fig. 2.1 Schematic diagrams of the preparation of (a) SN ion gel membrane composed of PVDF-HFP network and (b) SN ion gel membranes composed of cross-linkable polymer network.

2.2.4.2 Interpenetrating polymer network ion gels

PVDF-HFP/poly(EA-*co*-NSA) IPN ion gel was used as an example. First, 0.32 g of PVDF-HFP was dissolved in 4.12 g of acetone and stirred until completely dissolved. Subsequently, 0.3095 g poly(EA-*co*-NSA) was added to the PVDF-HFP solution and stirred for 30 min before 2.56 g [Emim][B(CN)$_4$], 0.0105 g DGBE, and 1.0 g acetone were added. After stirring for 10 min, the solution was sonicated for 1 min to remove air bubbles and then poured into an open mold. The mold was first heated in an oven at 50 °C for 24 h and then transferred to a hot plate at 70 °C for 24 h to evaporate the solvent to form an IPN ion gel. The [Emim][B(CN)$_4$] content in this sample was 80 wt%. The content of IL in the IPN ion gel was regulated by adjusting the mass of IL. A schematic

diagram detailing the preparation of the IPN ion gel is illustrated in **Fig. 2.2**.

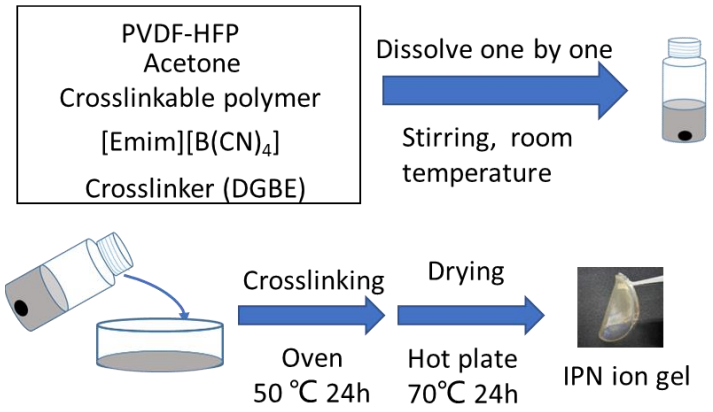

Fig. 2.2 Schematic diagram of the preparation of PVDF-HFP/cross-linkable polymer IPN ion gel membranes.

2.2.5 Characterization of ion gels

The mechanical properties of the ion gels were evaluated using a universal tester (EZ-LX, Shimadzu Co.), and the thickness of the samples was measured using a digital microscope system (Leica DMS300, Leica Microsystems Inc.). The strain rate was kept constant during ion gel stretching. The crystallinity of PVDF-HFP in the ion gels was assessed using an X-ray diffractometer (D2 PHASER, BRUKER) with a 2θ detection range of 10° to 40°. Measurements were made using Cu Kα radiation at a wavelength (λ) of 1.54 Å. In addition, the IL retention properties of the ion gels were evaluated using a universal tester (EZ-LX, Shimadzu Co.) [29]. The ion gel was compressed at 1.0 MPa for 1 min, then removed and the leaked IL on the sample surface was wiped off. The IL retention property was determined by the weight change of the ion gel before and after compression.

2.2.6 Evaluation of gas separation performance

A sweeping method was employed to assess the CO_2 separation performance of IPN ion gels. The gas permeation setup and membrane cell utilized were consistent with those previously employed by our research group [24, 29]. The schematic is shown in **Fig. 2.3**. A 50/50 mol/mol mixture of CO_2 and N_2 served as the feed gas, with a total flow rate set at 200 ml/min, while Argon was employed as the purge gas at a flow rate of 20 ml/min. The flow rate and pressure of the gases were regulated using a mass-flow controller (Hemmi Slide Rule Co., Ltd.) and a back-pressure regulator, respectively. On the permeate side, the pressure was kept at atmospheric pressure. Gas chromatography (GC-8A, Shimadzu Co.) was employed to determine the quantity of CO_2 and N_2 permeating through the membrane. Steady-state data for the gas permeation test were attained when the difference in GC peak area between adjacent measurements was less than 1%.

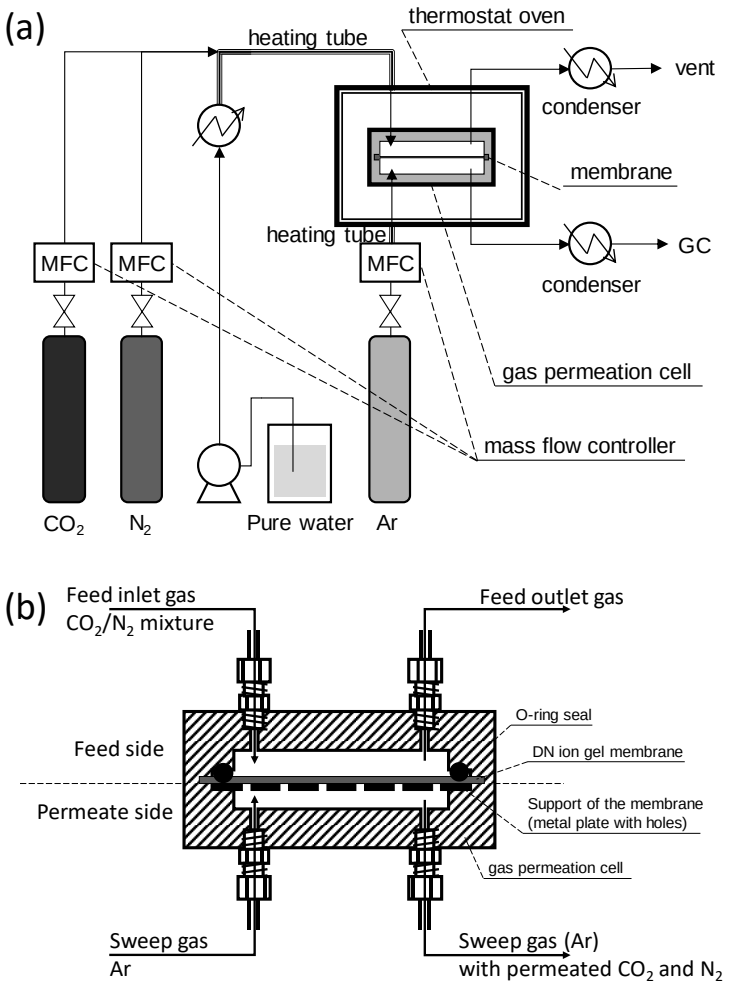

Fig. 2.3 Schematic illustrations of (a) the apparatus of the gas permeation test and (b) gas permeation cell.

2.3 Results and discussion

2.3.1 Characterization of ion gels composed of [Emim][B(CN)4], PVDF-HFP, and cross-linkable polymer

In the developed SN and IPN ion gels, the semi-crystalline polymer network was able to provide the ion gels with high mechanical strength [35-37]. Therefore, PVDF-HFP as a rigid semi-crystalline polymer can be expected to prepare ion gels with high mechanical strength. We first examined the mechanical strength of the PVDF-

HFP/[Emim][B(CN)$_4$] SN ion gel. **Fig. 2.4** shows the uniaxial and cyclic tensile stress-strain curves of PVDF-HFP SN ion gels with high fracture stress (429 kPa) at 80 wt% IL content. In **Fig. 2.4b**, the apparent hysteresis loop of the PVDF-HFP SN ion gel indicates that the PVDF-HFP network can dissipate the energy of the load. In other words, the fracture of the PVDF-HFP network contributes to the dissipation of the loading energy to provide mechanical strength to the ion gel.

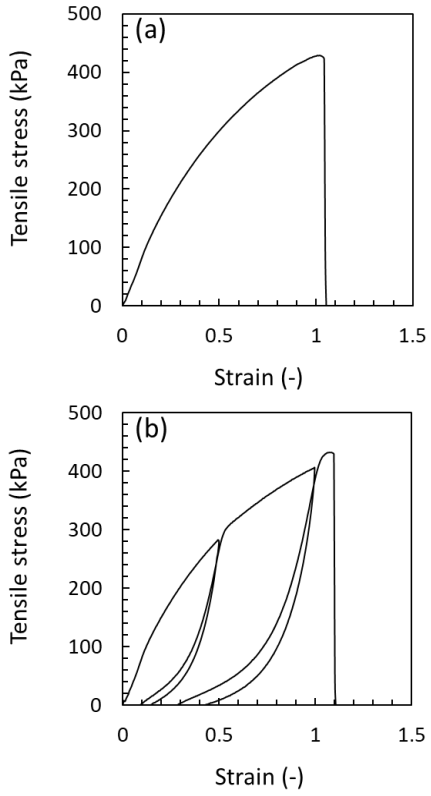

Fig. 2.4 Mechanical properties of an SN ion gel composed of 80 wt% [Emim][B(CN)$_4$] and 20 wt% PVDF-HFP network: (a) uniaxial tensile stress–strain curve, (b) cyclic tensile stress–strain curves.

To investigate the reason for the mechanical strength provided by the PVDF-HFP network, we performed XRD characterization of the PVDF-HFP SN ion gel, and the

results are shown in **Fig. 2.5**. In this figure, the PVDF crystallization peak of PVDF is evident near 20° in the PVDF-HFP SN ion gel, which indicates that the PVDF network was well formed in the PVDF-HFP SN ion gel and that the disruption of the network is conducive to the dissipation of the loading energy. However, the SN ion gels with a semi-crystalline polymer network showed poor IL retention ability [29, 38]. For ion gel membranes, high IL content is favorable for obtaining high CO_2 separation performance. Therefore, it is important to evaluate the IL retention capacity of ion gels. We evaluated the IL retention capacity of the PVDF-HFP SN ion gel. In **Fig. 2.6a**, the PVDF-HFP SN ion gel exhibits significant IL leakage, although the SN ion gel did not break when compressed at 1.0 MPa for 1 min.

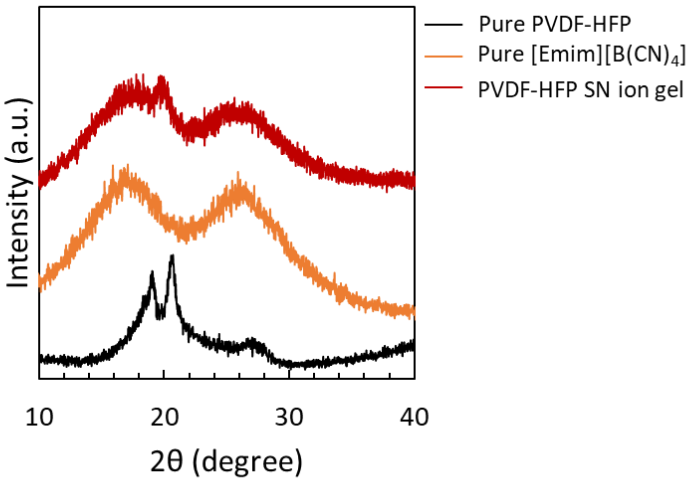

Fig. 2.5 XRD patterns of Pure PVDF-HFP, pure [Emim][$B(CN)_4$], and PVDF-HFP SN ion gel.

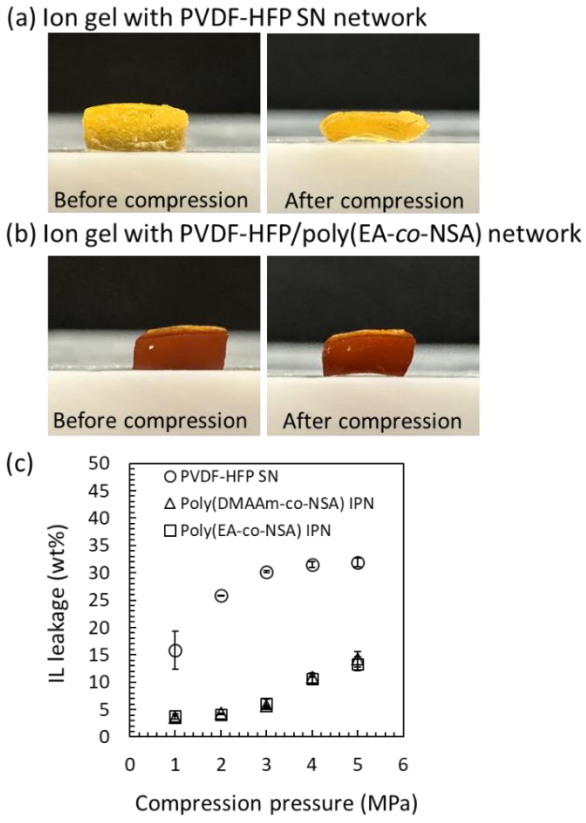

Fig. 2.6 Compressive stability of an IPN ion gel with poly(EA-*co*-NSA) as the cross-linkable polymer network: (a) photos of the SN ion gel with a PVDF-HFP network before and after compression at 1 MPa, (b) photos of the IPN ion gel with a PVDF-HFP/poly(EA-*co*-NSA) network before and after compression at 1 MPa and (c) relationship between IL leakage and applied pressure.

To enhance the IL retention of SN ion gels, we interpenetrated the cross-linkable polymer network into the SN ion gel. The cross-linkable polymer has good compatibility with the IL and is good for fabricating tough IPN ion gel membranes with high IL retention. We first conducted uniaxial and cyclic tensile tests on SN ion gels formed by various cross-linkable polymer networks and [Emim][$B(CN)_4$], with the results depicted in **Fig. 2.7**. Despite the mechanical strength of SN ion gels not very high, the successful

fabrication of cross-linkable polymer SN ion gels implied the promise of these cross-linkable polymers in enhancing the IL retention properties of PVDF-HFP SN ion gel. Subsequently, we prepared PVDF-HFP/cross-linkable polymer IPN ion gels and evaluated their IL retention properties. The results are depicted in **Figs. 2.6c** and **2.8**. In these ion gels, poly(DMAAm-*co*-NSA) and poly(EA-*co*-NSA) networks notably enhanced the IL retention properties of PVDF-HFP SN ion gels. This suggests that PDMAAm and PEA exhibit commendable compatibility with IL.

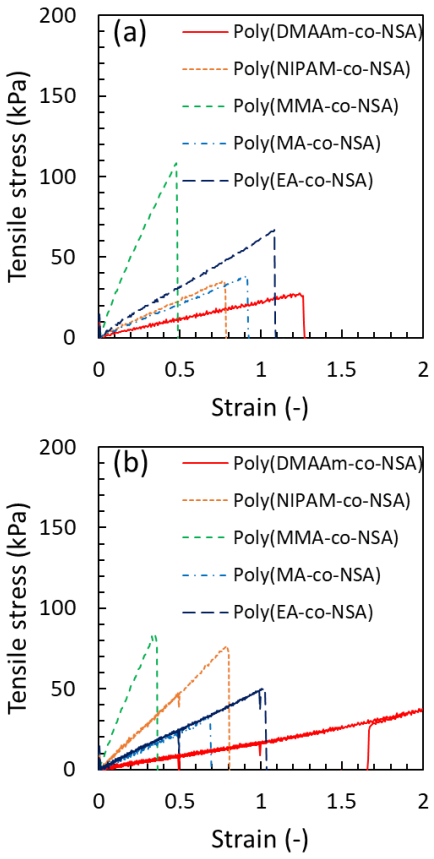

Fig. 2.7 Mechanical properties of single-network ion gels composed of 80 wt% [Emim][$B(CN)_4$] and cross-linkable polymers: (a) uniaxial tensile stress–strain curves, (b) cyclic tensile stress–strain curves.

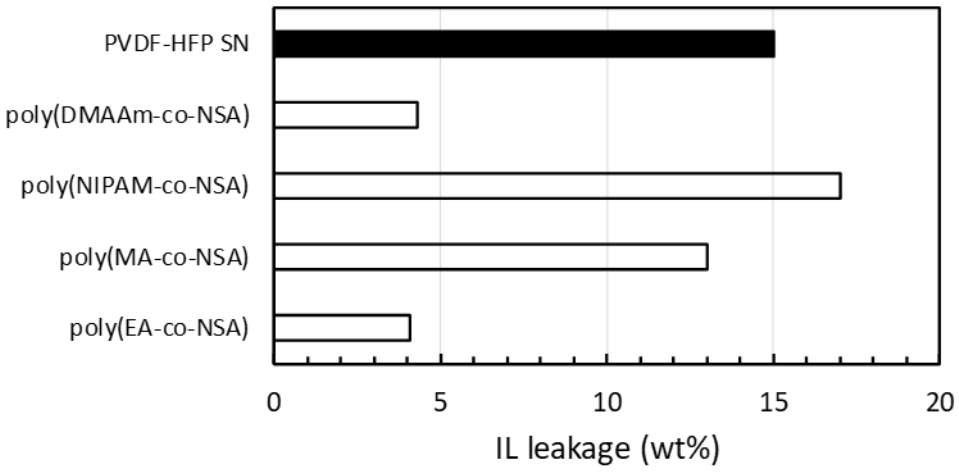

Fig. 2.8 IL-holding properties of the SN ion gel composed of a PVDF-HFP network and the IPN ion gels. The ion gel was compressed at 1.0 MPa for 1 min.

In addition to evaluating IL retention, we also assessed the mechanical strength of these IPN ion gels, with the results depicted in **Fig. 2.9**. Except for the PVDF-HFP/poly(NIPAM-*co*-NSA) IPN ion gels, which exhibited poor mechanical strength and the other IPN ion gels demonstrated good mechanical strength. Moreover, upon comparison of **Figs. 2.9a** and **2.6b**, it becomes apparent that the PVDF-HFP/poly(EA-*co*-NSA) IPN ion gels not only exhibit good mechanical strength but also display good compression resistance.

To deeply understand the toughening mechanism of IPN ion gels, we conducted XRD tests to assess the PVDF crystallinity of the prepared IPN ion gels. The XRD patterns are presented in **Fig. 2.10**. In the case of the PVDF-HFP/poly(MMA-*co*-NSA) and PVDF-HFP/poly(NIPAM-*co*-NSA) IPN ion gels, no discernible crystallization peaks of PVDF were evident near 20°. This absence suggests that these two IPN ion gels have not formed the crystalline of PVDF, consequently hindering the dissipation of energy as

sacrificial bonds and resulting in lower mechanical strength. Conversely, prominent PVDF crystallization peaks were observed in the remaining IPN ion gels, indicating the presence of enough PVDF crystalline regions to dissipate energy. This observation is further supported by the evident hysteresis lines observed in **Fig. 2.9b** for the other IPN ion gels. These findings underscore the significance of employing appropriate cross-linkable polymers to ensure that IPN ion gels with semi-crystalline polymer networks exhibit excellent IL retention and high mechanical strength.

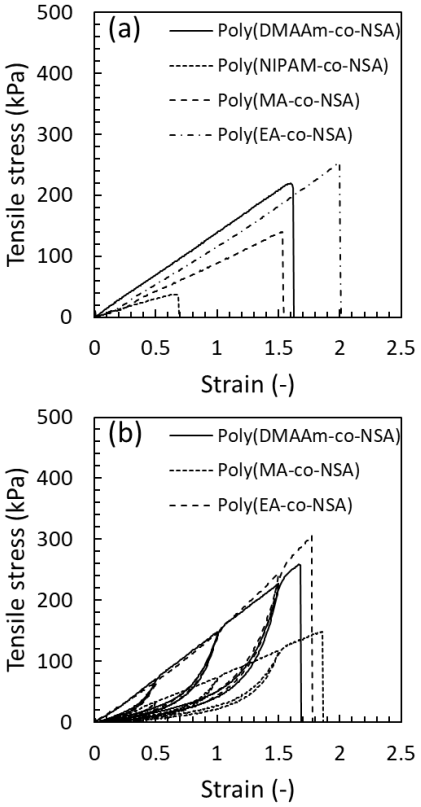

Fig. 2.9 Mechanical properties of IPN ion gels composed of 80 wt% [Emim][$B(CN)_4$] and interpenetrating PVDF-HFP/cross-linkable polymer networks: (a) uniaxial tensile stress–strain curves of IPN ion gels containing different cross-linkable polymer networks, (b) cyclic tensile stress–strain curves of IPN ion gels containing different cross-linkable polymer networks.

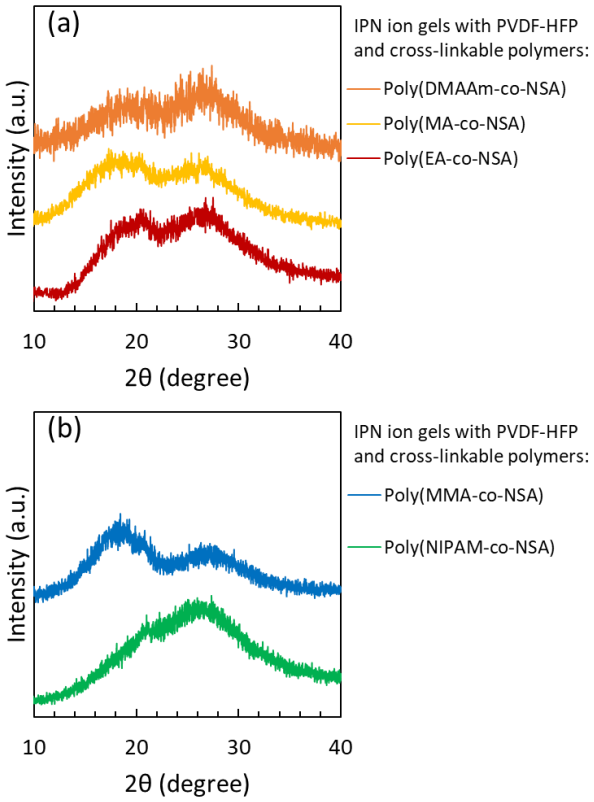

Fig. 2.10 XRD patterns of (a) IPN ion gels with PVDF-HFP/poly(DMAAm-*co*-NSA), PVDF-HFP/poly(MA-*co*-NSA), and PVDF-HFP/poly(EA-*co*-NSA) networks; and (b) IPN ion gels with PVDF-HFP/poly(MMA-*co*-NSA) and PVDF-HFP/poly(NIPAM-*co*-NSA) networks.

2.3.2 CO_2 permeation property of an IPN ion gel membrane containing [Emim][B(CN)$_4$]

IPN ion gels with the PVDF-HFP/poly(EA-*co*-NSA) network exhibit high mechanical strength and good IL retention properties. Hence, in this study, IPN ion gels prepared with the PVDF-HFP/poly(EA-*co*-NSA) network and [Emim][B(CN)$_4$] were selected for testing the CO_2 permeation properties.

As previously mentioned, the PVDF-HFP/poly(EA-*co*-NSA) IPN ion gel demonstrated exceptional pressure resistance. Therefore, this study first assessed the pressure resistance of IPN ion gels with varying [Emim][B(CN)$_4$] contents. We analyzed the CO_2 permeability and CO_2/N_2 permselectivity of IPN ion gels with different IL contents across various transmembrane pressure differences. The results are depicted in **Fig. 2.11**. At an IL content of 80 wt%, the IPN ion gels maintained stable CO_2/N_2 permselectivity even at a transmembrane pressure difference of 250 kPa. Although rupture occurred in this IPN ion gel at a transmembrane pressure difference of 300 kPa. It is noteworthy that in practical applications, due to the membrane material being sealed within the membrane module, there exists a CO_2 partial pressure difference between the feed gas and the permeate gas during permeate gas handling. Therefore, CO_2 separation membranes are required to possess a pressure resistance of at least 100 kPa. Therefore, the pressure resistance demonstrated by the PVDF-HFP/poly(EA-*co*-NSA) IPN ion gel containing 80 wt% IL is deemed sufficient to fulfill this criterion.

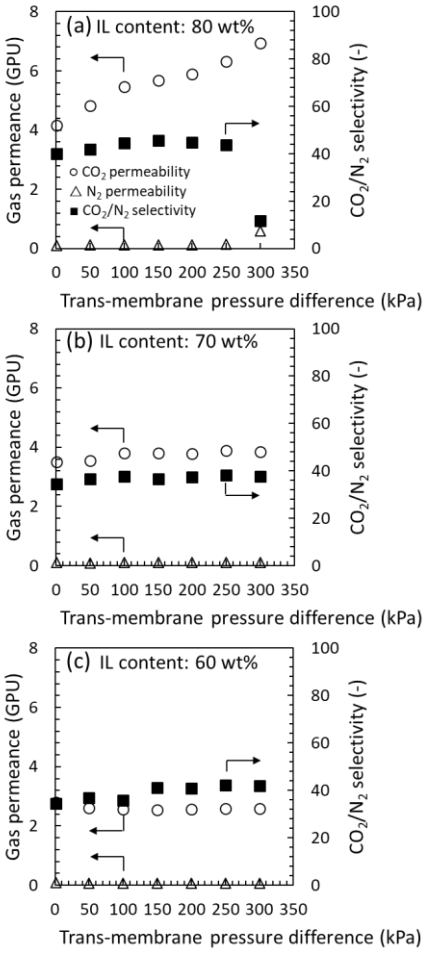

Fig. 2.11 Pressure resistance of IPN ion gel membranes with different IL contents: (a) 80 wt%, (b) 70 wt%, and (c) 60 wt%. The gas permeability was evaluated using a 50/50 mol/mol CO_2/N_2 mixed gas at 30 °C under dry conditions.

Furthermore, we observed an unexpected increase in the CO_2 permeability of IPN ion gel membranes with higher IL content as the transmembrane pressure difference increased. Generally, the CO_2 permeability of ion gel membranes remains unaffected by changes in the transmembrane pressure difference. This is because the adsorption of CO_2 by [Emim][$B(CN)_4$] follows Henry's law ([39-41]) and the gas permeation mechanism of ion gels adheres to the solution-diffusion principle [42-45]. There is no dependence of

CO_2 permeability and transmembrane pressure difference of ion gels.

However, the observed increase in CO_2 permeability of the IPN ion gels devised in this study with escalating feed gas pressure was unexpected. One possible explanation for this phenomenon is the variation in the thickness of IPN ion gels with high IL content under different transmembrane pressure differences. We compared Young's modulus of IPN ion gel membranes with varying IL contents, and the results are illustrated in **Fig. 2.12**. The Young's modulus of the IPN ion gel membrane containing 80 wt% IL was less than 100 kPa, indicating it is soft. This softness could potentially reduce the membrane thickness under pressurized conditions, thereby increasing the CO_2 permeability of the ion gel membrane with high IL content as the transmembrane pressure difference rises. In contrast, the CO_2 permeability of the IPN ion gel with 60 wt% IL remained unaffected by changes in the transmembrane pressure difference. This is attributed to the high Young's modulus of the ion gel with low IL content, rendering the membrane more rigid and less susceptible to thickness reduction with changes in the transmembrane pressure difference. These findings suggest that ion gel membranes with high IL content are also viable for practical applications.

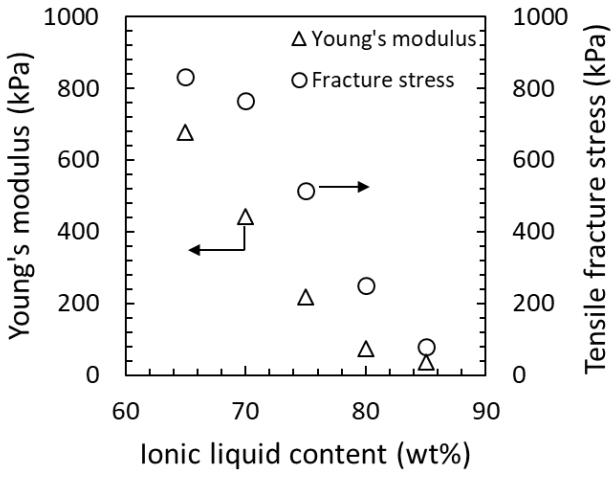

Fig. 2.12 Young's modulus and tensile fracture stress of IPN ion gel membranes with different IL contents.

Subsequently, we explored the impact of temperature on the CO_2 permeability and CO_2/N_2 permselectivity of IPN ion gels containing 80 wt% [Emim][$B(CN)_4$]. It has been noted that the CO_2/N_2 permselectivity should exceed 20 for CO_2 separation membranes employed in capturing CO_2 from the exhaust gas of coal-fired power plants [46]. Most CO_2 capture technologies focus on treating the flue gas post-desulfurization, where the temperature is typically around 50 °C [46]. Hence, the CO_2/N_2 permselectivity of separation membranes utilized for CO_2 treatment should ideally surpass 20 at 50 °C. **Fig. 2.13** depicts the temperature dependence of gas permeabilities and the CO_2/N_2 permselectivity of the designed IPN ion gel. The findings align closely with previous reports [47, 48]. As temperature rises, CO_2 permeability increases while CO_2/N_2 permselectivity decreases [48-50]. This behavior can be attributed to the gas permeation of polymeric membranes following a solution-diffusion mechanism.

This behavior can be attributed to the gas permeation of polymeric membranes following a solution-diffusion mechanism. The gas permeability (P)(mol·m/(m^2·s·Pa)) can be expressed as the product of the diffusion coefficient (D) (m^2/s) and the solubility coefficient (S) (mol /(m^3·Pa)).

$$P = D \cdot S \tag{1}$$

Moreover, the temperature dependence of D and S can be described by the Arrhenius equation and the Van't Hoff relationship.

$$\mathrm{D} = D_0 \exp\left(-\frac{E_D}{RT}\right) \tag{2}$$

$$\mathrm{S} = S_0 \exp\left(-\frac{\Delta H_s}{RT}\right) \tag{3}$$

where D_0 and S_0 are pre-exponential factors, R denotes the gas constant, and T signifies the temperature. E_D (kJ/mol) and ΔH_s (kJ/mol) are the activation energy of gas diffusion and the partial molar enthalpy of gas absorption, respectively. Combining Equations (1) through (3), the gas permeability can be expressed with E_D and ΔH_s as follows:

$$l_n P = l_n(D \cdot S) = l_n(D_0 \cdot S_0) - \frac{E_D + \Delta H_s}{RT} \quad (4)$$

Gas adsorption is indeed an exothermic process, with ΔHs being negative. As the absolute value of ΔHs is smaller than E_D, i.e. the $E_D + \Delta Hs > 0$, the gas permeabilities increase when the temperature increases [48]. Because the N_2 is more temperature-sensitive than CO_2, the increase in N_2 permeability higher than CO_2, resulting in a decrease in the selectivity of CO_2/N_2 with rising temperature. Despite this, the IPN ion gel developed in this study exhibits a CO_2/N_2 selectivity of approximately 30 at 50 °C, indicating its potential for capturing CO_2 from coal combustion flue gas.

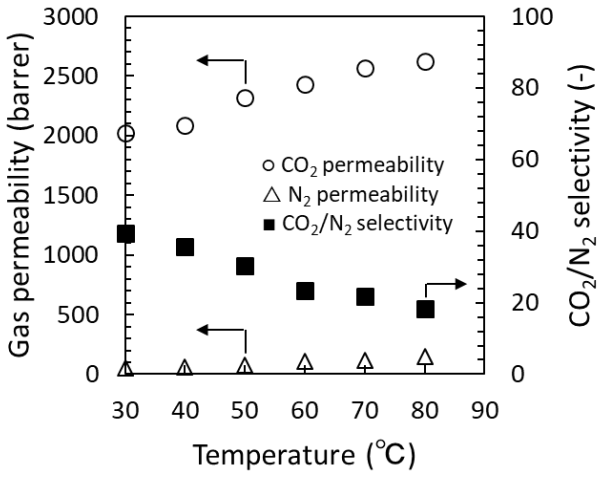

Fig. 2.13 Temperature dependence of the gas permeabilities and CO_2/N_2 selectivity of the IPN ion gel membrane containing 80 wt% [Emim][$B(CN)_4$]. The gas permeability was evaluated using a 50/50 mol/mol CO_2/N_2 mixed gas under dry and atmospheric pressure conditions.

It has been noted in previous studies that an increase in the IL content of ion gel membranes leads to a corresponding increase in CO_2 permeability [24]. Hence, we evaluated the impact of IL content on CO_2 permeability and CO_2/N_2 selectivity. The results are illustrated in **Fig. 2.14**. It shows that the CO_2 permeability and CO_2/N_2 selectivity of the developed IPN ion gel membranes far exceed those of IPN ion gel membranes containing [Emim][Tf_2N] as previously designed by our group. This enhancement can be attributed to the exceptional CO_2 solubility, low viscosity, and high CO_2/N_2 solubility selectivity offered by [Emim][$B(CN)_4$]. Moreover, at an [Emim][$B(CN)_4$] content of 85 wt%, the CO_2 permeability reaches 2243 barrer with a CO_2/N_2 permselectivity of 43. This performance is over that of other IL-based CO_2 separation membranes and near the upper limits of the Robeson bound, as depicted in **Fig. 2.15**. Therefore, the IPN ion gel designed in this study has great potential to separate CO_2.

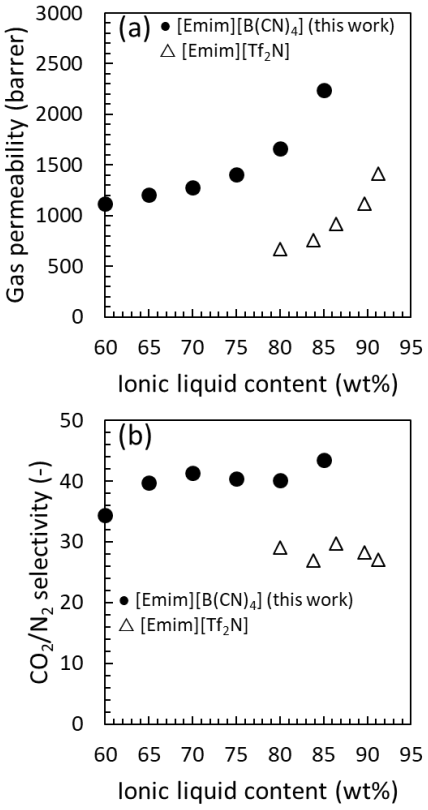

Fig. 2.14 Effect of IL content on the (a) CO_2 permeability and (b) CO_2/N_2 selectivity of tough ion gel membranes. [24] The cross-linkable polymer network of the IPN ion gel membrane with [Emim][$B(CN)_4$] is poly(EA-*co*-NSA). The gel network of the tough ion gel membranes containing [Emim][Tf_2N] is PVDF-HFP/poly(DMAAm-*co*-NSA) IPN.

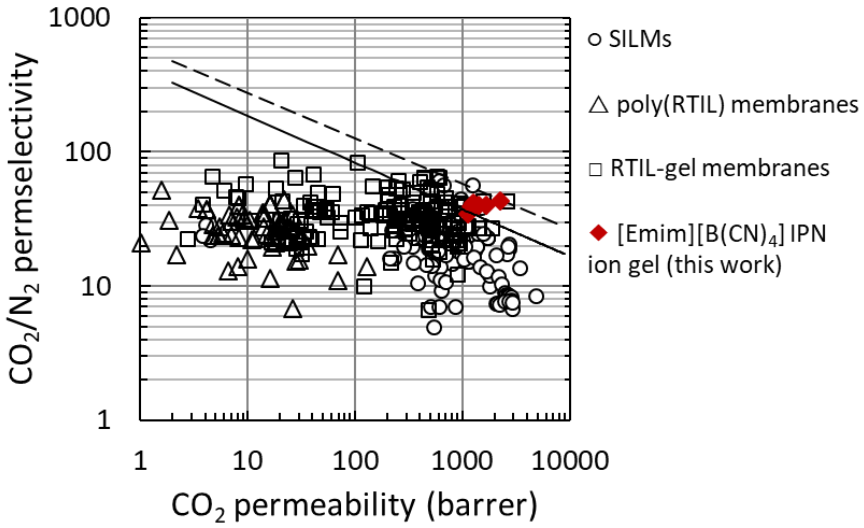

Fig. 2.15 Comparison of the CO_2 separation performance of the developed IPN ion gel membrane containing [Emim][$B(CN)_4$] and previously reported IL-based membranes. The solid and broken straight lines are the upper bounds of polymer membranes reported in 2008 and 2019, respectively [51, 52].

As mentioned in the previous part, glassy polymer membranes, exemplified by PIM, are recognized as promising materials for high-performance CO_2 separation membranes owing to their high CO_2 permeability. However, a notable drawback is their tendency for CO_2 permeability to decrease over time [5, 6, 53-55]. To assess the long-term stability of the IPN ion gel membranes fabricated in this study, we conducted long-term stability on IPN ion gel membranes with 80 wt% IL content. As depicted in **Fig. 2.16**, the CO_2 permeability of the IPN ion gel membranes exhibited no signs of decline during extended operation periods. This can be attributed to the inherent flexibility of the ion gel membrane, which effectively prevents physical aging and is a characteristic that sets IPN ion gel membranes apart from glassy polymer membranes.

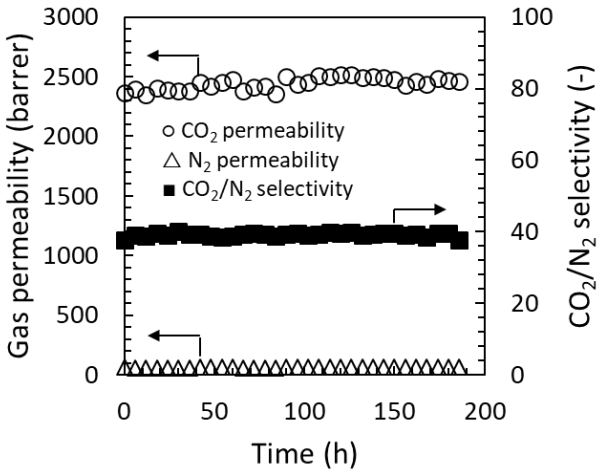

Fig. 2.16 Long-term stability during the gas permeation process of the IPN ion gel membrane with the IL content of 85 wt%. The gas permeability was evaluated using a 50/50 mol/mol CO_2/N_2 mixed gas at 30 °C under dry and atmospheric pressure conditions.

In conclusion, considering the CO_2 separation performance and long-term stability under elevated pressure and temperature conditions, IPN ion gels composed of cross-linkable polymer and semi-crystalline polymer networks, emerge as promising candidates for high-performance CO_2 separation membrane materials.

2.4 Conclusions

In this study, we successfully designed a tough IPN ion gel membrane composed of PVDF-HFP, poly(EA-*co*-NSA), and [Emim][$B(CN)_4$]. The good compatibility between the semi-crystalline polymer PVDF-HFP network and the poly(EA-*co*-NSA) network with [Emim][$B(CN)_4$], thereby providing the ion gel with superior mechanical strength and IL retention properties. These attributes endowed the IPN ion gels with exceptional CO_2 separation performance, even under varying pressure and high-temperature

conditions. Notably, the IPN ion gel membranes attained an impressive IL content of 85 wt%, a CO_2 permeability of 2400 barrer, and a CO_2/N_2 permselectivity of 40. Moreover, the CO_2 permeability remained consistent even after 200 h of testing. In summary, the developed PVDF-HFP/poly(EA-*co*-NSA) IPN ion gel stands poised as a highly promising CO_2 separation membrane material, well-suited for applications in carbon capture.

References

[1] D.J. Soeder, Fossil Fuels and Climate Change, Cham, 2021, 155-185

[2] K.O. Yoro, M.O. Daramola, Chapter 1-CO_2 emission sources, greenhouse gases, and the global warming effect, 2020, 3-28

[3] S. Bandehali, A.E. Amooghin, H. Sanaeepur, et al., Polymers of intrinsic microporosity and thermally rearranged polymer membranes for highly efficient gas separation, Separation and Purification Technology, 278, 2021, 119513.

[4] L.M. Robeson, M.E. Dose, B.D. Freeman, D.R. Paul, Analysis of the transport properties of thermally rearranged (TR) polymers and polymers of intrinsic microporosity (PIM) relative to upper bound performance, Journal of Membrane Science, 525, 2017, 18-24.

[5] M.M. Merrick, R. Sujanani, B.D. Freeman, Glassy polymers: Historical findings, membrane applications, and unresolved questions regarding physical aging, Polymer, 211, 2020, 123176.

[6] Z.X. Low, P.M. Budd, N.B. McKeown, D.A. Patterson, Gas permeation properties, physical aging, and its mitigation in high free volume glassy polymers, Chemical reviews, 118(12), 2018, 5871-5911.

[7] M. Sadrzadeh, E. Saljoughi, K. Shahidi, T. Mohammadi, Preparation and characterization of a composite PDMS membrane on CA support, Polymers for Advanced Technologies, 21(8), 2010, 568-577.

[8] M. Sadrzadeh, M. Amirilargani, K. Shahidi, T. Mohammadi, Pure and mixed gas permeation through a composite polydimethylsiloxane membrane, Polymers for Advanced Technologies, 22(5), 2011, 586-597.

[9] G.L. Zhuang, C.F. Wu, M.Y. Wey, H.H. Tseng, Impacts of green synthesis process on

asymmetric hybrid PDMS membrane for efficient CO_2/N_2 separation, Membranes, 11(1), 2021, 9.

[10] Z. Dai, R.D. Noble, D.L. Gin, et al., Combination of ionic liquids with membrane technology: A new approach for CO_2 separation, Journal of Membrane Science, 497, 2016, 1-20.

[11] R. Couto, L. Neves, P. Simões, I. Coelhoso, Supported ionic liquid membranes and ion-jelly® membranes with [BMIM][DCA]: comparison of its performance for CO_2 separation, Membranes, 5(1), 2015, 13-21.

[12] P. Scovazzo, J. Kieft, D.A. Finan, et al., Gas separations using non-hexafluorophosphate [PF6]−anion supported ionic liquid membranes, Journal of Membrane Science, 238(1), 2004, 57-63.

[13] P. Luis, L. Neves, C. Afonso, et al., Facilitated transport of CO_2 and SO_2 through supported ionic liquid membranes (SILMs), Desalination, 245(1-3), 2009, 485-493.

[14] L. Neves, N. Nemestóthy, V. Alves, et al., Separation of biohydrogen by supported ionic liquid membranes, Desalination, 240(1-3), 2009, 311-315.

[15] B.S. Ghanem, R. Swaidan, X. Ma, et al., Energy-efficient hydrogen separation by AB-type ladder-polymer molecular sieves, Advanced Materials, 26(39), 2014, 6696-6700.

[16] S. Kim, H.J. Jo, Y.M. Lee, Sorption and transport of small gas molecules in thermally rearranged (TR) polybenzoxazole membranes based on 2, 2-bis (3-amino-4-hydroxyphenyl)-hexafluoropropane (bisAPAF) and 4, 4′-hexafluoroisopropylidene diphthalic anhydride (6FDA), Journal of Membrane Science, 441, 2013, 1-8.

[17] C. Moya, J. Palomar, M. Gonzalez Miquel, et al., Diffusion coefficients of CO_2 in ionic liquids estimated by gravimetry, Industrial & Engineering Chemistry Research, 53(35), 2014, 13782-13789.

[18] S.G. Kazarian, B.J. Briscoe, T. Welton, Combining ionic liquids and supercritical fluids: ATR-IR study of CO_2 dissolved in two ionic liquids at high pressures, Chemical Communications, (20), 2000, 2047-2048.

[19] C.P. Fredlake, J.M. Crosthwaite, D.G. Hert, et al., Thermophysical properties of imidazolium-based ionic liquids, Journal of Chemical & Engineering Data, 49(4), 2004, 954-964.

[20] T. Makino, M. Kanakubo, T. Umecky, CO_2 solubilities in ammonium bis(trifluoromethanesulfonyl)amide ionic liquids: Effects of ester and ether groups, Journal of Chemical & Engineering Data, 59(5), 2014, 1435-1440.

[21] R. Babarao, S. Dai, D. Jiang, Understanding the high solubility of CO_2 in an ionic liquid with the tetracyanoborate anion, The Journal of Physical Chemistry B, 115(32), 2011, 9789-9794.

[22] H. Liu, S. Dai, D. Jiang, Structure and dynamics of CO_2 and N_2 in a tetracyanoborate based ionic liquid, Physical Chemistry Chemical Physics, 16(5), 2014, 1909-1913.

[23] S.M. Mahurin, P.C. Hillesheim, J.S. Yeary, et al., High CO_2 solubility, permeability and selectivity in ionic liquids with the tetracyanoborate anion, RSC Advances, 2(31), 2012, 11813-11819.

[24] E. Kamio, M. Minakata, Y. Iida, et al., Inorganic/organic double-network ion gel membrane with a high ionic liquid content for CO_2 separation, Polymer Journal, 53(1), 2021, 137-147.

[25] T. Matsunaga, T. Sakai, Y. Akagi, et al., Structure characterization of tetra-PEG gel by small-angle neutron scattering, Macromolecules, 42(4), 2009, 1344-1351.

[26] E. Kamio, T. Yasui, Y. Iida, et al., Inorganic/organic double-network gels containing ionic liquids, Advanced Materials, 29(47), 2017, 1704118.

[27] F. Moghadam, E. Kamio, H. Matsuyama, High CO_2 separation performance of amino acid ionic liquid-based double network ion gel membranes in low CO_2 concentration gas mixtures under humid conditions, Journal of Membrane Science, 525, 2017, 290-297.

[28] Y. Gu, E.L. Cussler, T.P. Lodge, ABA-triblock copolymer ion gels for CO_2 separation applications, Journal of Membrane Science, 423-424, 2012, 20-26.

[29] J. Zhang, E. Kamio, A. Matsuoka, et al., Novel tough ion-gel-based CO_2 separation membrane with interpenetrating polymer network composed of semicrystalline and cross-linkable polymers, Industrial & Engineering Chemistry Research, 61(13), 2022, 4648-4658.

[30] F. Moghadam, E. Kamio, A. Yoshizumi, H. Matsuyama, An amino acid ionic liquid-based tough ion gel membrane for CO_2 capture, Chemical Communications, 51(71), 2015, 13658-13661.

[31] E. Kamio, M. Minakata, H. Nakamura, et al., Tough ion gels composed of coordinatively crosslinked polymer networks using ZIF-8 nanoparticles as multifunctional crosslinkers, Soft Matter, 18(25), 2022, 4725-4736.

[32] F. Moghadam, E. Kamio, T. Yoshioka, H. Matsuyama, New approach for the fabrication of double-network ion-gel membranes with high CO_2/N_2 separation performance based on facilitated transport, Journal of Membrane Science, 530, 2017, 166-175.

[33] T. Ueki, M. Watanabe, Polymers in ionic liquids: dawn of neoteric solvents and innovative materials, Bulletin of the Chemical Society of Japan, 85(1), 2012, 33-50.

[34] E. Kamio, M. Kinoshita, T. Yasui, et al., Preparation of inorganic/organic double-network ion gels using a cross-linkable polymer in an open system, Macromolecules, 53(19), 2020, 8529-8538.

[35] P.J. Driest, D.J. Dijkstra, D. Stamatialis, D.W. Grijpma, Structure-property relations in semi-crystalline combinatorial poly(urethane-isocyanurate)-type hydrogels, Polymer International, 71(9), 2022, 1055-1061.

[36] A. Perez, E. Kynaston, C. Lindsay, N. Ballard, Designed incorporation of semi-crystalline domains into structured latex particles via solvent-aided emulsion polymerization, Polymer Chemistry, 13(39), 2022, 5636-5646.

[37] H.Z. Chen, P. Li, T. S. Chung, PVDF/ionic liquid polymer blends with superior separation performance for removing CO_2 from hydrogen and flue gas, International Journal of Hydrogen Energy, 37(16), 2012, 11796-11804.

[38] Z. Chen, Q. Gui, Y. Wang, Dynamic chemistry in ionic liquid-based conductor, Green Chemical Engineering, 2(4), 2021, 346-358.

[39] S.M. Mahurin, P.C. Hillesheim, J.S. Yeary, et al., High CO_2 solubility, permeability and selectivity in ionic liquids with the tetracyanoborate anion, RSC advances, 2(31), 2012, 11813-11819.

[40] A.J. Silveira, S. Pereda, F.W. Tavares, C.R.A. Abreu, A molecular dynamics study of the solvation of carbon dioxide and other compounds in the ionic liquids [emim][$B(CN)_4$] and [emim][NTf_2], Fluid Phase Equilibria, 491, 2019, 1-11.

[41] H. Liu, S. Dai, D. Jiang, Molecular Dynamics simulation of anion effect on solubility, diffusivity, and permeability of carbon dioxide in ionic liquids, Industrial & Engineering Chemistry Research, 53(25), 2014, 10485-10490.

[42] S. Kasahara, E. Kamio, R. Minami, H. Matsuyama, A facilitated transport ion-gel membrane for propylene/propane separation using silver ion as a carrier, Journal of Membrane Science, 431, 2013, 121-130.

[43] P. Bernardo, J.C. Jansen, F. Bazzarelli, et al., Gas transport properties of

Pebax®/room temperature ionic liquid gel membranes, Separation and Purification Technology, 97, 2012, 73-82.

[44] H.J. Min, Y.J. Kim, M. Kang, et al., Crystalline elastomeric block copolymer/ionic liquid membranes with enhanced mechanical strength and gas separation properties, Journal of Membrane Science, 660, 2022, 120837.

[45] X. Yan, S. Anguille, M. Bendahan, P. Moulin, Ionic liquids combined with membrane separation processes: A review, Separation and Purification Technology, 222, 2019, 230-253.

[46] T.C. Merkel, H. Lin, X. Wei, R. Baker, Power plant post-combustion carbon dioxide capture: An opportunity for membranes, Journal of Membrane Science, 359(1), 2010, 126-139.

[47] J. Zhang, E. Kamio, A. Matsuoka, et al., Development of a micro-double-network ion gel-based CO_2 separation membrane from nonvolatile network precursors, Industrial & Engineering Chemistry Research, 60(34), 2021, 12640-12649.

[48] C. Zhang, W. Zhang, H. Gao, et al., Synthesis and gas transport properties of poly(ionic liquid) based semi-interpenetrating polymer network membranes for CO_2/N_2 separation, Journal of Membrane Science, 528, 2017, 72-81.

[49] A. Alentiev, Y. Yampolskii, Correlation of Gas Permeability and diffusivity with selectivity: orientations of the clouds of the data points and the effects of temperature, Industrial & Engineering Chemistry Research, 52(26), 2013, 8864-8874.

[50] B.W. Rowe, L.M. Robeson, B.D. Freeman, D.R. Paul, Influence of temperature on the upper bound: Theoretical considerations and comparison with experimental results, Journal of Membrane Science, 360(1), 2010, 58-69.

[51] L.M. Robeson, The upper bound revisited, Journal of Membrane Science, 320(1),

2008, 390-400.

[52] B. Comesaña-Gándara, J. Chen, C.G. Bezzu, et al., Redefining the Robeson upper bounds for CO_2/CH_4 and CO_2/N_2 separations using a series of ultrapermeable benzotriptycene-based polymers of intrinsic microporosity, Energy & Environmental Science, 12(9), 2019, 2733-2740.

[53] B.W. Rowe, B.D. Freeman, D.R. Paul, Influence of previous history on physical aging in thin glassy polymer films as gas separation membranes, Polymer, 51(16), 2010, 3784-3792.

[54] A.A. Shamsabadi, R.M. Behbahani, F. Seidi, M. Soroush, Physical aging of polyetherimide membranes, Journal of Natural Gas Science and Engineering, 27, 2015, 651-660.

[55] P. Bernardo, F. Bazzarelli, F. Tasselli, et al., Effect of physical aging on the gas transport and sorption in PIM-1 membranes, Polymer, 113, 2017, 283-294.

Chapter 3

Development of a double-network ion gel membrane composed of a CO_2-philic ionic liquid, semi-crystalline polymer network, and tetra-armed polyethylene glycol network

3.1 Introduction

Exhaust gases from fossil fuel combustion are the main source of CO_2. To reduce the concentration of CO_2 in the atmosphere, we need to capture CO_2 from the flue gases emitted from power plants [1, 2]. Membrane separation technology has attracted much attention because of its low energy consumption and high separation efficiency [3, 4]. Polymer membranes, as the longest studied CO_2 separation membranes, the most prominent issue is the trade-off between gas permeability and gas selectivity [5-7]. In this regard, researchers have developed new types of CO_2 separation membranes to break through the upper limit of CO_2 separation performance [8-11]. However, among these polymer membranes, CO_2 permeability and CO_2/N_2 selectivity of glassy polymer membranes have reduced at high temperatures and humid environments [12-16]. In addition, some rubbery polymer membranes have a CO_2/N_2 selectivity of less than 20 at high temperatures, which is not enough to meet the requirements of practical CO_2 separation [17].

IL-based gel membranes, called ion gel membranes, have emerged as a good IL-

based membrane material [10, 11, 18, 19]. Tough ion gel membranes with higher IL content show high CO_2 permeability and maintain CO_2/N_2 selectivity. As a result, ion gel membranes with high IL content stand out as strong contenders for high-performance CO_2 separation membranes specifically designed to capture CO_2 from flue gas. However, ion gel membranes with high IL content still encounter a major problem of poor mechanical strength. To solve this issue, various types of tough ion gels have been developed [20-27].

One famous example is the double-network (DN) ion gel, which interpenetrates with two polymer networks [21, 27-32]. The first network in the DN gel is rigid and brittle, serving as a sacrificial bond to dissipate energy. Conversely, the second network is soft and highly ductile, referred to as the "hidden length," and does not very easily break even under large deformation. The combined action of these two networks gives the DN gel excellent mechanical strength. The crystal structure of the semi-crystalline polymer in tough ion gel membranes helps dissipate applied load energy and acts as cross-linking points in the gel network [33-35]. However, the IL retention of SN ion gels is poor due to their limited compatibility with IL. To address this issue, as discussed earlier, we improved the IL retention of ion gels by interpenetrating another polymer with superior IL compatibility [18, 24, 36]. Nonetheless, this can harm the mechanical strength of the ion gel. Drawing inspiration from the toughening mechanism in DN gels, the semi-crystalline polymer network can serve as the first polymer network, functioning as a sacrificial bond, thereby imparting toughness to the ion gel when applied load energy. In addition, introducing another IL-philic ductile polymer network to interpenetrate with the semi-crystalline polymer network, not only can increase the IL retention properties but also the mechanical strength of the SN ion gels can be improved. Therefore, the second polymer network should have high stretchability and high affinity for CO_2.

The 1-ethyl-3-methylimidazolium tricyanomethanide ([Emim][$C(CN)_3$]) has been selected due to its reported high CO_2 solubility and low viscosity, making it an ideal choice as the IL for the ion gel membranes designed in this study [37]. In addition, polyethylene glycol (PEG) has demonstrated excellent compatibility with [Emim][$C(CN)_3$] [38], and ion gels based on tetra-PEG networks comprising various PEG functional groups have exhibited exceptional ductility, thereby fulfilling the requisite characteristics of the hidden length of ion gels [39]. Moreover, as demonstrated previously, semi-crystalline polymers can serve as sacrificial bonds. Pebax 1657, a commercially available polymer composed of polyamide blocks (PA) and PEG blocks, is known for its brittleness [40-43]. For Pebax 1657, the polyamide blocks form a crystalline structure capable of acting as cross-linking points in the gel network and dissipating loading energy [18, 24, 36]. Therefore, this study focuses on the development of tough DN ion gel membranes composed of [Emim][$C(CN)_3$], Pebax 1657, and tetra-PEG, with a particular emphasis on their mechanical properties and toughening mechanisms. Additionally, the influence of temperature, humidity, and IL content on the CO_2 separation performances of the ion gels was evaluated.

3.2 Experimental

3.2.1 Materials

[Emim][$C(CN)_3$], obtained from Tokyo Chemical Industry Co., Ltd., was used as received without further purification. For the fabrication of the tetra-PEG network, we utilized precursors including 4-arm PEG with thiol termini (tetra-PEG-SH) and 4-arm polyethylene glycol with maleimide termini (tetra-PEG-MA), both procured from YUKA SANGYO Co. Ltd. The molecular weights of tetra-PEG-SH and tetra-PEG-MA were 20

kg/mol and 40 kg/mol, respectively. These tetra-PEG precursors were dissolved in acetonitrile (FUJIFILM Wako Pure Chemical Co). Furthermore, we employed 2-methylimidazole, sourced from Sigma-Aldrich Co., as received to expedite the Michael addition reaction. Pebax 1657, the first polymer network, was purchased from Arkema Inc.

To know the enhancement in mechanical strength attributed to the stretchable hidden length, poly(DMAAm-*co*-NSA) was employed as the second polymer network, facilitating comparative analysis of the mechanical strengths of prepared ion gels. Poly(DMAAm-*co*-NSA) synthesis was conducted through free-radical polymerization utilizing dimethyl acrylamide (DMAAm) and N-succinimidyl acrylate (NSA) monomers, with azobisisobutyronitrile (FUJIFILM Wako Pure Chemical Co.) serving as a radical initiator [18]. The monomers, sourced from Sigma-Aldrich, were used as received. Super-dehydrated 1,4-dioxane (FUJIFILM Wako Pure Chemical Co.) as the solvent. Purification of the synthesized poly(DMAAm-*co*-NSA) via precipitation was conducted using tetrahydrofuran and *n*-hexane as good and poor solvents, respectively procured from FUJIFILM Wako Pure Chemical Industries Ltd. For establishing a poly(DMAAm-*co*-NSA) network, diethylene glycol bis(3-aminopropyl) ether (DGBE, Tokyo Chemical Industry Co. Ltd.) was utilized as the crosslinker, employed as received.

3.2.2 Preparation of ion gel membranes

In this study, we fabricated five ion gel membranes: Pebax 1657 SN ion gel, tetra-PEG SN ion gel, poly(DMAAm-*co*-NSA) SN ion gel, Pebax 1657/poly(DMAAm-*co*-NSA) IPN ion gel, and Pebax 1657/tetra-PEG IPN ion gel, alongside two polymer membranes: Pebax 1657 and tetra-PEG. Below are the detailed preparation methods.

3.2.2.1 Pebax 1657 SN ion gel

First, the Pebax 1657 solution was prepared by adding Pebax 1657 particles at a concentration of 10 wt% to an ethanol/water (75/25 wt%) mixture. The mixture was then heated and stirred in an oil bath at 100 °C under reflux condensation until completely dissolved. Subsequently, 2.0 g of [Emim][C(CN)$_3$] was mixed with the Pebax 1657 solution (5.0 g), stirred for 5 min, sonicated for 1 min to remove air bubbles, and then poured into an open mold. The solution was dried in an oven at 30 °C for 24 h. Afterward, the gel was extracted from the mold and dried on a hot plate at 70 °C for 24 h. **Fig. 3.1** shows a schematic of the preparation method of Pebax 1657 SN ion gel. The [Emim][C(CN)$_3$] content in the Pebax 1657 SN ion gels was adjusted within the range of 0-80 wt%.

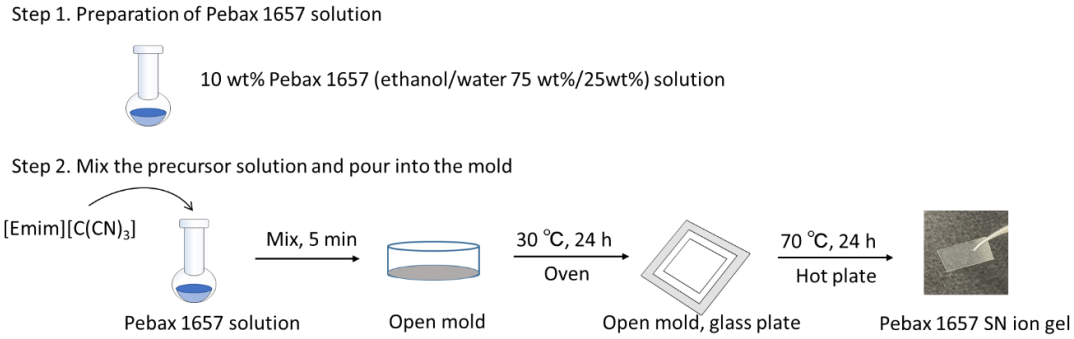

Fig. 3.1 Schematic representation of the preparation of Pebax 1657 SN ion gel.

3.2.2.2 Tetra-PEG SN ion gel

Tetra-PEG SN ion gels were synthesized via Michael addition using tetra-PEG-SH and tetra-PEG-MA [39, 44]. First, 2-methylimidazole (1.0 wt%) was dissolved in acetonitrile. A portion of the 2-methylimidazole solution (0.07 g) was then added to a mixture of tetra-PEG-MA (0.25 g) and acetonitrile (1.09 g). Subsequently, [Emim][C(CN)$_3$] (0.75 g) was added to the mixture, and the solution was stirred until a

clear solution was obtained (solution A). In parallel, tetra-PEG-SH (0.125 g) and IL (0.75 g) were dissolved in acetonitrile (1.09 g) and stirred for 30 min to form solution B. Solutions A and B were combined and stirred for 1 min. The mixed solution was then injected into a closed mold composed of two glass plates and a spacer using a syringe. The mold was subsequently heated in an oven at 50 °C for 24 h to facilitate the formation of the tetra-PEG network. The resulting ion gel was extracted from the mold, placed on a glass plate, and further heated on a hot plate at 70 °C for 24 h. **Fig. 3.2** shows a schematic of the preparation of tetra-PEG SN ion gel. The [Emim][C(CN)$_3$] content of the tetra-PEG SN ion gels ranged from 0-92.5 wt%.

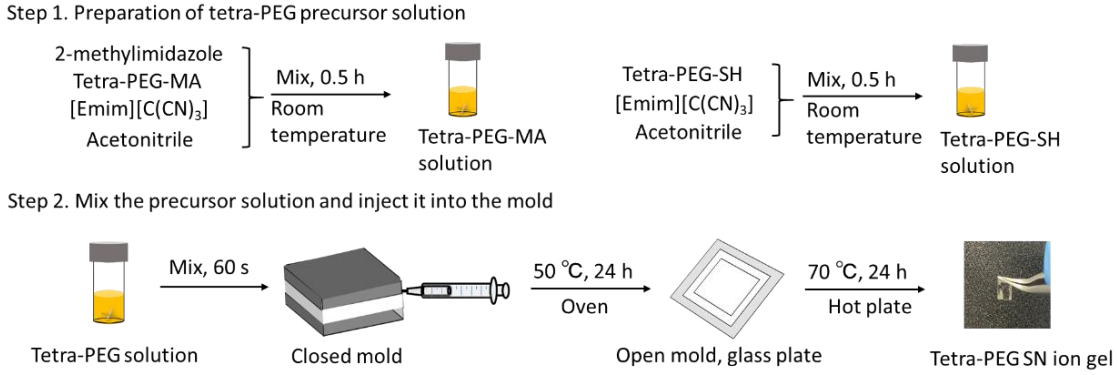

Fig. 3.2 Schematic representation of the preparation of tetra-PEG SN ion gel.

3.2.2.3 Pebax 1657/tetra-PEG IPN ion gel

For the preparation of Pebax 1657/tetra-PEG IPN ion gel membranes, Pebax 1657 solution was first prepared by dissolving Pebax particles in an ethanol/water mixture. Simultaneously, two solutions, A and B, were prepared. Solution A consisted of 2-methylimidazole (1.0 wt%, 0.025 g), [Emim][C(CN)$_3$] (0.75 g), tetra-PEG-MA (0.125 g), and acetonitrile (1.018 g), while solution B composed of tetra-PEG-SH (0.0625 g), IL (0.75 g), and acetonitrile (1.018 g). The prepared Pebax 1657 solution and solutions A

and B were mixed, stirred for 30 s, and then injected into a closed mold. The mold was heated in an oven at 50 °C for 24 h. Afterward, the resulting gel was removed from the mold, placed on a glass plate, and then heated on a hot plate at 70 °C for 24 h. The weight ratio of Pebax 1657 to tetra-PEG in the IPN ion gel was 50/50 wt%, and the IL content was 80 wt%. **Fig. 3.3** illustrates a schematic diagram of the preparation process. Variations in the component ratios of each component in the IPN ion gel were achieved by adjusting the weight of IL and polymers. **Table 3.1** provides details of the weights of components in IPN ion gels.

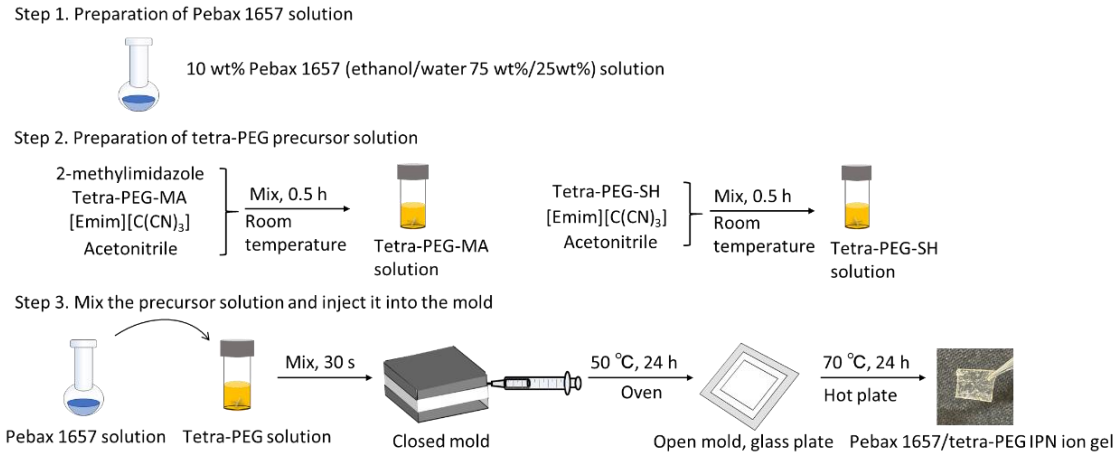

Fig. 3.3 Schematic representation of the preparation of Pebax 1657/tetra-PEG IPN ion gel.

Table 3.1 Weights of Pebax 1657 solution, tetra-PEG-SH, and tetra-PEG-MA used to prepare ion gels with different [Emim][C(CN)$_3$] contents.

Contents (wt%)			IL (g)	10 wt% Pebax 1657 solution (g)	Tetra-PEG-SH (g)	Tetra-PEG-MA (g)	Characterization
Pebax 1657	tetra-PEG	IL					
20	0	80	1.5	3.75	/	/	Mechanical strength test **Figs. 3.4, 3.5, 3.6, and 3.7**
19.5	0.5	80	1.5	3.656	0.0031	0.0062	
19	1	80	1.5	3.5625	0.0063	0.0125	
18	2	80	1.5	3.375	0.0125	0.025	
17	3	80	1.5	3.1875	0.0188	0.0375	

	16.5	3.5	80	1.5	3.094	0.0219	0.0438	
	16	4	80	1.5	3.0	0.025	0.05	
	15	5	80	1.5	2.8125	0.0313	0.0625	
	14	6	80	1.5	2.625	0.0375	0.075	
	12	8	80	1.5	2.25	0.05	0.1	
†	10	10	80	1.5	1.875	0.0625	0.125	
	9	11	80	1.5	1.6875	0.0688	0.1375	
	8	12	80	1.5	1.5	0.075	0.15	
	0	20	80	1.5	/	0.125	0.25	
	3.75	3.75	92.5	1.5	0.608	0.0203	0.0405	Mechanical strength and gas permeation tests*
	5	5	90	1.5	0.833	0.0278	0.0556	
	6.25	6.25	87.5	1.5	1.071	0.0357	0.0714	
	7.5	7.5	85	1.5	1.324	0.0441	0.0882	
	10	10	80	1.5	1.875	0.0625	0.125	
	57	38	5	0.075	8.55	0.19	0.38	XRD measurement **Fig. 3.8a**
	55.8	37.2	7	0.075	5.95	0.1329	0.2657	
	54	36	10	0.075	4.05	0.09	0.18	
	52.8	35.2	12	0.075	3.3	0.0734	0.1467	
	51	34	15	0.075	2.55	0.0567	0.1133	
	48	32	20	0.075	1.8	0.04	0.08	
	0	90	10	0.15	/	0.45	0.9	XRD measurement **Fig. 3.8b**
	45	45	10	0.15	6.75	0.225	0.45	
	54	36	10	0.075	4.05	0.09	0.18	
	85.5	4.5	10	0.15	12.825	0.0225	0.045	
	90	0	10	0.15	13.5	/	/	
	47.5	47.5	5	0.075	7.125	0.2375	0.475	XRD measurement **Fig. 3.9a**
	46.5	46.5	7	0.075	4.982	0.1661	0.3321	
	45	45	10	0.15	6.75	0.225	0.45	
	44	44	12	0.075	2.75	0.0917	0.1833	
	42.5	42.5	15	0.075	2.125	0.0708	0.1417	
	40	40	20	0.075	1.5	0.05	0.1	

†: This sample was used for the gas permeation tests; *: These samples were used for the mechanical strength test (**Fig. 3.5**) and the gas permeation test (**Fig. 3.16**).

3.2.2.4 Poly(DMAAm-co-NSA) SN ion gel

Poly(DMAAm-*co*-NSA) SN ion gels were prepared following the procedure outlined in the previous chapter [24]. Initially, poly(DMAAm-*co*-NSA) (1.24 g) was dissolved in ethanol/water (10.24 g, 75/25 wt%) and stirred for 30 min. Subsequently, IL (5.12 g) and the cross-linker DGBE (0.042 g) were added to the solution and sonicated to remove air bubbles. The resulting solution was then poured into an open mold. The mold was heated in an oven at 50 °C for 24 h and then transferred to a hot plate at 70 °C for drying for 24 h. The IL content of the poly(DMAAm-*co*-NSA) SN ion gel was 80 wt%.

3.2.2.5 Pebax 1657/poly(DMAAm-co-NSA) IPN ion gel

The Pebax 1657/poly(DMAAm-*co*-NSA) IPN ion gel was prepared through the following procedure. Poly(DMAAm-*co*-NSA) (0.31 g) was completely dissolved in a mixture of ethanol/water (1.12 g). Subsequently, Pebax 1657 solution (1.60 g) was added to the mixture and stirred for 5 min. Then, [Emim][$C(CN)_3$] (1.28 g) and DGBE (0.005 g) were added to the solution, followed by sonication for 1 min to remove air bubbles. The resulting solution was then poured into an open mold. The mold was heated in an oven at 50 °C for 24 h and then dried on a hot plate at 70 °C for 24 h. Pebax 1657/poly(DMAAm-*co*-NSA) IPN ion gel membranes were prepared by adjusting the [Emim][$C(CN)_3$] and polymer content for use under different test conditions. Detailed information on the content of each component is provided in **Table 3.2**.

Table 3.2 Weights of Pebax 1657 solution and poly(DMAAm-*co*-NSA) used to prepare ion gels with different [Emim][C(CN)$_3$] contents.

	Contents (wt%)			IL (g)	10 wt% Pebax 1657 solution (g)	Poly(DMAAm-*co*-NSA) (g)	Characterization
	Pebax 1657	poly(DMAAm-*co*-NSA)	IL				
	47.5	47.5	5	0.0168	1.60	0.160	Mechanical strength test (**Fig. 3.4**) and XRD measurement (**Fig. 3.9**)
	46.5	46.5	7	0.0241	1.60	0.160	
	45	45	10	0.0356	1.60	0.160	
	44	44	12	0.0436	1.60	0.160	
	42.5	42.5	15	0.0565	1.60	0.160	
	40	40	20	0.08	1.60	0.160	
†	10	10	80	1.28	1.60	0.160	
†	20	0	80	1.50	3.75	/	
†	0	20	80	1.28	/	0.309	

†: These samples were used for the mechanical strength test in **Fig. 3.4** as Pebax 1657/poly(DMAAm-*co*-NSA) IPN, Pebax 1657 SN, and Poly(DMAAm-*co*-NSA) SN.

3.2.2.6 Pebax 1657 membrane and tetra-PEG membrane

To provide comparison samples for X-ray diffraction (XRD) characterization, IL-free pure Pebax 1657 membrane and tetra-PEG membrane were prepared. The preparation methods were as follows. For Pebax 1657 membranes, Pebax 1657 (10 wt%) was dissolved in a mixture of ethanol/water (75/25 wt%) under refluxing and stirring at 100 °C. The resulting Pebax 1657 solution was poured into an open mold and dried in an oven at 50 °C for 48 h. For tetra-PEG membranes, first, 2-methylimidazole (1.0 wt%) was dissolved in acetonitrile. Then, 0.07 g of the 2-methylimidazole solution was added to a mixture of tetra-PEG-MA (0.25 g) and acetonitrile (1.09 g). Separately, tetra-PEG-SH (0.125 g) was dissolved in acetonitrile (1.09 g) and stirred for 30 min. The solutions of tetra-PEG-MA and tetra-PEG-SH were mixed and stirred for 1 minute before being injected into a sealed mold. The mold was treated in an oven at 30 °C for 24 h to form a gel. Subsequently, the obtained gel was removed from the glass plate and dried on a hot

plate at 70 °C for 24 h to remove solvent.

3.2.2.7 Pebax 1657/tetra-PEG composite membrane and Pebax 1657/poly(DMAAm-co-NSA) composite membrane

To reduce the influence of IL on the crystalline network formation of Pebax 1657, we fabricated IL-free polymer composite membranes. These composite membranes were designed to possess a network structure similar to the ion gel. Therefore, the polymer composite membranes were synthesized using ion gels as precursors. The fabrication process for the polymer composite membranes was as follows. First, Pebax 1657/tetra-PEG IPN and Pebax/poly(DMAAm-*co*-NSA) IPN ion gel samples were prepared. The compositions of Pebax 1657/tetra-PEG and Pebax/poly(DMAAm-*co*-NSA) were varied at 2.0, 3.0, 4.0, and 5.0 g/g. Subsequently, 0.4 g of the prepared Pebax 1657/tetra-PEG and Pebax 1657/poly(DMAAm-*co*-NSA) ion gels were soaked in ethanol (80.0 g) at room temperature for 24 h to extract IL from the gels. After 24 h, the samples immersed in ethanol were collected and rinsed multiple times with ethanol. Finally, the samples were vacuum-dried at 90 °C for 24 h to yield polymer composite membranes.

3.2.3 Characterization of ionic gel membranes and composite membranes

To evaluate the mechanical properties of the ion gels following the measurements and procedures outlined in Chapter 2.

To examine the formation of crystalline regions in the network of the semi-crystalline polymer Pebax 1657, X-ray diffraction (XRD, Cu Kα, D2 PHASER, BRUKER) tests were conducted on the prepared ion gels and composite membranes, the sample scanning angle 2θ in the range of 15° to 30°.

The [Emim][$C(CN)_3$] retention after compression of the ion gels was assessed using

a universal testing machine. The measurement facilities and procedures are consistent with the previous Chapter 2.

For the gas separation performance test, the experimental setup and membrane cell were identical to those used in the previous chapter [29, 45-47]. A gas mixture of CO_2 and N_2 was employed as the feed gas, while Ar gas as the purge gas. The feed gas composition was categorized as either 50/50 mol/mol or 10/90 mol/mol, depending on the test conditions. The total flow rate on the feed side was kept at 200 ml/min, with the purge gas flow rate maintained at 20 ml/min. To study the effect of relative humidity on gas separation performance, Milli-Q water was vaporized using a high-temperature vaporizer. The double-ended plunger pump (Nihon Seimitsu Kagaku Co., Ltd.) changes the flow rate of water supplied to the vaporizer. The evaluation method for ensuring stable separation performance of the ion gel remains consistent with Chapter 2. To examine how temperature, humidity, and IL content affect the separation performance of ion gel membranes at atmospheric pressure, the gas permeation test conditions are detailed in **Table 3.3**.

Table 3.3 Experimental conditions of the gas permeation tests.

(a) Temperature dependence		
[Emim][C(CN)$_3$] content		80 wt%
Temperature		30-80 ℃
Pressure @feed and permeate sides		atmospheric
Trans-membrane pressure difference		0 kPa
Gas flow rate (dry basis)	CO_2	100 cm^3/min
	N_2	100 cm^3/min
	Ar	20 cm^3/min
Relative humidity of the feed gas		0% (dry)
(b) Effect of relative humidity		
[Emim][C(CN)$_3$] content		80 wt%

Temperature		80 ℃
Pressure @feed and permeate sides		atmospheric
Trans-membrane pressure difference		0 kPa
Gas flow rate (dry basis)	CO_2	100 cm^3/min
	N_2	100 cm^3/min
	Ar	20 cm^3/min
Relative humidity of the feed gas		0 – 80%
(c) Long-term stability test		
[Emim][$C(CN)_3$] content		80 wt%
Temperature		80 ℃
Pressure @feed and permeate sides		atmospheric
Trans-membrane pressure difference		0 kPa
Gas flow rate (dry basis)	CO_2	20 cm^3/min
	N_2	180 cm^3/min
	Ar	20 cm^3/min
Relative humidity of the feed gas		80%
Time		240 h
(d) Effect of IL content		
[Emim][$C(CN)_3$] content		80-92.5 wt%
Temperature		30 ℃
Pressure @feed and permeate sides		atmospheric
Trans-membrane pressure difference		0 kPa
Gas flow rate (dry basis)	CO_2	100 cm^3/min
	N_2	100 cm^3/min
	Ar	20 cm^3/min
Relative humidity of the feed gas		0%

3.3 Results and discussion

3.3.1 Mechanical properties of prepared ion gels

Double-network gels possess a distinctive interpenetrating network structure and toughness, resulting in superior mechanical strength compared to SN gels of any polymer constituting the double-network [21, 27, 48]. However, this principle doesn't hold for our previously developed IPN ion gels comprising a semi-crystalline polymer as the first network [18, 24]. In these IPN ion gels, the toughening mechanism of the double network couldn't be realized due to the limited stretchability of the second polymer network. Essentially, the low ductility of the second polymer network prevents it from serving as a hidden length to delay the fracture of ion gels. Hence, in this study, to create an ion gel with a DN principle and the semi-crystalline polymer network as a sacrificial bond, we introduced a tetra-PEG network with high ductility into the ion gel. In this chapter, we will explore the mechanical properties of ion gels prepared with Pebax 1657 and tetra-PEG network interpenetration.

We first evaluated the mechanical strength of ion gels prepared using Pebax 1657, tetra-PEG, and poly(DMAAm-*co*-NSA) as polymer networks. **Fig. 3.4** illustrates the stress-strain curves of these ion gels. Based on the stress-strain curves, the fracture energies of Pebax 1657 SN, Pebax 1657/poly(DMAAm-*co*-NSA) IPN, Pebax 1657/tetra-PEG IPN, and tetra-PEG SN ion gels were measured at 290 kJ/m^3, 46 kJ/m^3, 474 kJ/m^3, and 315 kJ/m^3, respectively. Notably, the mechanical strength of Pebax 1657/poly(DMAAm-*co*-NSA) IPN ion gel was lower than that of Pebax 1657 SN ion gel. In contrast, the mechanical strength of Pebax 1657/tetra-PEG IPN ion gels surpassed that of both Pebax 1657 SN and tetra-PEG SN ion gels. This observation suggests that the tetra-PEG network functions as a hidden length, enhancing the mechanical strength of the

ion gels.

To further elucidate the toughening mechanism of Pebax 1657/tetra-PEG IPN ion gels, cyclic tensile tests were conducted on Pebax 1657/tetra-PEG IPN ion gels with different tetra-PEG contents. As shown in **Fig. 3.4b**, all Pebax 1657/tetra-PEG IPN ion gels except tetra-PEG SN ion gel exhibited hysteresis loops. This suggests the break of the sacrificial bond causes energy dissipation [49-51]. In other words, the Pebax 1657/tetra-PEG IPN ion gel dissipates energy by fracture of crystalline regions. To assess the toughening effect of the tetra-PEG network in the Pebax 1657/tetra-PEG IPN ion gel, we measured Young's modulus of the IPN ion gel after elongation. As shown in **Fig. 3.4c**, the results show that Young's modulus of the IPN ion gel decreases with decreasing Pebax network content, which suggests that the rigidity of the ion gel is dominated by the Pebax 1657 network. As the number of cycles increases, Young's modulus of the ion gels approaches that of the tetra-PEG SN ion gels, indicating that the tetra-PEG network is ductile even under strong stretching. Essentially, the tetra-PEG network acts as a hidden length, preventing macro-destruction of the ion gel.

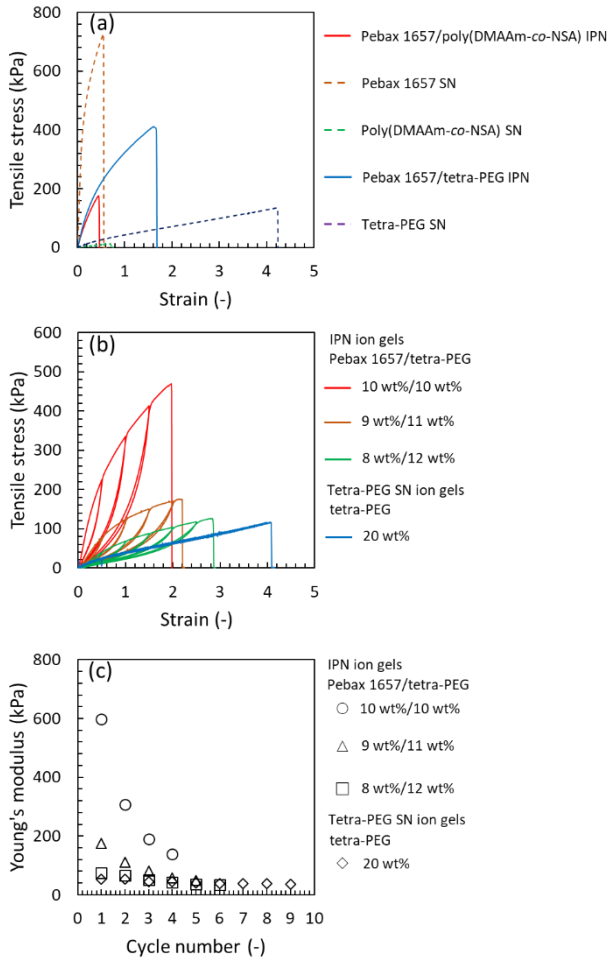

Fig. 3.4 Mechanical properties of the prepared ion gels. (a) Uniaxial tensile stress-strain curves of Pebax 1657 SN, poly(DMAAm-*co*-NSA) SN, Pebax 1657/poly(DMAAm-*co*-NSA) IPN, tetra-PEG SN, and Pebax 1657/tetra-PEG IPN ion gels. (b) Cyclic tensile stress-strain curves of Pebax 1657/tetra-PEG IPN ion gels with different tetra-PEG contents. (c) Young's modulus of Pebax 1657/tetra-PEG IPN ion gels with different tetra-PEG contents after elongation. The ion gels involved in this experiment all contain 80 wt% of [Emim][$C(CN)_3$].

To further investigate the influence of the tetra-PEG network on the mechanical properties of IPN ion gels, we studied the correlation between fracture strain and tetra-

PEG content in Pebax 1657/tetra-PEG IPN and tetra-PEG SN ion gels, as shown in **Fig. 3.5**. In this study, three series of tetra-PEG-based ion gel membranes were used: tetra-PEG SN ion gel, IPN ion gel with different IL contents but consistent Pebax 1657/tetra-PEG ratio, and IPN ion gel with different Pebax 1657/tetra-PEG network ratio while maintaining the same IL content in the ion gel. In this figure, the fracture strain of these ion gels is mainly affected by the tetra-PEG network. Furthermore, this result reaffirms that the tetra-PEG network serves as a hidden length that effectively delays the breakage of Pebax 1657/tetra-PEG IPN ion gels. Based on the toughening mechanism observed in the Pebax 1657/tetra-PEG IPN ion gel, it is clear that the Pebax 1657 network acts as sacrificial bonds, dissipating energy, while the tetra-PEG network acts as a hidden length, preventing the gel breaks, thereby complying with the DN principle [51]. Therefore, the Pebax 1657/tetra-PEG IPN ion gel developed in this study can be regarded as a type of DN ion gel.

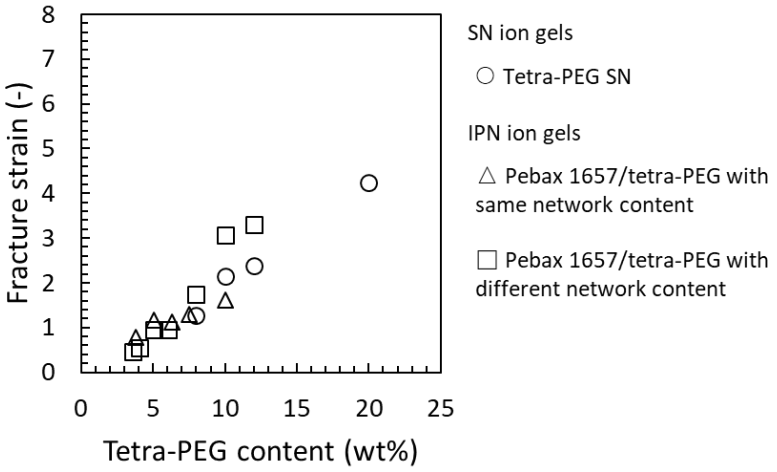

Fig. 3.5 Relationship between fracture strain and tetra-PEG content in ion gels. Circles: tetra-PEG SN ion gels, triangles: Pebax 1657/tetra-PEG IPN ion gels with fixed polymer network weight ratios but different IL contents, squares: Pebax 1657/tetra-PEG IPN ion

gels with 80 wt% IL but different polymer network weight ratios.

3.3.2 Toughening of tetra-PEG networks in Pebax 1657/tetra-PEG IPN ion gels

We have found the tetra-PEG network exerts a significant influence on the fracture strain of ion gels. Increased fracture strains may also enhance dissipated energy by promoting the rupture of sacrificial bonds. This is because as the degree of gel stretching increases, the fragmentation of the first polymer into smaller clusters can dissipate load energy. Consequently, increasing the content of the tetra-PEG network can extend the tensile length. However, in ion gels with fixed IL/IPN ratios, an increase in the hidden length leads to a reduction in sacrificial bonds, potentially diminishing energy dissipation. Thus, the mechanical strength of Pebax 1657/tetra-PEG IPN ion gels may hinge upon the balance between sacrificial bonds and hidden length. Therefore, there exists an optimal network ratio between the Pebax network and the tetra-PEG network. To validate the optimal composition of the polymer network for maximizing the mechanical properties of IPN ion gels, we conducted uniaxial tensile tests on IPN ion gels with a fixed IL content of 80 wt% but varying Pebax 1657/tetra-PEG ratios. The results are illustrated in **Fig. 3.6**. The curves in **Fig. 3.6a** were utilized to compute the relationship between fracture energy and strain, and tetra-PEG content (**Figs. 3.6b** and **3.6c**). As anticipated, the fracture strain exhibited an increase in tetra-PEG content (**Fig. 3.6c**). Notably, at a tetra-PEG content of 10 wt%, the fracture energy of the IPN ion gels peaked (**Fig. 3.6b**). However, with further increases in tetra-PEG content, the sacrificial bond of the Pebax network decreased, consequently leading to a decline in the fracture energy of the ion gels. If these considerations are correct, the dissipation energy of the gel would be expected to reach its maximum at 10 wt% tetra-PEG content, followed by a decrease. Therefore, we

conducted cyclic tensile tests on IPN ion gels with various Pebax 1657/tetra-PEG network compositions to explore the relationship between dissipation energy and tetra-PEG network content. The results are depicted in **Fig. 3.7**. It illustrates the relationship between dissipated energy and tetra-PEG network content of the ion gels, confirming that the dissipation energy of the ion gel peaks at a tetra-PEG content of 10 wt%, aligning with our expectations.

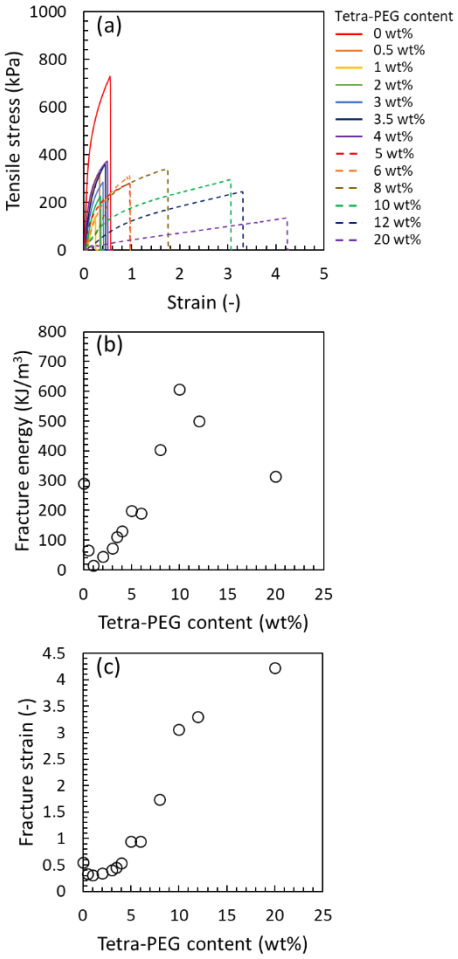

Fig. 3.6 Effect of tetra-PEG content on the mechanical properties of Pebax 1657/tetra-PEG IPN ion gels. (a) Uniaxial tensile stress-strain curves of ion gels with different tetra-PEG contents. (b) Fracture energy (c) Dependence of fracture strain on tetra-PEG content. The [Emim][C(CN)$_3$] content in the ion gels was fixed at 80 wt%.

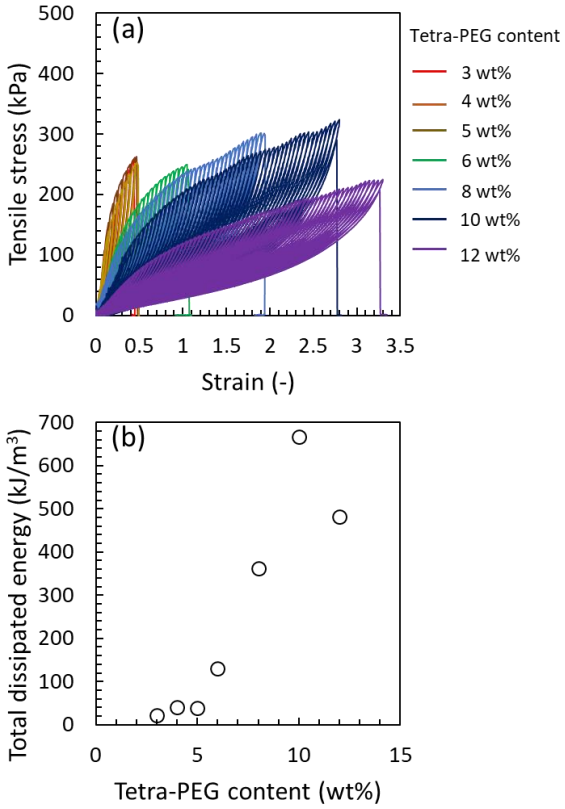

Fig. 3.7 Effect of tetra-PEG content on energy dissipation in Pebax 1657/tetra-PEG IPN ion gels. (a) Cyclic tensile stress-strain curves and (b) total dissipated energy of Pebax 1657/tetra-PEG IPN ion gels with different tetra-PEG contents. The [Emim][C(CN)$_3$] content in the ion gels was fixed at 80 wt%.

3.3.3 Evaluation of semi-crystalline structure formation in Pebax 1657/tetra-PEG ion gel membranes

Based on **Fig. 3.6b**, it was noted that the fracture energy of the gels experienced a sharp decline when the tetra-PEG content was below 2 wt% and the fracture energy of the IPN ion gels was lower than that of the Pebax 1657 SN ion gels. This significant reduction in fracture energy upon adding a small quantity of tetra-PEG suggests that tetra-

PEG prevents the formation of the sacrificial bond Pebax 1657 network. To deeper into the suppression of polyamide block formation in Pebax 1657 by the tetra-PEG network, XRD measurements were conducted on ion gels with varying polymer network compositions. Due to ionic liquids also influence the formation of semi-crystalline polymer networks in ion gels [24]. Consequently, we conducted XRD measurements of ion gels with varying [Emim][$C(CN)_3$] contents and Pebax 1657/tetra-PEG compositions. The XRD spectra displayed in **Fig. 3.8**. The diffraction peaks observed at 19° and 23° correspond to crystalline PEG chains of the tetra-PEG network [52] while the diffraction peak at 24° is attributed to crystalline PA chains of the Pebax 1657 network [53].

We first explored the impact of [Emim][$C(CN)_3$] content on the crystallinity of the gel network formed in Pebax 1657/tetra-PEG IPN ion gels, with the Pebax 1657/tetra-PEG ratio fixed at 12/8 wt%. The XRD pattern is depicted in **Fig. 3.8a**. The intensity of peaks associated with the tetra-PEG network in the ion gel markedly decreased with increasing IL content. Conversely, the effect of IL content on the crystallinity of the Pebax 1657 network was relatively minor. Thus, high IL content inhibited the formation of the crystalline tetra-PEG network while leaving the formation of the semi-crystalline Pebax 1657 network unaffected. Subsequently, we investigated the impact of Pebax 1657/tetra-PEG compositions on the crystallinity of the gel network. To minimize the influence of IL on the crystallinity of the tetra-PEG network, the content of [Emim][$C(CN)_3$] was fixed at 10 wt%. **Fig. 3.8b** revealed that the strength of Pebax 1657 peaks decreased with increasing tetra-PEG network content. This suggests that the tetra-PEG network prevented the formation of the crystalline region in the Pebax 1657 network, consistent with the results of tensile tests.

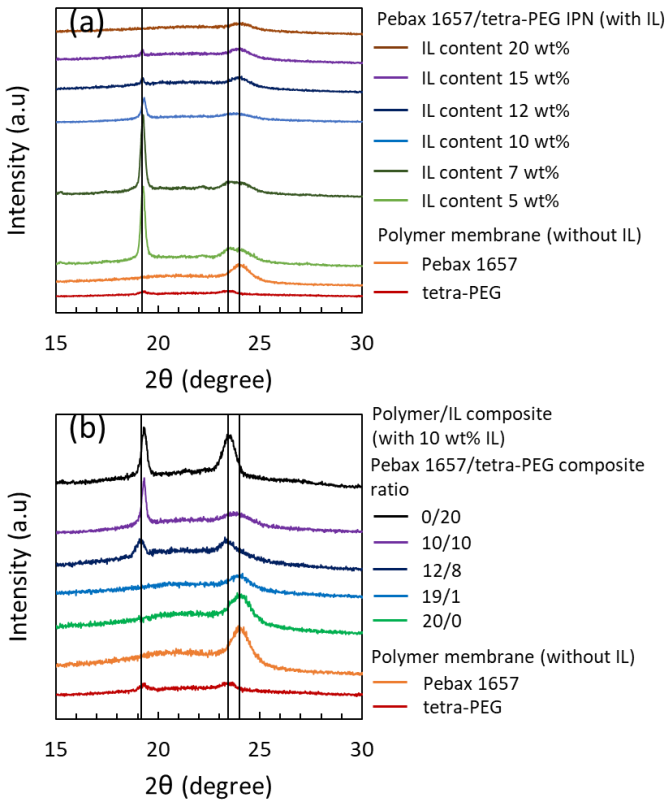

Fig. 3.8 Effect of [Emim][C(CN)$_3$] and tetra-PEG content on the crystallinity of Pebax 1657/tetra-PEG IPN ion gels. (a) XRD patterns of ion gels with different [Emim][C(CN)$_3$] contents, the composition of the Pebax 1657/tetra-PEG network was fixed at 12/8. (b) XRD patterns of Pebax 1657/tetra-PEG IPN ion gels with different Pebax 1657/tetra-PEG compositions. The [Emim][C(CN)$_3$] content was fixed at 10 wt%. XRD patterns of polymer films without ionic liquids were used as a reference.

To further examine the influence of tetra-PEG network content on the formation of semi-crystalline Pebax 1657 networks, we compared the XRD spectra of Pebax 1657/tetra-PEG IPN, Pebax 1657/poly(DMAAm-*co*-NSA) IPN, and Pebax 1657 SN ion gels. The content of the Pebax 1657 network varied within the same range in these ion gels. The results of the XRD spectra are illustrated in **Fig. 3.9**. In **Fig. 3.9a**, the Pebax

1657/tetra-PEG IPN ion gel exhibits relatively low peak intensities corresponding to the Pebax 1657 network and lower than the Pebax 1657/poly(DMAAm-*co*-NSA) IPN and the Pebax 1657 SN ion gels. These results strongly indicate that the tetra-PEG network effectively prevents the formation of the semi-crystalline Pebax network. Additionally, to minimize the influence of IL on the test results, we prepared IL-free polymer composite membranes consisting of Pebax 1657 and tetra-PEG (or poly(DMAAm-*co*-NSA)) networks and conducted XRD tests. The results are presented in **Fig. 3.10**. Similar to **Fig. 3.9**, the peak intensity of the semi-crystalline network decreased upon the addition of the tetra-PEG network to the membranes, while the Pebax 1657/poly(DMAAm-*co*-NSA) composite membranes exhibited negligible changes in peak intensity. This further validates the effect of the tetra-PEG network on the crystalline regions in the Pebax 1657 network.

Based on the analysis of the mechanical properties and structure of Pebax 1657/tetra-PEG IPN ion gels, when the semi-crystalline polymer is the 1st network in DN ion gel, the soft and highly stretchable tetra-PEG network may not be an optimal polymer network. Although it worked as a hidden length to sustain the deformation. This is because it hinders the formation of the semi-crystalline polymer network. Therefore, there is a need to design a polymer network that does not interact with the semi-crystalline polymer network, yet can still be highly stretched as the second polymer network, to further enhance the mechanical strength of DN ion gels.

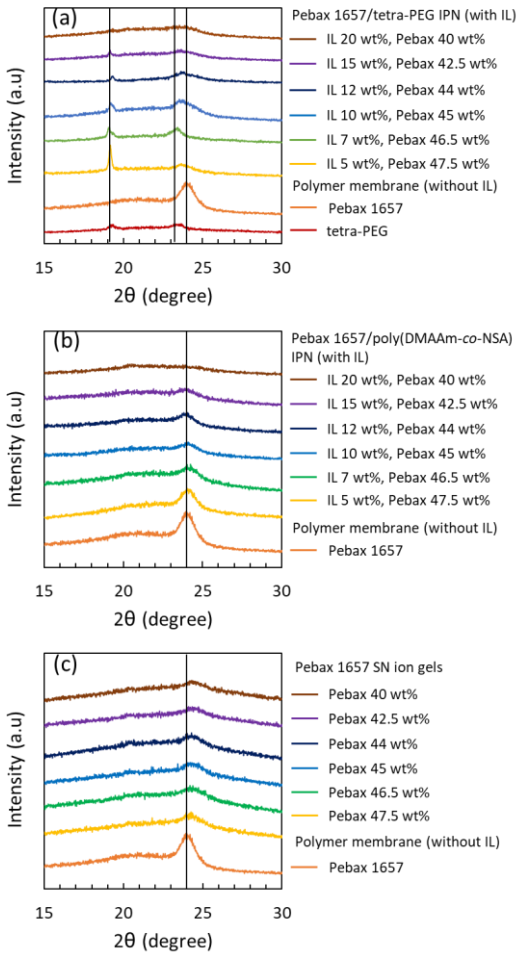

Fig. 3.9 Effect of tetra-PEG and poly(DMAAm-*co*-NSA) networks and IL concentration on the crystallinity of the Pebax 1657 network. XRD patterns of (a) Pebax 1657/tetra-PEG IPN, (b) Pebax 1657/poly(DMAAm-*co*-NSA) IPN, and (c) Pebax 1657 SN ion gels. Pebax 1657 concentration was fixed in these ion gels. XRD patterns of IL-free polymer membranes are shown for reference.

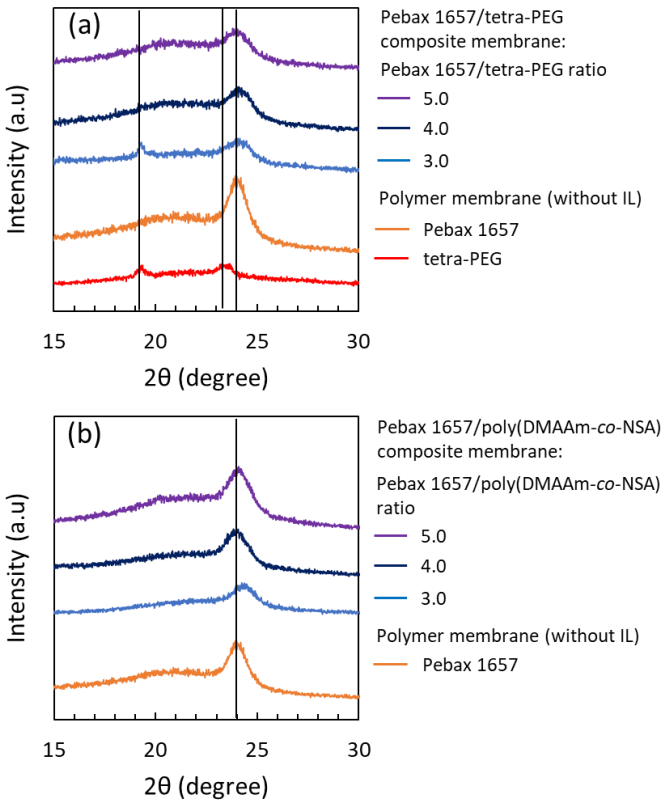

Fig. 3.10 Influence of the content of the second polymer network on the formation of a crystalline Pebax 1657 network. (a) XRD patterns of Pebax 1657/tetra-PEG composite membranes for different Pebax 1657/tetra-PEG network weight ratios. (b) XRD patterns of Pebax 1657/poly(DMAAm-*co*-NSA) composite membranes for different Pebax 1657/poly(DMAAm-*co*-NSA) network weight ratios.

3.3.4 IL retention property of Pebax 1657/tetra-PEG IPN ion gel membranes

Mechanical properties and IL retention properties are key factors affecting the CO_2 separation performance of ion gels [25, 54]. As previously discussed, Pebax 1657/tetra-PEG IPN ion gels exhibit high mechanical strength. Hence, it is need to assess the IL retention property of the ion gel. It can be anticipated that Pebax 1657/tetra-PEG IPN ion gels would demonstrate high IL retention properties owing to the good compatibility

between PEG and [Emim][C(CN)$_3$]. We investigated the impact of tetra-PEG network content in IPN ion gels on the retention capacity of [Emim][C(CN)$_3$]. **Fig. 3.11** reveals that the amount of IL retained by Pebax 1657/tetra-PEG IPN ion gels for 1 minute at 1.0 MPa increased with the rise in tetra-PEG network content. Remarkably, when the tetra-PEG content was at 10 wt%, the ion gel exhibited the highest mechanical strength and retained over 95% of the IL. Therefore, only a negligible amount of [Emim][C(CN)$_3$] might leak from the gel under low pressures. In other words, the ion gel membranes comprise 80 wt% [Emim][C(CN)$_3$], 10 wt% Pebax 1657, and 10 wt% tetra-PEG can be used for CO_2 separation tests.

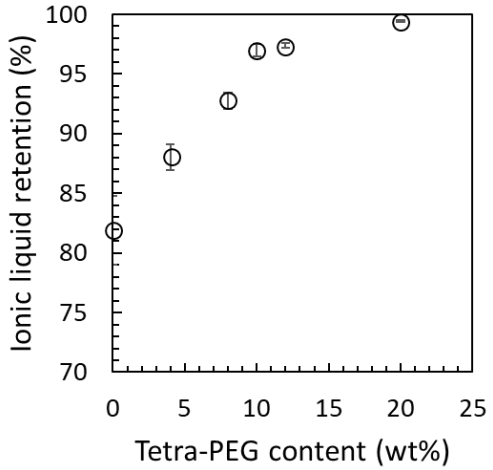

Fig. 3.11 Ionic liquid retained by Pebax 1657/tetra-PEG IPN ion gels as a function of tetra-PEG content. The [Emim][C(CN)$_3$] content in the ion gel was fixed at 80 wt%.

3.3.5 Gas separation performances of Pebax 1657/tetra-PEG IPN ion gel membranes

In practical applications, after the waste gas emitted from coal-fired power plants is treated with desulphurization, the flue gas temperature is reduced to below 80 °C [17, 55,

56]. Based on this, we assessed the CO_2 permeability and CO_2/N_2 selectivity of IPN ion gels at elevated temperatures up to 80 °C. As depicted in **Fig. 3.12**, the CO_2 permeability increased with rising temperature. When the temperature reached 80 °C, the CO_2 permeability had reached approximately 1500 barrer. On the contrary, since the temperature sensitivity of N_2 is higher than that of CO_2, the increase in N_2 permeability is higher than that of CO_2, and the CO_2/N_2 selectivity of the ion gel membrane decreases with increasing temperature. Nevertheless, even at 80 °C, the selectivity still exceeded 20. This excellent CO_2/N_2 selectivity meets the industrial requirements for CO_2 separation membranes utilized in capturing CO_2 from flue gas in coal-fired power plants [17, 57]. Therefore, the IPN ion gel membrane designed in this study is suitable for CO_2 capture from flue gas at high temperatures.

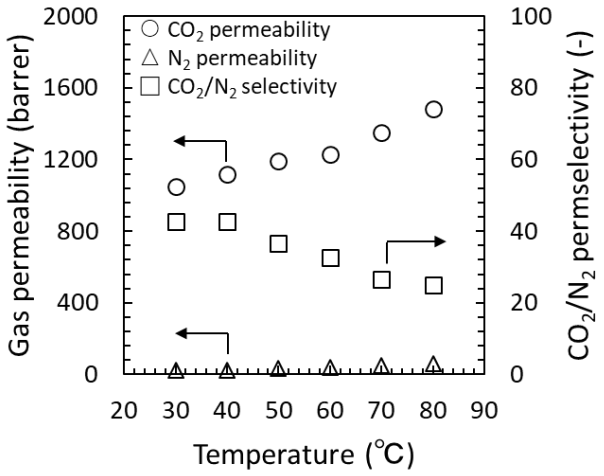

Fig. 3.12 Effect of temperature on CO_2 and N_2 permeability and CO_2/N_2 selectivity of Pebax 1657/tetra-PEG IPN ion gel membranes containing 80 wt% [Emim][$C(CN)_3$]. A dry CO_2/N_2 mixture of composition 50/50 mol/mol was supplied as feed gas at atmospheric pressure.

In addition to carbon dioxide and nitrogen, the desulfurization flue gas treatment process also contains some water vapor. Therefore, in addition to considering the effect of temperature on the CO_2 permeability of ion gels, relative humidity also needs to be considered [16, 58]. Typically, the CO_2 permeability and CO_2/N_2 selectivity of high-performance CO_2 separation membranes, composed of glassy polymers decreases as the relative humidity in the feed gas rises [14-16, 59-61]. In contrast, the CO_2 permeability of IPN ion gels developed in this study exhibited an increase with rising humidity, while maintaining unaffected CO_2/N_2 permselectivity (**Fig. 3.13**). As the viscosity of the ionic liquid in the ion gel membrane decreases upon absorption of water vapor, the diffusion coefficients of CO_2 and N_2 in the ion gel increase, thereby increasing the permeability of the two gases. However, since the diffusion coefficients of CO_2 and N_2 increase at the same time, the selectivity of CO_2/N_2 remains almost constant. In conclusion, the ion gel membrane demonstrated a CO_2 permeability of 2000 barrer and CO_2/N_2 selectivity of 25 at 80 °C and relative humidity of 80%. Notably, the CO_2 separation performance of the ion gel membrane remained stable even after long-term stability tests lasting over 10 days (**Fig. 3.14**). This stability indicates minimal IL leakage from the gel membrane during the test period. Hence, Pebax 1657/tetra-PEG IPN ion gel membranes containing [Emim][$C(CN)_3$] hold promise as CO_2 separation membranes for capturing CO_2 from flue gas emitted by coal-fired power plants.

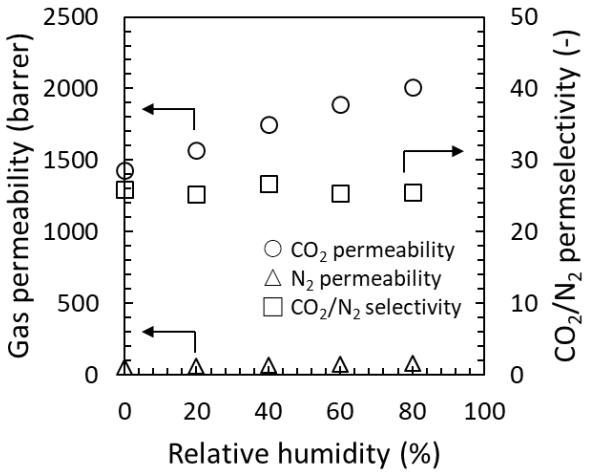

Fig. 3.13 Effect of relative humidity on CO_2 and N_2 permeability and CO_2/N_2 permselectivity of Pebax 1657/tetra-PEG IPN ion gel membranes containing 80 wt% IL. The experiments were carried out using a feed gas consisting of 50/50 mol/mol of CO_2/N_2 (dry basis) with a certain relative humidity, 80 °C, and atmospheric pressure.

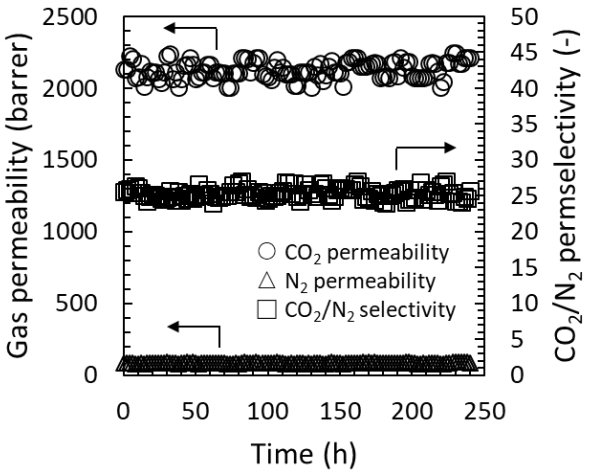

Fig. 3.14 Long-term stability of Pebax 1657/tetra-PEG IPN ion gel membranes containing 80 wt% [Emim][$C(CN)_3$]. The CO_2/N_2 composition of the feed gas was 10/90 mol/mol (dry basis). The relative humidity of the feed gas was maintained at 80%. The

experiments were carried out at 80 °C and atmospheric pressure.

In addition to temperature and humidity, we evaluated the effect of transmembrane pressure difference on the CO_2 separation performance of Pebax 1657/tetra-PEG IPN ion gels, and the results are consistent with the other IL-based membranes (**Fig. 3.15**). Due to the high mechanical strength of the ion gel, the Pebax 1657/tetra-PEG IPN ion gel did not rupture even at 500 kPa transmembrane pressure difference. Meanwhile, due to the high compatibility of IL and tetra-PEG network, only a small amount of IL overflowed under high transmembrane pressure difference did not affect the CO_2 separation performance of the IPN ion gel.

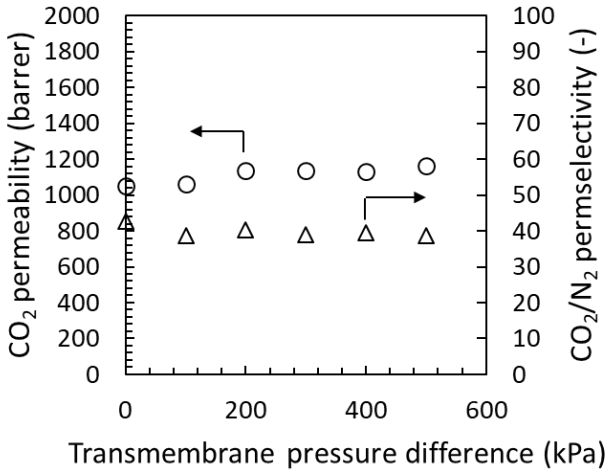

Fig. 3.15 Pressure resistance of Pebax 1657/tetra-PEG IPN ion gel membranes containing 80 wt% [Emim][$C(CN)_3$]. The experiment was performed using a feed gas consisting of 50/50 mol/mol of CO_2/N_2 at 30 °C and dry conditions.

Finally, we investigated the effect of IL content on the CO_2 permeability and CO_2/N_2 selectivity of Pebax 1657/tetra-PEG IPN ion gels. In **Fig. 3.16**, as expected, the CO_2

permeability of the Pebax 1657/tetra-PEG IPN ion gel showed an increasing trend with increasing IL content, up to 92.5 wt%. The ability of the designed IPN ion gels to reach an IL content above 90 wt% and to be tested for gas properties is mainly due to the high mechanical strength and effective IL holding property of the ion gel. In addition, the CO_2 permeability of the IPN ion gel containing 92.5 wt% IL reached 3100 barrer, which is higher than that of other ionic liquid-based CO_2 separation membranes previously reported and covered in **Fig. 3.17** [18, 24].

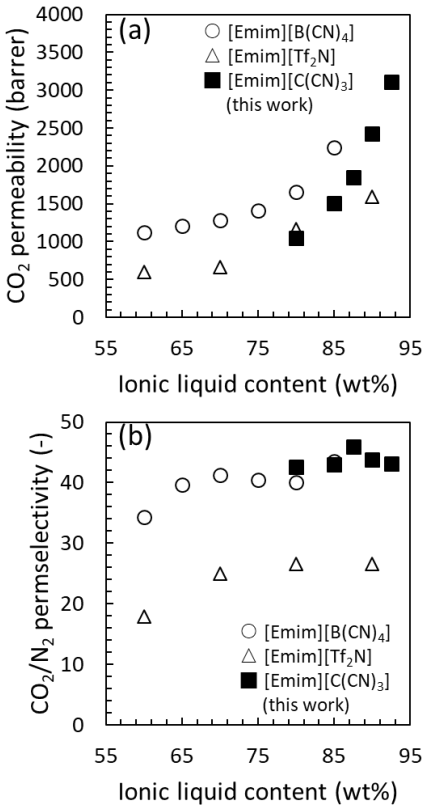

Fig. 3.16 Effect of IL content on (a) CO_2 permeability and (b) CO_2/N_2 selectivity of Pebax 1657/tetra-PEG ion gel membranes. The feed gas contained 50/50 mol/mol CO_2/N_2. The experiments were carried out at 30 °C, atmospheric pressure, and dry conditions.

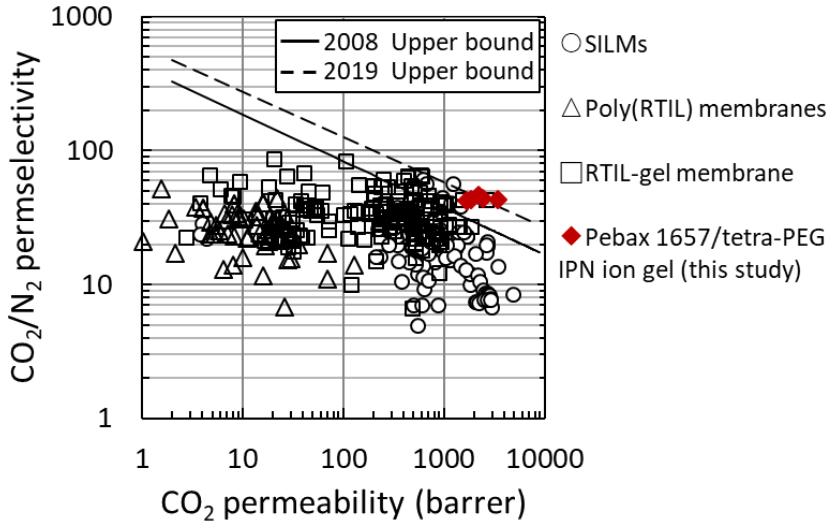

Fig. 3.17 Comparison of the CO_2 separation performance of the developed Pebax 1657/tetra-PEG IPN ion gel with previously reported IL-based membranes. The solid and dashed lines are the upper limits of the polymeric membranes reported [9, 10].

The ion gels developed in this study showcased outstanding mechanical strength and good IL retention. They demonstrated long-term stability in CO_2 separation performance even under high-temperature and high-humidity conditions. Therefore, the Pebax 1657/tetra-PEG IPN ion gel emerges as a highly promising candidate for CO_2 separation membrane applications in the treatment of flue gas emanating from coal-fired power plants.

3.4 Conclusions

In this study, we developed a tough ionic liquid-based CO_2 separation membrane. This ion gel membrane comprises [Emim][$C(CN)_3$], a Pebax 1657 network, and a tetra-PEG network. The remarkable ductility of the tetra-PEG network serves as a hidden length, effectively delaying gel network rupture even under large elongation. Meanwhile,

the Pebax 1657 network acts as a sacrificial bond to dissipate the loading energy, and the synergistic action of the double network gives the ion gel high mechanical strength. Thanks to the superior mechanical strength of the ion gel, we were able to increase the IL content to 92.5 wt%, resulting in a CO_2 permeability of 3100 barrer and a CO_2/N_2 selectivity of 43. In addition, the CO_2 separation performance of the ion gel was good even under high temperature and high humidity tests, which meets the requirements of CO_2 separation membranes for flue gas from coal-fired power plants.

Reference

[1] R. Quadrelli, S. Peterson, The energy-climate challenge: Recent trends in CO_2 emissions from fuel combustion, Energy Policy, 35(11), 2007, 5938-5952.

[2] H. Fu, K. Xue, Z. Li, et al., Study on the performance of CO_2 capture from flue gas with ceramic and PTFE membrane contactors, Energy, 263, 2023, 125677.

[3] M.K. Mondal, H.K. Balsora, P. Varshney, Progress and trends in CO_2 capture/separation technologies: A review, Energy, 46(1), 2012, 431-441.

[4] H. Wu, Q. Li, M. Sheng, et al., Membrane technology for CO_2 capture: From pilot-scale investigation of two-stage plant to actual system design, Journal of Membrane Science, 624, 2021, 119137.

[5] Y. Han, W.S.W. Ho, Recent advances in polymeric membranes for CO_2 capture, Chinese Journal of Chemical Engineering, 26(11), 2018, 2238-2254.

[6] Y. Han, W.S.W. Ho, Polymeric membranes for CO_2 separation and capture, Journal of Membrane Science, 628, 2021, 119244.

[7] Y. Han, Y. Yang, W.S.W. Ho, Recent progress in the engineering of polymeric membranes for CO_2 capture from flue gas, Membranes, 10(11), 2020, 365.

[8] L.M. Robeson, Correlation of separation factor versus permeability for polymeric membranes, Journal of Membrane Science, 62(2), 1991, 165-185.

[9] L.M. Robeson, The upper bound revisited, Journal of Membrane Science, 320(1), 2008, 390-400.

[10] B. Comesaña-Gándara, J. Chen, C.G. Bezzu, et al., Redefining the Robeson upper bounds for CO_2/CH_4 and CO_2/N_2 separations using a series of ultrapermeable benzotriptycene-based polymers of intrinsic microporosity, Energy & Environmental Science, 12(9), 2019, 2733-2740.

[11] E. Kamio, T. Yoshioka, H. Matsuyama, Recent advances in carbon dioxide separation membranes: A review, Journal of Chemical Engineering of Japan, 56(1), 2023, 2222000.

[12] P.M. Budd, N.B. McKeown, B.S. Ghanem, et al., Gas permeation parameters and other physicochemical properties of a polymer of intrinsic microporosity: Polybenzodioxane PIM-1, Journal of Membrane Science, 325(2), 2008, 851-860.

[13] E. Lasseuguette, R. Malpass Evans, M. Carta, et al., Temperature and pressure dependence of gas permeation in a microporous Tröger's base polymer, Membranes, 8(4), 2018, 132.

[14] G.Q. Chen, C.A. Scholes, G.G. Qiao, et al., Water vapor permeation in polyimide membranes, Journal of Membrane Science, 379(1-2), 2011, 479-487.

[15] L. Ansaloni, M. Minelli, M.G. Baschetti, et al., Effect of relative humidity and temperature on gas transport in Matrimid®: Experimental study and modeling, Journal of membrane science, 471, 2014, 392-401.

[16] E. Lasseuguette, M. Carta, S. Brandani, M.C. Ferrari, Effect of humidity and flue gas impurities on CO_2 permeation of a polymer of intrinsic microporosity for post-combustion capture, International Journal of Greenhouse Gas Control, 50, 2016, 93-99.

[17] T.C. Merkel, H. Lin, X. Wei, et al., Power plant post-combustion carbon dioxide capture: An opportunity for membranes, Journal of Membrane Science, 359(1), 2010, 126-139.

[18] S. He, E. Kamio, J. Zhang, et al., Development of an ion gel membrane containing a CO_2-philic ionic liquid in interpenetrating semi-crystalline and crosslinkable polymer networks, Journal of Membrane Science, 685, 2023, 121912.

[19] A.R. Nabais, S. Ahmed, M. Younis, et al., Mixed matrix membranes based on ionic liquids and porous organic polymers for selective CO_2 separation, Journal of Membrane

Science, 660, 2022, 120841.

[20] T. Watanabe, E. Oe, Y. Mizutani, T. Ono, Toughening of poly(ionic liquid)-based ion gels with cellulose nanofibers as a sacrificial network, Soft Matter, 19(15), 2023, 2745-2754.

[21] E. Kamio, T. Yasui, Y. Iida, et al., Inorganic/organic double-network gels containing ionic liquids, Advanced Materials, 29(47), 2017, 1704118.

[22] Y. Yu, X. Yang, C. Zhang, et al., A tough double-network ion gel membrane based on poly (ionic liquid) for efficient carbon capture, Separation and Purification Technology, 331, 2024, 125591.

[23] E. Hayashi, M.L. Thomas, K. Hashimoto, et al., Application of protic ionic liquids to CO_2 separation in a sulfonated polyimide-derived ion gel membrane, ACS Applied Polymer Materials, 1(6), 2019, 1579-1589.

[24] J. Zhang, E. Kamio, A. Matsuoka, et al., Novel tough ion-gel-based CO_2 separation membrane with interpenetrating polymer network composed of semicrystalline and cross-linkable polymers, Industrial & Engineering Chemistry Research, 61(13), 2022, 4648-4658.

[25] F. Ranjbaran, E. Kamio, H. Matsuyama, Ion gel membrane with tunable inorganic/organic composite network for CO_2 separation, Industrial & Engineering Chemistry Research, 56(44), 2017, 12763-12772.

[26] V.A. Kusuma, C. Chen, J.S. Baker, et al., The effect of poly(ethylene oxide) cross-linking structure on the mechanical properties and CO_2 separation performance of an ion gel membrane, Polymer, 180, 2019, 121666.

[27] F. Moghadam, E. Kamio, A. Yoshizumi, H. Matsuyama, An amino acid ionic liquid-based tough ion gel membrane for CO_2 capture, Chemical Communications, 51(71), 2015,

13658-13661.

[28] F. Moghadam, E. Kamio, T. Yoshioka, H. Matsuyama, New approach for the fabrication of double-network ion-gel membranes with high CO_2/N_2 separation performance based on facilitated transport, Journal of Membrane Science, 530, 2017, 166-175.

[29] F. Moghadam, E. Kamio, H. Matsuyama, High CO_2 separation performance of amino acid ionic liquid-based double network ion gel membranes in low CO_2 concentration gas mixtures under humid conditions, Journal of Membrane Science, 525, 2017, 290-297.

[30] E. Kamio, M. Kinoshita, T. Yasui, et al., Preparation of inorganic/organic double-network ion gels using a cross-linkable polymer in an open system, Macromolecules, 53(19), 2020, 8529-8538.

[31] E. Kamio, M. Minakata, Y. Iida, et al., Inorganic/organic double-network ion gel membrane with a high ionic liquid content for CO_2 separation, Polymer Journal, 53(1), 2021, 137-147.

[32] T. Yasui, E. Kamio, H. Matsuyama, Inorganic/organic double-network ion gels with partially developed silica-particle network, Langmuir, 34(36), 2018, 10622-10633.

[33] H.Z. Chen, P. Li, T.S. Chung, PVDF/ionic liquid polymer blends with superior separation performance for removing CO_2 from hydrogen and flue gas, International Journal of Hydrogen Energy, 37(16), 2012, 11796-11804.

[34] J.C. Jansen, G. Clarizia, P. Bernardo, et al., Gas transport properties and pervaporation performance of fluoropolymer gel membranes based on pure and mixed ionic liquids, Separation and Purification Technology, 109, 2013, 87-97.

[35] Z. Dai, R.D. Noble, D.L. Gin, et al., Combination of ionic liquids with membrane technology: A new approach for CO_2 separation, Journal of Membrane Science, 497, 2016,

1-20.

[36] J. Zhang, E. Kamio, A. Matsuoka, et al., Fundamental investigation on the development of composite membrane with a thin ion gel layer for CO_2 separation, Journal of Membrane Science, 663, 2022, 121032.

[37] K. Huang, H.L. Peng, Solubilities of carbon dioxide in 1-Ethyl-3-methylimidazolium thiocyanate, 1-ethyl-3-methylimidazolium dicyanamide, and 1-ethyl-3-methylimidazolium tricyanomethanide at (298.2 to 373.2) K and (0 to 300.0) kPa, Journal of Chemical & Engineering Data, 62(12), 2017, 4108-4116.

[38] A.P.S. Martins, A. Fdz De Añastro, J.L. Olmedo-Martínez, et al., Influence of anion structure on thermal, mechanical and CO_2 solubility properties of UV-cross-linked poly(ethylene glycol) diacrylate iongels, Membranes, 10(3), 2020, 46.

[39] K. Fujii, H. Asai, T. Ueki, et al., High-performance ion gel with tetra-PEG network, Soft Matter, 8(6), 2012, 1756-1759.

[40] W. Fam, J. Mansouri, H. Li, et al., Effect of inorganic salt blending on the CO_2 separation performance and morphology of pebax1657/ionic liquid gel membranes, Industrial & Engineering Chemistry Research, 58(8), 2019, 3304-3313.

[41] H. Rabiee, A. Ghadimi, T. Mohammadi, Gas transport properties of reverse-selective poly(ether-b-amide6)/[Emim][BF_4] gel membranes for CO_2/light gases separation, Journal of Membrane Science, 476, 2015, 286-302.

[42] E. Ghasemi Estahbanati, M. Omidkhah, A. Ebadi Amooghin, Preparation and characterization of novel Ionic liquid/Pebax membranes for efficient CO_2/light gases separation, Journal of Industrial and Engineering Chemistry, 51, 2017, 77-89.

[43] P. Bernardo, J.C. Jansen, F. Bazzarelli, et al., Gas transport properties of Pebax®/room temperature ionic liquid gel membranes, Separation and Purification

Technology, 97, 2012, 73-82.

[44] S. Ishii, H. Kokubo, K. Hashimoto, et al., Tetra-PEG network containing ionic liquid synthesized via michael addition reaction and its application to polymer actuator, Macromolecules, 50(7), 2017, 2906-2915.

[45] E. Kamio, S. Kasahara, F. Moghadam, H. Matsuyama, Development of facilitated transport membranes composed of a dense gel layer containing CO_2 carrier formed on porous cylindrical support membranes, Chemical Engineering Research and Design, 153, 2020, 284-293.

[46] S. Kasahara, E. Kamio, T. Ishigami, H. Matsuyama, Effect of water in ionic liquids on CO_2 permeability in amino acid ionic liquid-based facilitated transport membranes, Journal of Membrane Science, 415-416, 2012, 168-175.

[47] S. Kasahara, E. Kamio, T. Ishigami, H. Matsuyama, Amino acid ionic liquid-based facilitated transport membranes for CO_2 separation, Chemical Communications, 48(55), 2012, 6903-6905.

[48] J.P. Gong, Y. Katsuyama, T. Kurokawa, Y. Osada, Double-network hydrogels with extremely high mechanical strength, Advanced Materials, 15(14), 2003, 1155-1158.

[49] T. Yasui, Y. Zheng, T. Nakajima, et al., Rate-independent self-healing double network hydrogels using a thixotropic sacrificial network, Macromolecules, 55(21), 2022, 9547-9557.

[50] M.A. Haque, T. Kurokawa, G. Kamita, J.P. Gong, Lamellar bilayers as reversible sacrificial bonds to toughen hydrogel: Hysteresis, self-recovery, fatigue resistance, and crack blunting, Macromolecules, 44(22), 2011, 8916-8924.

[51] J.P. Gong, Why are double network hydrogels so tough?, Soft Matter, 6(12), 2010, 2583-2590.

[52] Y. Nomoto, T. Matsunaga, T. Sakai, et al., Structure and physical properties of dried Tetra-PEG gel, Polymer, 52(18), 2011, 4123-4128.

[53] M. Isanejad, N. Azizi, T. Mohammadi, Pebax membrane for CO_2/CH_4 separation: Effects of various solvents on morphology and performance, Journal of Applied Polymer Science, 134(9), 2017.

[54] F. Ranjbaran, E. Kamio, H. Matsuyama, Inorganic/organic composite ion gel membrane with high mechanical strength and high CO_2 separation performance, Journal of Membrane Science, 544, 2017, 252-260.

[55] A.A. Olajire, CO_2 capture and separation technologies for end-of-pipe applications – A review, Energy, 35(6), 2010, 2610-2628.

[56] M. Songolzadeh, M. Soleimani, M. Takht Ravanchi, R. Songolzadeh, Carbon dioxide separation from flue gases: A technological review emphasizing reduction in greenhouse gas emissions, The Scientific World Journal, 2014, 2014, 828131.

[57] P.T. Nguyen, B.A. Voss, E.F. Wiesenauer, et al., Physically gelled room-temperature ionic liquid-based composite membranes for CO_2/N_2 separation: Effect of composition and thickness on membrane properties and performance, Industrial & Engineering Chemistry Research, 52(26), 2013, 8812-8821.

[58] J.C. Abanades, B. Arias, A. Lyngfelt, et al., Emerging CO_2 capture systems, International Journal of Greenhouse Gas Control, 40, 2015, 126-166.

[59] C.A. Scholes, S. Kanehashi, G.W. Stevens, S.E. Kentish, Water permeability and competitive permeation with CO_2 and CH_4 in perfluorinated polymeric membranes, Separation and Purification Technology, 147, 2015, 203-209.

[60] A. Fuoco, B. Satilmis, T. Uyar, et al., Comparison of pure and mixed gas permeation of the highly fluorinated polymer of intrinsic microporosity PIM-2 under dry and humid

conditions: Experiment and modelling, Journal of Membrane Science, 594, 2020, 117460.
[61] E. Lasseuguette, M. C. Ferrari, S. Brandani, Humidity impact on the gas permeability of PIM-1 membrane for post-combustion application, Energy Procedia, 63, 2014, 194-201.

Chapter 4

Highly selective CO_2 permeable double-network ion gel membrane containing 1-ethyl-3-methylimidazolium dicyanamide

4.1 Introduction

In recent years, CO_2 separation membranes utilizing ionic liquids (ILs) as CO_2 separation media have garnered significant interest [1-4]. ILs are nonvolatile organic salts with customizable chemical structures, allowing them to be fine-tuned for specific tasks. For instance, imidazolium-type ILs that contain an anion with cyano groups are known for their selective CO_2 absorption [5-10]. Such ILs, with their high selectivity for CO_2 absorption, can serve as effective CO_2 separation media, including CO_2 absorbents and CO_2 separation membranes [11-15]. Studies have shown that CO_2 separation membranes incorporating ILs with selective CO_2 absorbability exhibit high CO_2/N_2 permselectivity, ranging from approximately 30 to 60 [16-21]. The CO_2/N_2 permselectivity of ionic liquid (IL)-based CO_2 separation membranes surpasses that of the latest polymer membranes made from polymers of intrinsic microporosity (PIMs) and thermally rearranged (TR) polymers [22-29]. Moreover, the CO_2/N_2 permselectivity of IL-based CO_2 separation membranes is on par with that of polymer membranes composed of PEG-based polymers known for their high affinity with CO_2 [30-33]. Additionally, some IL-based CO_2 separation membranes have been found to exhibit high CO_2 permeability. Recent studies

have reported that ion gel membranes containing significant amounts of IL demonstrate exceptional CO_2 permeability [4, 20, 34-37]. Ion gel membranes with an IL content of 80 wt% or higher exhibit significantly greater CO_2 permeability compared to PEG-based polymer membranes (100 to 500 barrer) [4, 38-43]. Consequently, ion gels enriched with a CO_2-philic IL are promising materials for high-performance CO_2 separation membranes, offering both high permeability and excellent CO_2 selectivity.

The CO_2/N_2 permselectivity of an ion gel membrane containing a high content of an IL is largely determined by the properties of the IL within the gel [4, 44-46]. Consequently, developing an ion gel membrane with high CO_2/N_2 permselectivity requires using an IL with a high CO_2/N_2 solubility selectivity. Among the various ILs available, 1-ethyl-3-methylimidazolium dicyanamide ([Emim][DCA]) stands out with a very high CO_2/N_2 solubility selectivity of approximately 45-60 [47, 48]. This makes [Emim][DCA] a promising candidate for developing high-performance ion gel-based CO_2 separation membranes. Moreover, the CO_2 permeability of the ion gel membrane increases exponentially with the IL content in the membrane [41-43]. An ion gel with a high content of 1-ethyl-3-methylimidazolium dicyanamide ([Emim][DCA]) can be used as a material for creating an ion gel-based CO_2 separation membrane that offers both high permeability and high selectivity in CO_2 separation. In recent years, researchers have reported the fabrication of highly tough ion gels by forming a unique gel network within an IL [37, 43, 49-54]. These tough ion gels exhibit high mechanical strength, allowing the IL content in the ion gel to be increased to over 90 wt%. As a result, tough ion gels with high IL content represent a promising material for CO_2 separation membranes capable of high-speed CO_2 permeation. In this study, we developed a tough ion gel with a high [Emim][DCA] content to create a CO_2 separation membrane that offers rapid and highly selective CO_2

permeation.

Research has shown that tough ion gels containing [Emim][DCA] can be developed by using polyvinyl alcohol (PVA) as a gel network [16, 55]. For instance, Klepić et al. developed an ion gel membrane with [Emim][DCA] and PVA as the gel network, evaluating its selective CO_2/H_2 permeation performance [16]. Additionally, Weng et al. demonstrated that a tough ion gel with [Emim][DCA] can be prepared by forming a composite network of PVA and polyvinylpyrrolidone (PVP) in [Emim][DCA] [55]. However, the [Emim][DCA] content in these ion gels was below 80 wt%. To use PVA-based tough ion gels with [Emim][DCA] as materials for CO_2 separation membranes, it is necessary to increase the [Emim][DCA] content. Notably, PVA forms a semi-crystalline structure in [Emim][DCA] gels [16, 55]. The semi-crystalline structure formed in PVA allows it to physically crosslink and create a three-dimensional network within [Emim][DCA], resulting in the gelation of [Emim][DCA] with PVA. Recently, we developed a tough double-network ion gel using a semi-crystalline polymer by establishing semi-crystalline physical crosslinking in an ionic liquid (IL) [43]. Generally, double network (DN) gels exhibit exceptional toughness due to energy dissipation caused by the internal rupture of the first network, which serves as a sacrificial bond when force is applied to the gel [56]. To efficiently dissipate the applied energy, a soft and stretchable second polymer network must be formed in the gel, highly entangled with the first network to provide hidden length. In this study, a second network made of poly(*N,N′*-dimethyl acrylamide) (PDMAAm), which exhibits good compatibility with [Emim][DCA], was formed through free radical polymerization of N,N'-dimethyl acrylamide (DMAAm) in an aqueous solution containing [Emim][DCA] and PVA. The mechanical and CO_2 permeation properties of the resulting ion gel membrane, composed

of [Emim][DCA] and a PVA/PDMAAm double-network (PVA/PDMAAm DN ion gel), were then evaluated.

4.2 Experimental

4.2.1 Reagents

[Emim][DCA] purchased from Tokyo Chemical Industry (TCI) Co., Ltd. was used as the IL. 99% hydrolyzed polyvinyl alcohol (PVA) purchased from Sigma-Aldrich Co. was used as the 1st network of the DN ion gel. *N,N*'-dimethylacrylamide used for the formation of PDMAAm network, which is the 2nd network of the DN ion gel, was purchased from TCI Co., Ltd. *N,N*'-methylenebis(acrylamide) (MBAA) purchased from Sigma-Aldrich Co. was used as a crosslinker for the PDMAAm network. 2-oxoglutaric acid (OA), purchased from TCI Co., Ltd., was used as a photoinitiator of the PDMAAm network formation reaction. All reagents were used without further purification.

4.2.2 Preparation of ion gel membranes

Fig. 4.1 illustrates the preparation process of three different types of ion gels: the single-network ion gel composed of a PVA network (PVA SN ion gel), the single-network ion gel composed of a PDMAAm network (PDMAAm SN ion gel), and the PVA/PDMAAm double-network ion gel (PVA/PDMAAm DN ion gel). The specific methods for preparing each type of ion gel are detailed below.

4.2.2.1 PVA SN ion gel

A PVA aqueous solution was prepared by stirring and dissolving 1.0 g of PVA powder in 9.0 g of pure water in a water bath at 95 °C for 2 hours. Then, 4.0 g of

[Emim][DCA] was added to the PVA solution and vigorously mixed for 5 minutes to create a precursor solution for the ion gel. The precursor solution was poured into an open mold and heated on a hot plate at 70 °C for 24 hours to remove the solvent (water). The resulting PVA SN ion gel had an [Emim][DCA] content of 80 wt%.

4.2.2.2 PDMAAm SN ion gel

To prepare a homogeneous [Emim][DCA]/DMAAm solution, 4.0 g of [Emim][DCA] and 1.0 g of DMAAm were mixed for 10 minutes in a glass vessel. Certain quantities of MBAA (0.4 mol% based on DMAAm) and OA (0.1 mol% based on DMAAm) were added to the [Emim][DCA]/DMAAm solution and completely dissolved through stirring. The resulting precursor solution was injected into a sealed mold, which consisted of a square die-cut polytetrafluoroethylene (PTFE) spacer sandwiched between two glass plates. Free radical polymerization of DMAAm was then carried out by irradiating the mold with 365 nm UV light for 9 hours to form a three-dimensional PDMAAm network. The [Emim][DCA] content in the PDMAAm SN ion gel was 80 wt%.

4.2.2.3 PVA/PDMAAm DN ion gel

The PVA/PDMAAm double-network ion gel, composed of an optimized PVA and PDMAAm double-network and 80 wt% [Emim][DCA], was prepared as follows. First, a PVA aqueous solution was prepared by dissolving 0.5 g of PVA powder in 4.5 g of pure water in a water bath at 95 °C for 2 hours. Next, 2.0 g of [Emim][DCA] was added to the PVA aqueous solution and dissolved through vigorous mixing for 5 minutes to create solution A. Separately, 0.5 g of DMAAm was dissolved in an [Emim][DCA] aqueous solution consisting of 2.0 g of [Emim][DCA] and 0.45 g of Milli-Q water to form the

[Emim][DCA]/DMAAm aqueous solution. In this solution, 0.0032 g of MBAA and 0.0007 g of OA were added and fully dissolved to form solution B. Solutions A and B were then combined and thoroughly mixed. The mixed solution was immediately injected into a sealed mold consisting of two glass plates and a PTFE spacer. The mold was irradiated with 365 nm UV light for 9 hours to form a PDMAAm network within the precursor solution. After 9 hours, the mold was opened, and the resulting gel was heated in an oven at 50 °C for 24 hours to evaporate the water. During the drying process, the PVA network formed within the ion gel. The ion gel was then removed from the mold and heated on a hot plate at 70 °C for 24 hours to remove any residual water. As a result, the PVA/PDMAAm double-network ion gel was successfully prepared.

When preparing double-network (DN) ion gels with varying [Emim][DCA] contents, the quantities of the reagents used to prepare the ion gels were adjusted. The preparation conditions are detailed in **Table 4.1**. Additionally, DN ion gels with different crosslinking degrees and varying PVA/PDMAAm compositions were prepared to optimize the mechanical strength of the DN ion gel. These preparation conditions are also presented in **Table 4.1**.

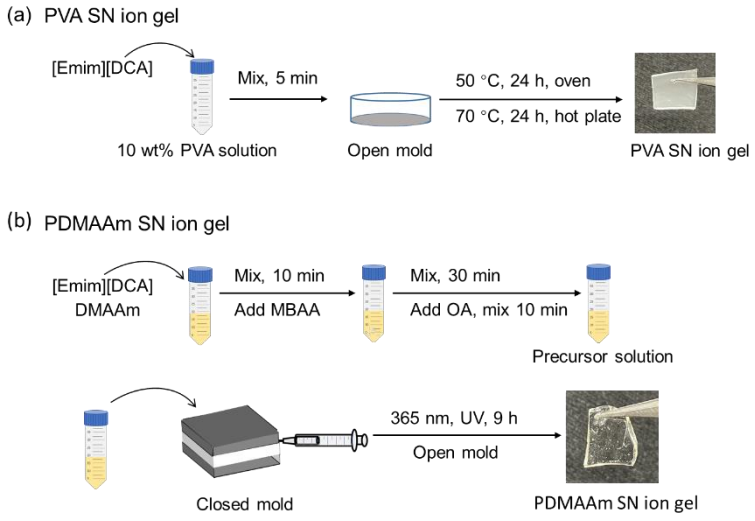

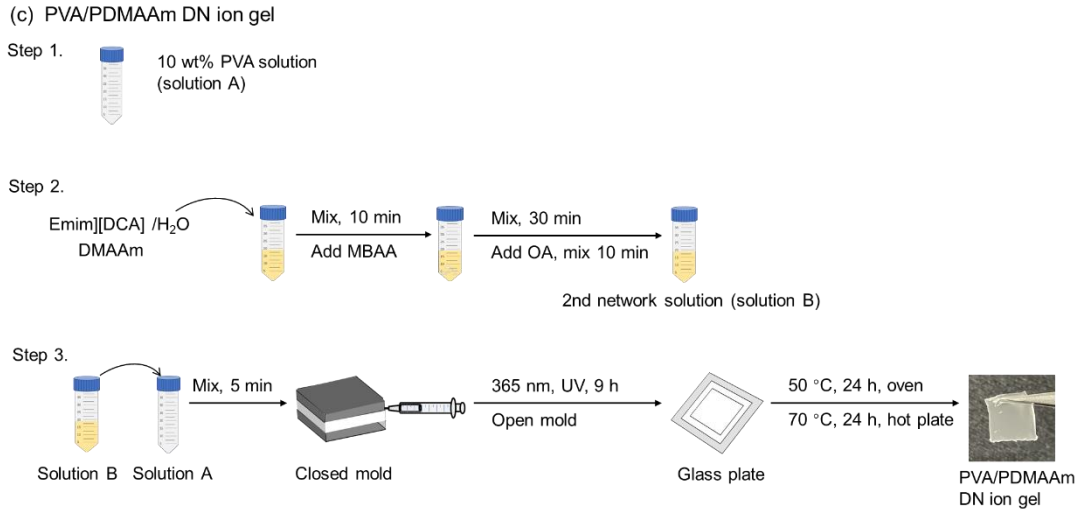

Fig. 4.1 Schematic diagram of the preparation of ion gels. (a) PVA SN ion gel, (b) PDMAAm SN ion gel, and (c) PVA/PDMAAm DN ion gel.

Table 4.1 Preparation conditions of PVA/PDMAAm DN ion gels.

Contents (wt%)			Weight of reagents used					characterization
PVA	DMAAm	IL	IL	PVA	DMAAm	MBAA	OA	
20	0	80	8.0	2.0	0	0	0	Mechanical
19	1	80	8.0	1.9	0.1	0.0006	0.0001	strength test
18	2	80	4.0	0.9	0.1	0.0006	0.0001	
16	4	80	4.0	0.8	0.2	0.0012	0.0003	Effect of
12	8	80	4.0	0.6	0.4	0.0025	0.0006	PVA/PDMAAm
10	10	80	4.0	0.5	0.5	0.0032	0.0007	composition
8	12	80	4.0	0.4	0.6	0.0037	0.0009	(**Fig. 4.3**)
6	14	80	4.0	0.3	0.7	0.0044	0.0010	(**Fig. 4.5(a)**)
0	20	80	4.0	0	1.0	0.0062	0.0015	
10	10	80	4.0	0.5	0.5	0.0008	0.0007	Mechanical
10	10	80	4.0	0.5	0.5	0.0016	0.0007	strength test
10	10	80	4.0	0.5	0.5	0.0024	0.0007	
10	10	80	4.0	0.5	0.5	0.0031	0.0007	Effect of
10	10	80	4.0	0.5	0.5	0.0040	0.0007	crosslinking
10	10	80	4.0	0.5	0.5	0.0048	0.0007	degree
10	10	80	4.0	0.5	0.5	0.0064	0.0007	(**Fig. 4.4**)

10	10	80	4.0	0.5	0.5	0.0156	0.0007	(**Fig. 4.5(b)**)
15	15	70	4.0	0.8571	0.8571	0.0053	0.0013	Mechanical
12.5	12.5	75	4.0	0.6667	0.6667	0.0041	0.0010	strength test
10	10	80	4.0	0.5	0.5	0.0031	0.0007	
8.75	8.75	82.5	4.0	0.4242	0.4242	0.0026	0.0006	Effect of IL
7.5	7.5	85	4.0	0.3529	0.3529	0.0022	0.0005	content
6.25	6.25	87.5	4.0	0.2857	0.2857	0.0018	0.0004	(**Fig. 4.7**)
5.5	5.5	89	4.0	0.2472	0.2472	0.0015	0.0004	
15	15	70	4.0	0.8571	0.8571	0.0053	0.0013	Gas
12.5	12.5	75	4.0	0.6667	0.6667	0.0041	0.0010	permeation
10	10	80	4.0	0.5	0.5	0.0031	0.0007	test
8.75	8.75	82.5	4.0	0.4242	0.4242	0.0026	0.0006	
7.5	7.5	85	4.0	0.3529	0.3529	0.0022	0.0005	Effect of IL
6.25	6.25	87.5	4.0	0.2857	0.2857	0.0018	0.0004	content
5.5	5.5	89	4.0	0.2472	0.2472	0.0015	0.0004	(**Fig. 4.8**)
4.5	4.5	91	8.0	0.3956	0.3956	0.0025	0.0006	
4	4	92	8.0	0.3478	0.3478	0.0022	0.0005	
3.5	3.5	93	8.0	0.3011	0.3011	0.0019	0.0004	

4.2.3 Characterization of ion gel membranes

4.2.3.1 Evaluation of mechanical properties

The mechanical strength of the ion gel membrane was evaluated using the same tensile apparatus used in Chapters 1 and 2. A cyclic stretching test was conducted to investigate the toughening mechanism of the PVA/PDMAAm DN ion gel, using specimens with the same geometry as those used in the uniaxial stretching tests. The ion gel specimen was stretched to a predetermined strain, ε_1, at a constant tensile speed of 100 mm/min, then immediately returned to its original length at the same speed. The ion gel was then stretched again at the same speed to a larger strain, ε_2, and then returned to its original length. This cycle of stretching and returning was repeated each time with an increase in the strain, for nth cycles until the ion gel ruptured. Here, ε_n (n = 1, 2, ...)

represents the maximum strain during the nth cycle, and ε represents the current nominal strain during that cycle. The failure stress, σ_n (kPa), at the nth tensile cycle was calculated as the ratio of the applied load to the initial cross-sectional area of the sample. The formulas for parameter calculation in this chapter are as follows:

$$\Delta U_{hys_n} = \int_0^{\varepsilon_n} \sigma_n \, d\varepsilon - \int_0^{\varepsilon_n} \sigma_{n+1} \, d\varepsilon \tag{1}$$

$$U_{hys_n} = \sum_{i=1}^{n} \Delta U_{hys_i} \tag{2}$$

$$W_n = U_{hys_n} + \int_0^{\varepsilon_n} \sigma_{n+1} \, d\varepsilon \tag{3}$$

$$\Delta U_{recover_n} = \int_0^{\varepsilon_n} \sigma_{n+1} \, d\varepsilon - \int_0^{\varepsilon_n} \sigma_{n,recover_n} \, d\varepsilon \tag{4}$$

$$\Delta U_{hys_n'} = \int_0^{\varepsilon_n} \sigma_n \, d\varepsilon - \int_0^{\varepsilon_n} \sigma_{n,return} d\varepsilon \tag{5}$$

4.2.3.2 Evaluation of IL holding property

Use the same universal testing machine as in Chapter 1 and Chapter 2 to evaluate the IL retention performance of the ion gel. Initially, the ion gel was cut into a disk with a diameter of 1.2 cm and recorded the weights. The ion gel sample was then compressed for 1.0 min at various compression pressures. The IL that leaked onto the surface of the compressed sample was wiped off, and the weight of the sample after compression was measured. The IL retention of the ion gel was assessed based on the change in the sample's weight before and after compression.

4.2.3.3 Gas separation performance of ion gel membranes

The CO_2/N_2 separation performance of the ion gel membrane was assessed using a sweep method following the same procedure as previously reported [43, 57]. This study

examined the effects of the [Emim][DCA] content in the DN ion gel membrane, transmembrane pressure difference, temperature, and relative humidity of the feed gas on the CO_2 and N_2 permeabilities, as well as the CO_2/N_2 permselectivity, of the DN ion gel membrane. For evaluations of the effects of [Emim][DCA] content, transmembrane pressure difference, and temperature, the CO_2/N_2 composition of the feed gas was adjusted to 50/50 mol/mol. To evaluate the effect of relative humidity, a humid feed gas with a CO_2/N_2 composition of 10/90 mol/mol was used. Additionally, the stability of the selective CO_2 permeation performance of the DN ion gel membrane was assessed using the humid feed gas with a CO_2/N_2 composition of 10/90 mol/mol. To evaluate the effect of [Emim][DCA] content in the DN ion gel membrane, the membranes were prepared under the conditions outlined in **Table 4.1**, and their CO_2 and N_2 permeation performances were assessed under the standard conditions mentioned earlier. For assessing the effect of a transmembrane pressure difference, the feed-side pressure was controlled within the range of 100 kPa to 500 kPa. When evaluating the effect of relative humidity, the humidity was adjusted from 0% to 80% at a temperature of 80 °C.

4.3 Results and discussion

4.3.1 Mechanical strength of the PVA/PDMAAm DN ion gel

A tough ion gel was successfully fabricated by forming PVA and PDMAAm networks within [Emim][DCA]. The stress-strain curve of the PVA/PDMAAm DN ion gel is illustrated in **Fig. 4.2a**. This evaluation used a DN ion gel with a double-network composition of 10/10 wt%, achieved using a precursor solution with an optimal MBAA concentration of 0.4 mol% (refer to **Figs. 4.3 and 4.4**). For comparison, the results for SN ion gels with either a PVA or PDMAAm network are also shown in **Fig. 4.2a**. The stress-

strain curves in **Fig. 4.2a** reveal that the mechanical strength of the DN ion gel is significantly higher than that of the SN ion gels. To investigate the toughening mechanism of the PVA/PDMAAm DN ion gel, a cyclic tensile stress-strain measurement was performed. The results are displayed in **Fig. 4.2b**. As shown in the figure, the DN ion gel exhibited a large hysteresis loop in the cyclic stress-strain curve, indicating that energy dissipation is the toughening mechanism of the PVA/PDMAAm DN ion gel. Additionally, while the PVA SN ion gel also demonstrated a clear hysteresis loop, the PDMAAm SN ion gel did not exhibit any hysteresis. This suggests that the PVA network in the DN ion gel dissipates the applied energy. Previous reports have indicated that the PVA network forms a semi-crystalline structure in [Emim][DCA] [16, 55, 58, 59]. This means that the loaded energy may be dissipated through the rupture of the semi-crystalline crosslinks in the PVA network formed within the ion gels. In other words, the PVA network acts as a sacrificial bond in the PVA/PDMAAm DN ion gel. Moreover, the excellent stretchability of the DN ion gel allows it to dissipate a large amount of energy before breaking. To further explore the toughening mechanism, we analyzed the dissipated energy in detail.

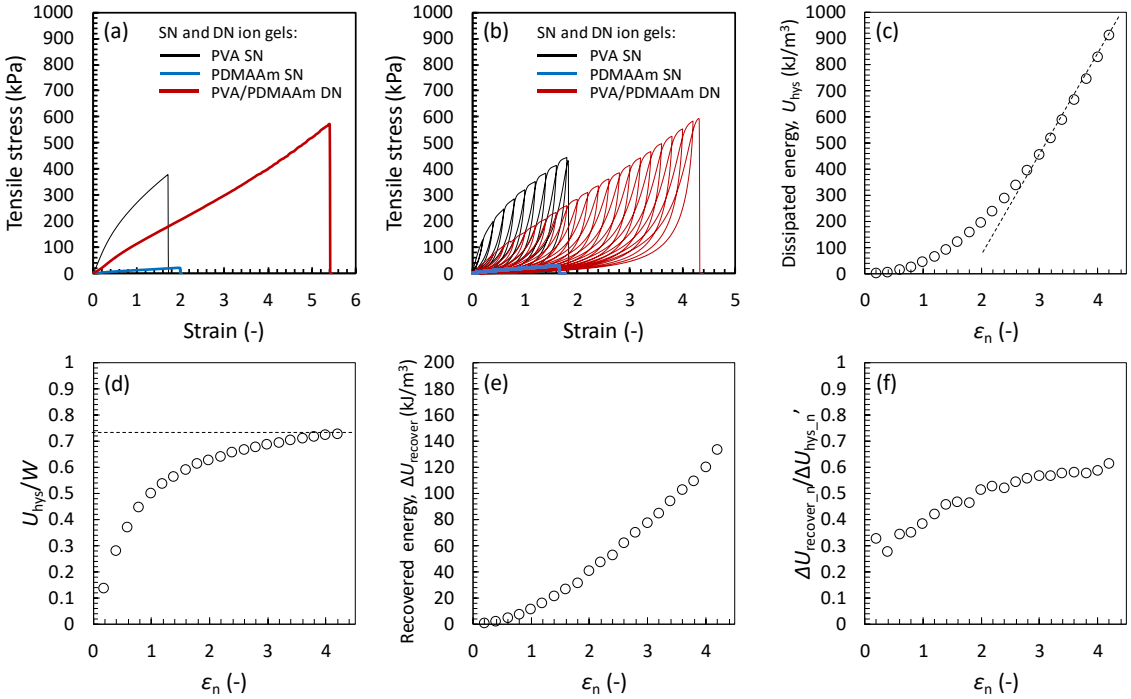

Fig. 4.2 Mechanical strength and toughening mechanism of PVA/PDMAAm DN ion gel. (a) Stress-strain curves of the PVA/PDMAAm DN ion gel, PVA SN ion gel, and PDMAAm SN ion gel. (b) Cyclic tensile stress loading-unloading curves of the PVA/PDMAAm DN, PVA SN, and PDMAAm SN ion gels. (c-f) Totally dissipated energy, U_{hys} (c), ratio of the irreversible work within the total work done by extension, U_{hys}/W (d), recovered energy dissipated, $\Delta U_{recover}$ (e), and ratio of the recovered energy and dissipated energy (f) at a certain ε_n. The [Emim][DCA] content in the ion gels was 80 wt%.

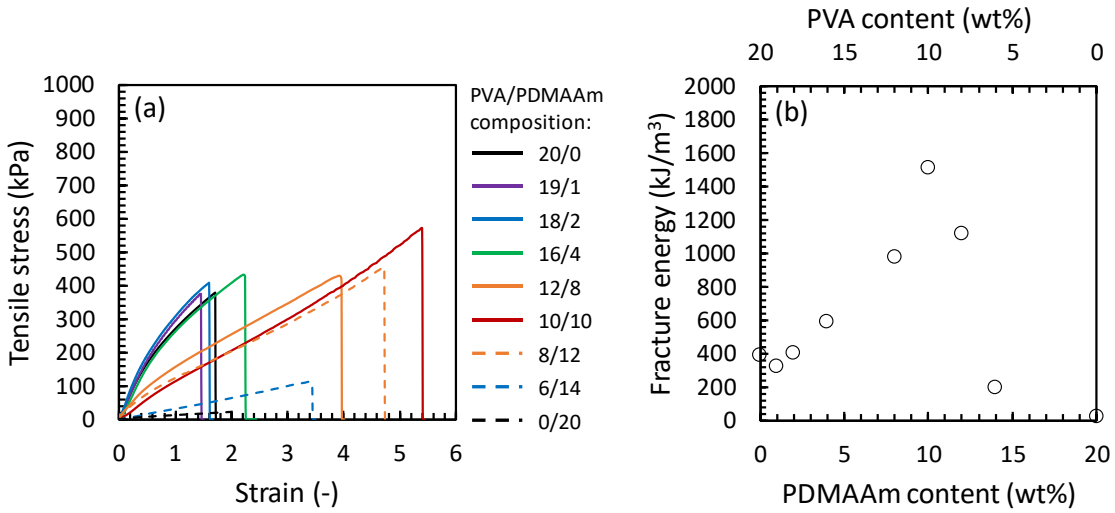

Fig. 4.3 Effect of PDMAAm network composition in PVA/PDMAAm DN on the mechanical properties of the DN ion gel. (a) Uniaxial tensile stress-strain curves and (b) fracture energy of the DN ion gels with different PVA/PDMAAm network compositions. The [Emim][DCA] content in the DN ion gels was 80 wt%.

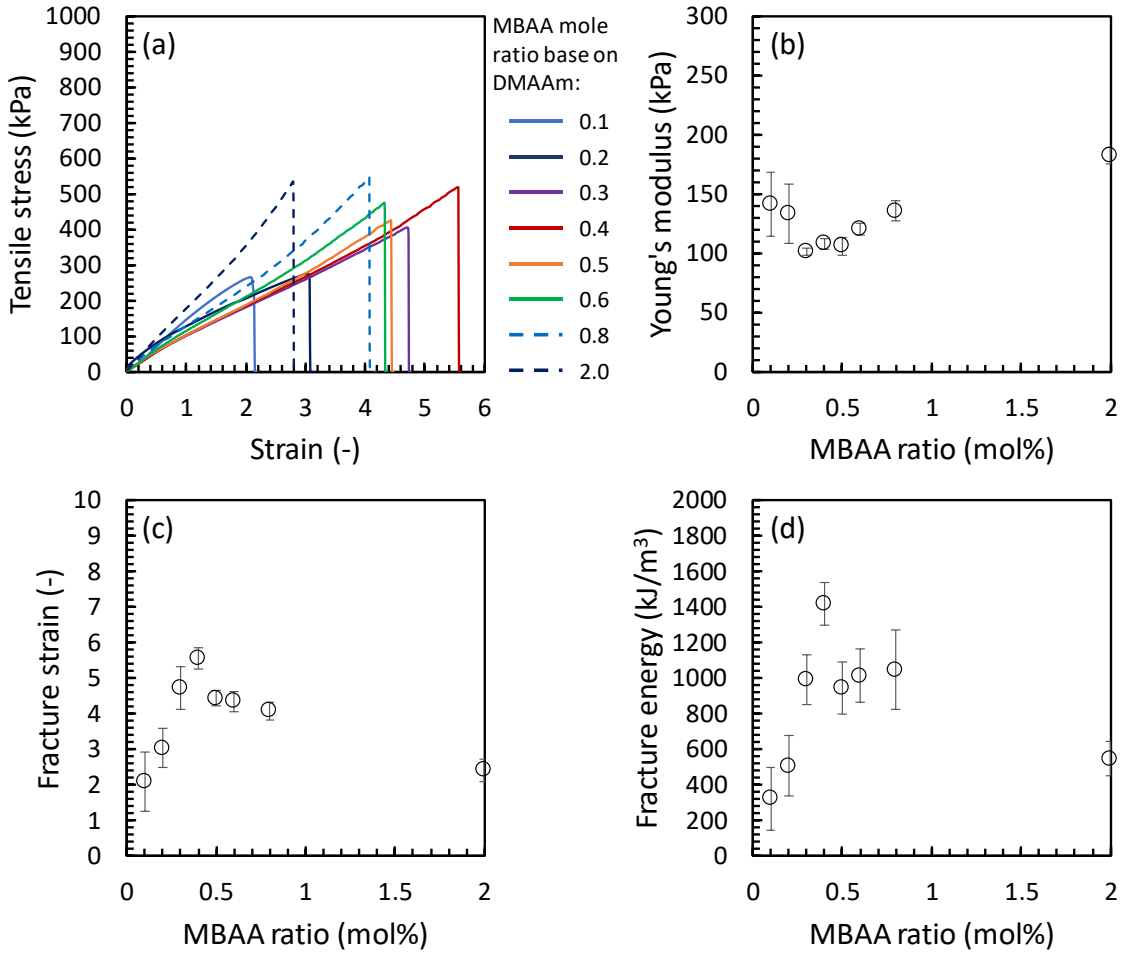

Fig. 4.4 Effect of crosslinking degree of the PDMAAm network on the mechanical properties of the PVA/PDMAAm DN ion gels. (a) Uniaxial tensile stress-strain curves, and effect of crosslinking degree on (b) Young's modulus, (c) fracture strain, and (d) fracture energy of the DN ion gels. The PVA/PDMAAm composition and the [Emim][DCA] content in the DN ion gels were 10/10 mol/mol and 80 wt%, respectively.

Fig. 4.2c shows the relationship between the total energy dissipated during the nth stretching cycle (U_{hys}, kJ/m³) and the maximum strain at the nth stretching cycle (ε_n) of the DN ion gel. U_{hys} is the sum of the dissipated energy at each stretching cycle (ΔU_{hys}, kJ/m³). The cyclic tensile stress loading-unloading curves of the DN ion gel (**Fig. 4.2b**)

demonstrate that the nth unloading curve overlaps with the (n+1)th loading curve up to ε_n. This overlap indicates that some of the dissipated energy during the nth stretching process is recovered during the stress unloading phase. The recovery of dissipated energy may occur due to the reformation of broken semi-crystalline crosslinks in the PVA network, as observed in the cyclic tensile stress-strain curve of the PVA SN ion gel (**Fig. 4.2b**). The overlapping area between the nth unloading and (n+1)th loading curves represents the energy recovered during the nth stress unloading process. Regarding U_{hys} during each stress loading-unloading cycle, it increased monotonically with ε_n (**Fig. 4.2c**). The slope $dU_{hys}/d\varepsilon_n$ remained constant beyond a strain of 3, indicating that the internal fracture of the semi-crystalline structure of the PVA network continued to occur with deformation until the ion gel broke. This suggests that both internal fracture of the semi-crystalline crosslinks in the PVA network and strain hardening in the PDMAAm network occurred continuously as the gel was stretched extensively.

To evaluate the efficiency of energy dissipation in the PVA/PDMAAm DN ion gel, the ratio U_{hys}/W at a certain strain ε_n was calculated. Here, U_{hys}/W represents the proportion of the irreversible work resulting from the internal fracture of the PVA network relative to the total work of extension, while W (kJ/mol) represents the total work performed to extend the DN ion gel to a given strain ε_n. As shown in **Fig. 4.2d**, U_{hys}/W approached a constant value of approximately 72% at higher elongations. This finding suggests that over 70% of the work was utilized for internal fracture of the PVA network. Although the U_{hys}/W value for the PVA/PDMAAm DN ion gel is lower than that of DN hydrogels (85%), it is higher than that of vulcanized rubbers (59–67%) [60-63]. Thus, the PVA network in the DN ion gel appears to stretch more than the network in vulcanized rubbers, but not to the same extent as the sacrificial bonds in DN hydrogels.

Another notable characteristic of the PVA/PDMAAm DN ion gel is its ability to regain toughness through the reconstruction of the physical semi-crystalline crosslinks in the PVA network. **Fig. 4.2e** illustrates the $\Delta U_{recover}$ of the DN ion gel at various strains ε_n. The $\Delta U_{recover}$ value rises steadily with increasing ε_n, indicating that the number of ruptured semi-crystalline crosslinks in the PVA network grows as strain increases, and a significant portion of them are reconstructed. As depicted in **Fig. 4.2f**, the recovery ratio—defined as the ratio of recovered energy from the nth to (n+1)th cycle compared to the dissipated energy in the nth cycle-reaches 60%. This substantial recovery of toughness in the PVA/PDMAAm DN ion gel is attributed to the reversible physical crosslinking of the PVA network.

The results in **Fig. 4.2** confirm that the developed ion gel with a PVA/PDMAAm network is a type of DN ion gel with a high degree of self-healing properties.

4.3.2 Consideration on the effect of PDMAAm network on the mechanical strength enhancement

The PVA/PDMAAm DN ion gel exhibits a distinctive feature compared to traditional DN gels. Typically, DN gels consist of an interpenetrating polymer network composed of a rigid, brittle first network and a soft, ductile second network [56]. The second network provides a "hidden length" to prevent the macroscopic failure of the DN gel, necessitating that it be highly stretchable [64]. As shown in **Fig. 4.2**, within the PVA/PDMAAm DN ion gel, the PVA and PDMAAm networks can serve as the first and second networks, respectively. Notably, the fracture strain of the PDMAAm SN ion gel is nearly equivalent to that of the PVA SN ion gel (**Fig. 4.2a**). This is an intriguing observation. In other words, the PDMAAm network acts as a hidden length although it

does not have highly stretchable property.

One possible explanation for the large fracture strain observed in the PVA/PDMAAm DN ion gel is the formation of hydrogen bonds between the PVA and PDMAAm networks. It has been reported that gels with networks capable of connecting through hydrogen bonding exhibit high mechanical strength and self-healing properties [65-67]. For instance, Tamate et al. described an ion gel comprising an IL-phobic poly(styrene) block and a hydrogen-bonding block composed of statistical copolymers of DMAAm and acrylic acid [65]. In their study, the carboxylic acid and carbonyl groups in the diblock copolymer were connected via hydrogen bonding, enhancing the mechanical strength of the ion gel. Similarly, in the PVA/PDMAAm DN ion gel, the hydroxyl (OH) group of PVA and the amide group of PDMAAm could form hydrogen bonds, thereby strengthening the ion gel. To investigate the potential formation of hydrogen bonds, we analyzed the FT-IR spectra of PVA/PDMAAm DN, PVA SN, and PDMAAm SN ion gels. However, no significant shift was observed in the carbonyl stretching band of the amide group in PDMAAm at 1622 cm^{-1} within the FT-IR spectra. Additionally, if hydrogen bonding were the primary factor contributing to the DN ion gel's toughness, the mechanical strength of the DN ion gel would be unlikely to depend significantly on the crosslinking degree of the PDMAAm network. Nevertheless, as shown in **Fig. 4.4**, the toughness of the DN ion gel was closely linked to the crosslinking degree of the PDMAAm network. This suggests that the large fracture strain of the PVA/PDMAAm DN ion gel may not be attributed to hydrogen bonding between PVA and PDMAAm.

To investigate the positive effect of the PDMAAm network on the mechanical strength enhancement of the PVA/PDMAAm DN ion gel, we analyzed the uniaxial stress-strain curves of the DN ion gels with varying compositions of the PVA/PDMAAm

networks and those of the DN ion gels with PDMAAm networks featuring different degrees of crosslinking. The stress-strain curves were interpreted using the Vilgis-Heinrich-Klüppel model [68], which accounts for parameters such as the limiting extensibility, n_e/T_e, and the elastic moduli that correspond to the crosslink constraints (G_c), and the topologically entanglement constraints (G_e).

$$\sigma = G_c(\lambda - \lambda^{-2})\left\{\frac{1 - T_e/n_e}{\left(1 - \frac{T_e}{n_e}\left(\lambda^2 + \frac{2}{\lambda} - 3\right)\right)^2} - \frac{T_e/n_e}{1 - \frac{T_e}{n_e}\left(\lambda^2 + \frac{2}{\lambda} - 3\right)}\right\} + 2G_e\left(\lambda^{-1/2} - \lambda^{-2}\right) \quad (1)$$

where λ is the deformation ratio ($\lambda = \varepsilon + 1$). Fitting results of the calculated and experimental stress-strain curves are shown in **Fig. 4.5(a) and (b)**. It is clearly shown that the calculated results well correlate with the experimental results.

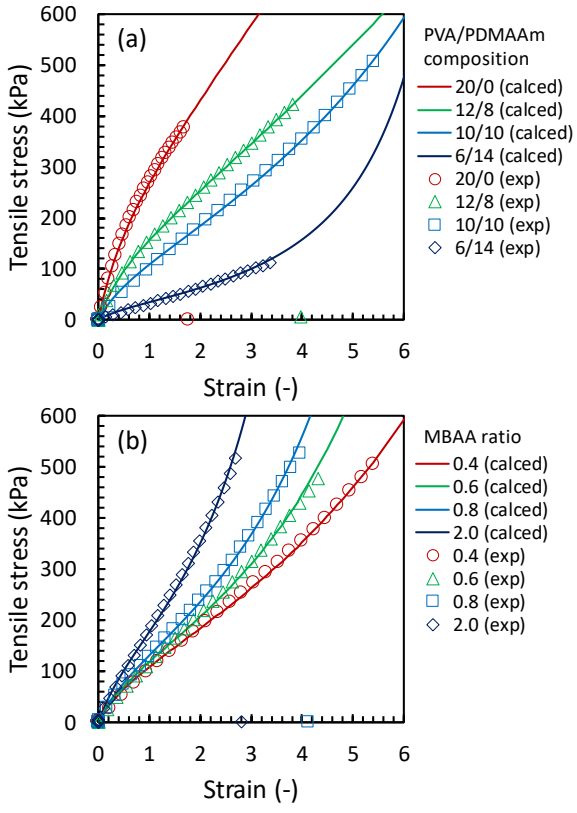

Fig. 4.5 Analysis of the stress-strain curves of the PVA/PDMAAm DN ion gels by Vilgis-Heinrich-Klüppel model. Stress-strain curves of the DN ion gels with (a) different compositions of PVA/PDMAAm networks and (b) the PDMAAm network with different crosslinking degree. Solid lines are calculated results. Plots are experimental results.

Table 4.2 Fitting parameters for Vilgis-Heinrich-Klüppel model calculation of the stress-strain curves of the PVA/PDMAAm DN ion gels.

(a) DN ion gels with different PVA/PDMAAm compositions

	PVA/PDMAAm composition (wt%)			
	20/0	12/8	10/10	6/14
n_e/T_e	n.d.	1035	303	98
G_c (kPa)	143	83	61	19
G_e (kPa)	20	11	1	0

DN ion gels were prepared under the condition of the MBAA mole ratio of 0.4 (mol/mol-DMAAm).

(b) DN ion gels with PDMAAm network with different crosslinking degree

	MBAA mole ratio (mol/mol-DMAAm)			
	0.4	0.6	0.8	2
n_e/T_e	303	153	112	56
G_c (kPa)	61	66	74	98
G_e (kPa)	1	1	1	1

DN ion gels were prepared under the condition of the PVA/PDMAAm composition of 10/10 wt%.

The model calculation fitting parameters are summarized in **Table 4.2**. In **Table 4.2a**, the fitting parameters for DN ion gels with various PVA/PDMAAm compositions prepared using an MBAA mole ratio of 0.4 (mol/mol-DMAAm), are presented. As the PVA composition decreased and the PDMAAm composition increased, both the elastic moduli G_c and G_e, which correspond respectively to crosslinking constraints and topological constraints, showed a decline. These trends suggest that the PVA network exhibited significant entanglement and cross-linking. Regarding the limiting extensibility

parameter, it also decreased as PVA composition decreased and PDMAAm composition increased. The observed trend can be attributed to the increase in permanent entanglement caused by the chemical crosslinking of PDMAAm. For the PVA SN ion gel with a PVA/PDMAAm composition of 20/0 wt%, the n_e/T_e parameter was infinite. This infinite n_e/T_e for the PVA SN ion gel, along with decreases in elastic moduli Gc and Ge as the PVA network composition decreases, is due to the reduction in PVA network content and suggests that the PVA network in the ion gel may be intricately entangled and physically crosslinked. Conversely, the fitting parameters for DN ion gels with different degrees of crosslinking in the PDMAAm network, prepared with a PVA/PDMAAm composition of 10/10 mol/mol, are presented in **Table 4.2b**. As the chemical crosslinking of PDMAAm increased, the elastic modulus G_c increased while the limiting extensibility n_e/T_e decreased. The rise in G_c can be attributed to the increase in permanent entanglements resulting from the chemical crosslinking of the PDMAAm network. Consequently, the fraction of permanent, or trapped, entanglements T_e increased, leading to a decrease in the mean number of statistical segments between two successive entanglements n_e. This resulted in a reduction in the limiting extensibility of n_e/T_e with the increased chemical crosslinking degree of the PDMAAm network.

As discussed earlier, the behavior of the determined parameters presented in **Table 4.2** is consistent with the properties of the physically crosslinked PVA and chemically crosslinked PDMAAm networks. Considering this, the increase in the fracture strain of the PVA/PDMAAm DN ion gel due to the introduction of the crosslinked PDMAAm network can be explained. When the PDMAAm network is moderately crosslinked, the PVA network becomes trapped at the crosslinking points of the PDMAAm network in a stretched state. As the gel is further stretched, some of the weaker physical crosslinking

in the PVA network breaks, dissipating the loaded energy. However, the remaining unbroken PVA network maintains trapping entanglements and serves as a multifunctional crosslinking medium for the PDMAAm networks. Consequently, the PDMAAm network, additionally crosslinked by the clusters of physically crosslinked PVA network, prevents macroscopic fracture of the DN ion gel and allows it to reach a highly elongated state.

4.3.3 [Emim][DCA] retention of PVA/PDMAAm DN ion gel

Another advantage of the PVA/PDMAAm DN ion gel is its excellent IL retention. After being compressed at 500 kPa, the DN ion gel retained over 95% of its IL content, while the PVA SN ion gel retained less than 70% (**Fig. 4.6a**). The strong IL retention of the DN ion gel is attributed to the high compatibility between [Emim][DCA] and PDMAAm. As shown in **Fig. 4.6b**, IL retention of over 95% was achieved when the composition of the PVA/PDMAAm networks was at least 10/10 wt%. Notably, the 10/10 wt% composition of the PVA/PDMAAm network provided the DN ion gel with the greatest toughness (**Fig. 4.3**), making it an excellent candidate for high-performance CO_2 separation membranes. Additionally, the high mechanical strength and superior IL retention of the DN ion gel allowed for an increase in [Emim][DCA] content.

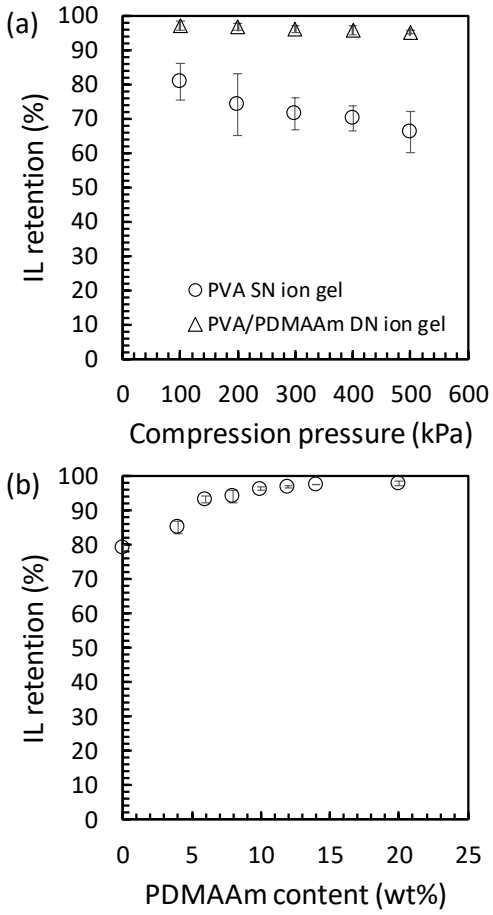

Fig. 4.6 IL holding property of the DN ion gel. (a) IL retention of PVA SN and PVA/PDMAAm DN ion gel under compression at different pressures. The composition of PVA/PDMAAm networks in the PVA/PDMAAm DN ion gel was 10/10 wt%. The [Emim][DCA] content in the DN and SN ion gels was 80 wt%. (b) Effect of the composition of the PDMAAm network in the PVA/PDMAAm double-network on the IL retention under compression at 100 kPa. The content of [Emim][DCA] in the ion gels was 80 wt%.

4.3.4 Effect of [Emim][DCA] content on the mechanical strength and CO_2 permeation performance of PVA/PDMAAm DN ion gel membrane

Figs. 4.7 and 4.8 illustrate the impact of [Emim][DCA] content on the mechanical

strength as well as the CO_2 and N_2 permeation properties of the DN ion gel membranes. Thanks to the high mechanical strength of the DN ion gel, the [Emim][DCA] content could be increased to approximately 90 wt% (**Fig. 4.7a**). Furthermore, the toughness of the PVA/PDMAAm DN ion gel significantly surpassed that of previously developed tough ion gels featuring semi-crystalline polymer networks (**Fig. 4.7b**).

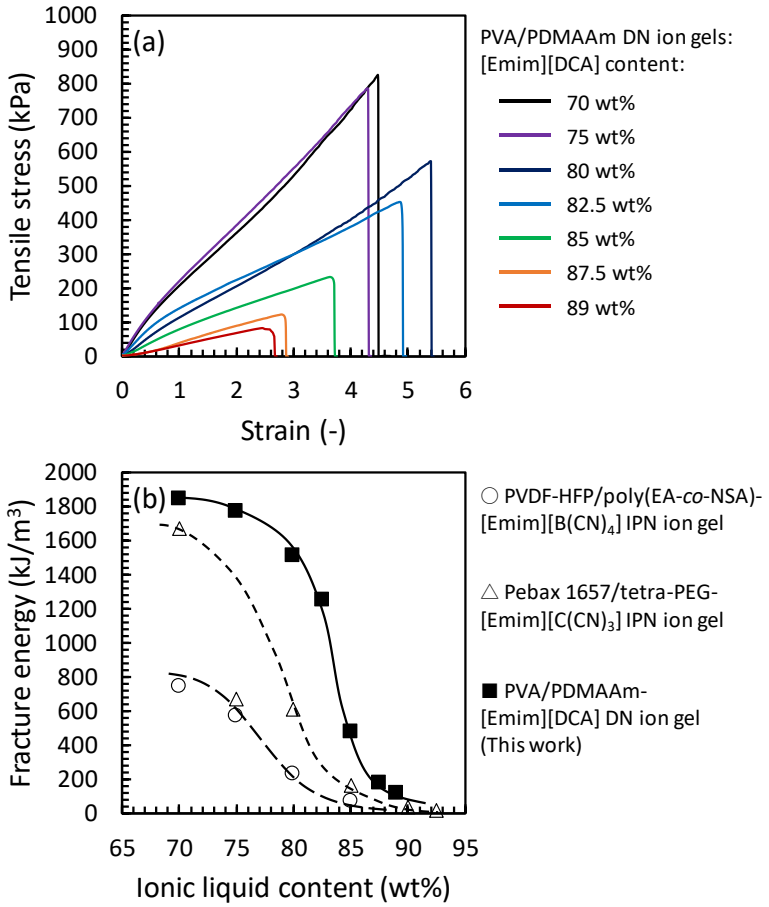

Fig. 4.7 Effect of IL content on the mechanical strength of the DN ion gel. (a) Uniaxial tensile stress-strain curves of the DN ion gels with different IL contents. (b) relationship between the fracture energy and the IL content. As the comparison, the data for the previously developed PVDF-HFP/poly(EA-*co*-NSA) IPN ion gels [37] and Pebax 1657/tetra-PEG IPN ion gels [43] were also plotted.

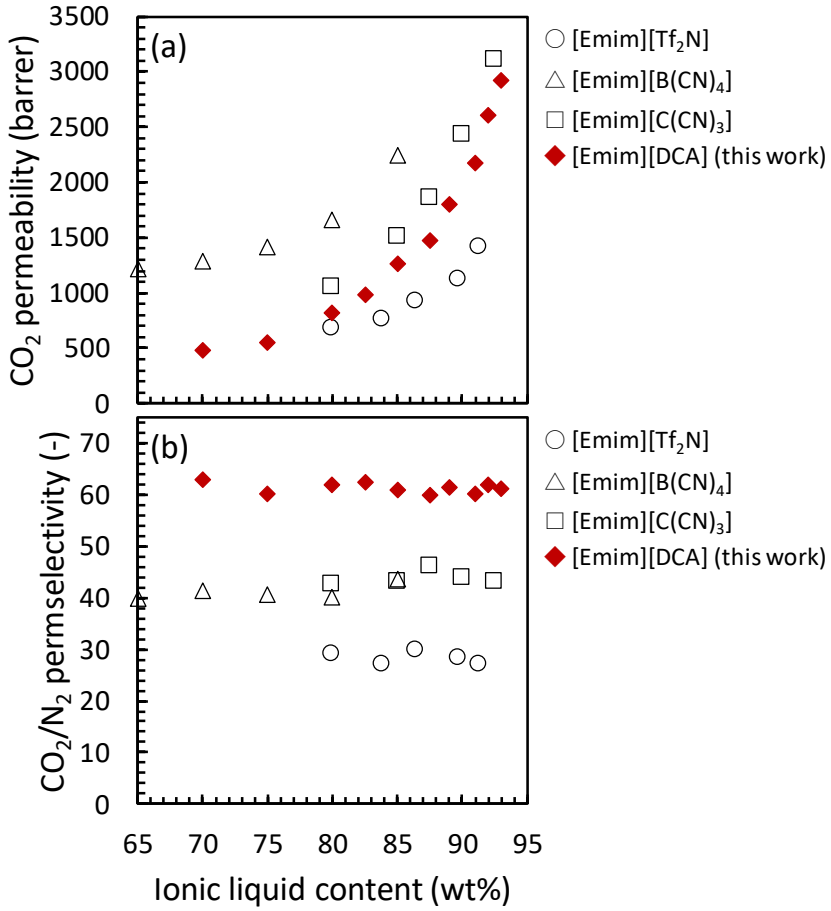

Fig. 4.8 Effect of IL content on the CO_2 separation performance of the ion gel membranes. (a) CO_2 and N_2 permeabilities of the ion gels and (b) CO_2/N_2 permselectivity of the ion gels. As the comparison, the data for the previously developed PVDF-HFP/poly(DMAAm-*co*-NSA) IPN ion gels [42], PVDF-HFP/poly(EA-*co*-NSA) IPN ion gels [37], and Pebax 1657/tetra-PEG IPN ion gels [43] were also plotted.

The maximum [Emim][DCA] content of the PVA/PDMAAm DN ion gel, which remained intact when handled and during gas permeation testing, was 93 wt%. Consistent with our previous findings, increasing the IL content effectively enhances the gas permeance of ion gel-based membranes [41-43]. We observed an exponential increase in the CO_2 permeability of an ion gel membrane as the IL content rose. This trend was also

evident in the PVA/PDMAAm DN ion gel membrane (**Fig. 4.8a**). Notably, the CO_2 permeability of the PVA/PDMAAm DN ion gel membrane is approximately 80% of that of the [Emim][$C(CN)_3$] containing Pebax 1657/tetra-PEG ion gel membrane. When the [Emim][DCA] content of the DN ion gel membrane reached 93 wt%, the CO_2 permeability soared to 2920 barrer, a substantial increase compared to other ion gel membranes. Additionally, the exceptionally high CO_2/N_2 permselectivity of the PVA/PDMAAm DN ion gel membrane containing [Emim][DCA] is significant and noteworthy. As illustrated in **Fig. 4.8b**, the CO_2/N_2 permselectivity exceeded 60, which is notably high. While PEG-based polymer membranes are known for their strong CO_2/N_2 permselectivity [30, 40, 69-71], even these membranes struggle to achieve such an elevated level of 60. Furthermore, as previously mentioned, the CO_2 permeability of PVA/PDMAAm DN ion gel membranes is notably high. When the [Emim][DCA] content of the ion gel membrane exceeds 90 wt%, the CO_2 permeability of the membrane is 10 times greater than that of PEG-based polymer membranes. Therefore, it is evident that the CO_2/N_2 separation performance of the PVA/PDMAAm DN ion gel membrane, which contains a substantial amount of [Emim][DCA], surpasses that of polymer membranes.

To evaluate the CO_2/N_2 separation performance of the PVA/PDMAAm DN ion gel membrane, its CO_2 permeabilities and CO_2/N_2 permselectivities were plotted alongside other IL-based and polymeric CO_2 separation membranes in **Fig. 4.9**. Due to its high CO_2/N_2 permselectivity, when the [Emim][DCA] content exceeded 80 wt%, the PVA/PDMAAm DN ion gel membrane demonstrated CO_2 separation performance beyond the 2019 upper bound [72]. Therefore, the PVA/PDMAAm DN ion gel membrane is considered a promising candidate for a high-performance CO_2 separation membrane.

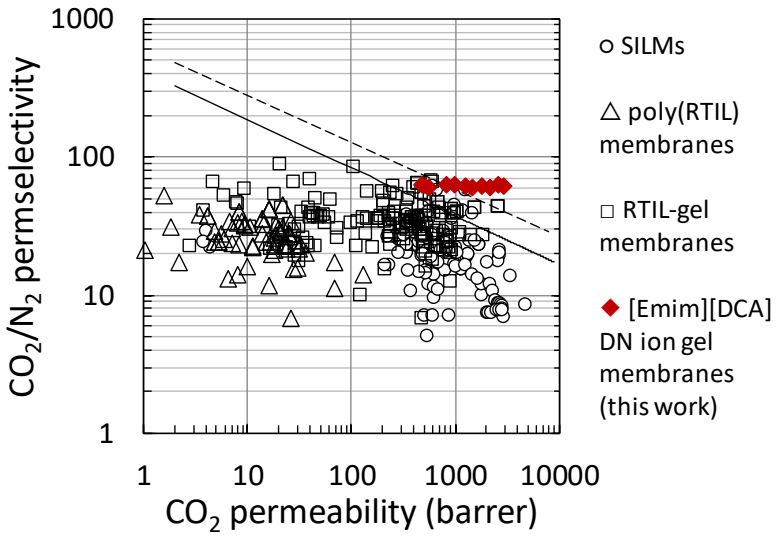

Fig. 4.9 Comparison of CO_2 permeability and CO_2/N_2 permselectivity of the PVA/PDMAAm DN ion gel membranes with different [Emim][DCA] contents and those of previously reported IL-based CO_2 separation membranes. The straight and dashed lines are the upper bounds of polymer membranes reported in 2008 [73] and 2019 [72], respectively.

4.3.5 CO_2 permeation performance of the PVA/PDMAAm DN ion gel membrane for CO_2 capture

As mentioned earlier, PVA/PDMAAm DN ion gel membranes have significant potential as high-performance CO_2 separation membranes. The relationship between CO_2/N_2 permselectivity and CO_2 permeability, known as a Robeson plot (as shown in **Fig. 4.9**), serves as a key indicator of a material's potential for CO_2 separation membranes. The data in **Fig. 4.9** is obtained for a dry CO_2/N_2 mixture at 30 °C under atmospheric pressure. However, in general, the CO_2 permeation properties of CO_2 separation membranes are strongly influenced by factors such as feed gas pressure, temperature, and relative humidity. For practical applications, it is essential to understand the CO_2

permeation performance of the membrane under different conditions. Therefore, the effects of various conditions on the CO_2 and N_2 permeation properties of the PVA/PDMAAm DN ion gel membrane were assessed. For this evaluation, the DN ion gel membrane composed of 10/10 wt% PVA/PDMAAm DN and 80 wt% [Emim][DCA] was used.

Fig. 4.10 illustrates the CO_2 and N_2 permeabilities as well as the CO_2/N_2 permselectivity of the PVA/PDMAAm DN ion gel membrane containing 80 wt% of [Emim][DCA]. The high mechanical strength of the DN ion gel membrane ensured it remained intact even under pressurized conditions, with a transmembrane pressure difference of up to 500 kPa. This demonstrates the membrane's ability to withstand pressurized environments. The CO_2 permeability and CO_2/N_2 permselectivity remained consistent at approximately 800 barrer and 60, respectively. The reason for the lack of dependency on CO_2 and N_2 permeability on the feed gas pressure is that the gas permeation of the DN ion gel membrane operates on a solution-diffusion mechanism.

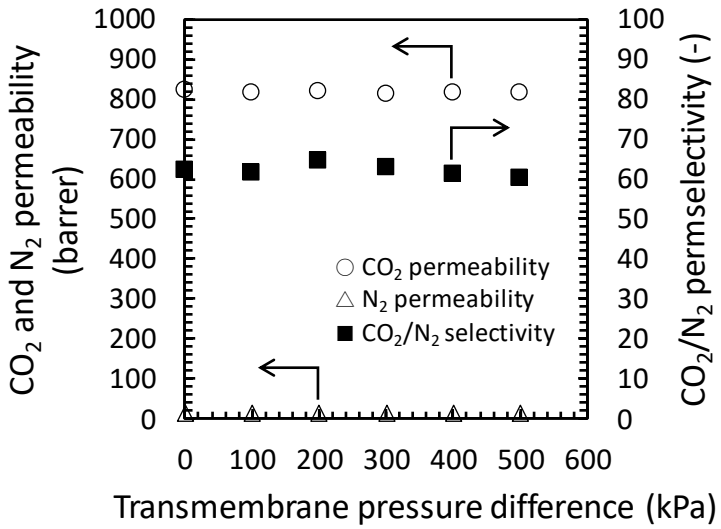

Fig. 4.10 Effect of transmembrane pressure difference on CO_2 permeability, N_2 permeability, and CO_2/N_2 permselectivity of PVA/PDMAAm DN ion gel membrane. The

feed gas consisted of 50/50 mol/mol CO_2/N_2. The experiment was performed at 30 °C under dry conditions.

In the process of capturing CO_2 from the exhaust gas of a coal-fired power plant, CO_2 separation occurs after the flue gas undergoes desulfurization [74]. Typically, the flue gas temperature following desulfurization falls below 80 °C [74]. **Fig. 4.11** demonstrates the impact of temperature on the CO_2 and N_2 permeabilities as well as the CO_2/N_2 permselectivity of the PVA/PDMAAm DN ion gel membrane. As the figure illustrates, CO_2 permeability increases with rising temperature. Despite the DN ion gel membrane containing only 80 wt% [Emim][DCA] in this study, the CO_2 permeability reached 1300 barrer at 80 °C. Conversely, the CO_2/N_2 permselectivity of the DN ion gel membrane decreased as the temperature rose. Nonetheless, owing to the exceptionally high CO_2/N_2 solubility selectivity of [Emim][DCA] [47, 48], the DN ion gel membrane maintained a high CO_2/N_2 permselectivity of 28 even at 80 °C.

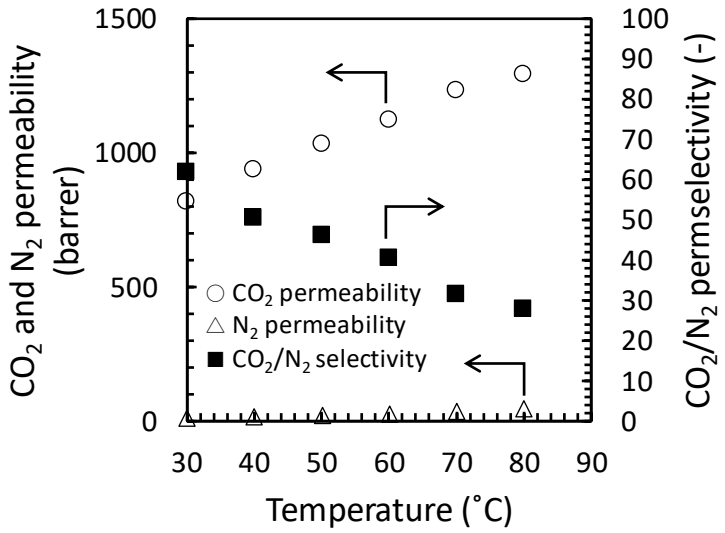

Fig. 4.11 Effect of temperature on CO_2 permeability, N_2 permeability, and CO_2/N_2 perrmselectivity of PVA/PDMAAm DN ion gel membrane. The feed gas consisted of

50/50 mol/mol CO_2/N_2. The gas permeation test was conducted under dry conditions at atmospheric pressure.

In addition, when a wet SO_2 removal process such as limestone slurry contactor or alkaline solution absorption is employed during the desulfurization process of flue gas, the flue gas becomes highly humid after desulfurization. Therefore, the impact of relative humidity on the CO_2 separation performance of membranes is as significant as the effect of temperature when designing a CO_2 capture process for flue gas. **Fig. 4.12** illustrates the CO_2 and N_2 permeabilities and CO_2/N_2 permselectivity of PVA/PDMAAm DN ion gel membranes at 80 °C using a 10/90 mol/mol CO_2/N_2 mixed gas with varying levels of relative humidity. As the figure shows, the CO_2 permeability of the DN ion gel membrane increases with rising relative humidity. At 80% relative humidity, the CO_2 permeability reached 2240 barrer, while maintaining a high CO_2/N_2 permselectivity of 28.

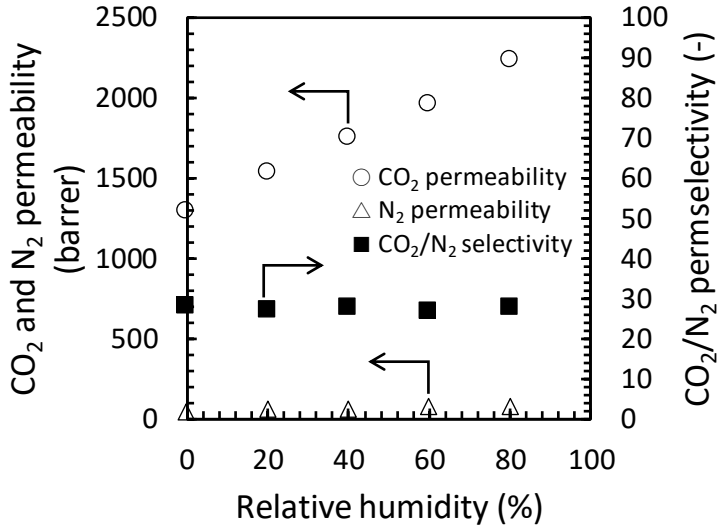

Fig. 4.12 Effect of humidity on CO_2 permeability, N_2 permeability, and CO_2/N_2 permselectivity of PVA/PDMAAm DN ion gel membrane. The feed gas consisted of 10/90 mol/mol CO_2/N_2. The gas permeation test was conducted at 80 °C under

atmospheric pressure condition.

Furthermore, the DN ion gel membrane maintained its excellent CO_2 separation performance consistently over 10 days in conditions of 80% relative humidity at 80 °C, as shown in **Fig. 4.13**. The stability of the membrane's CO_2 separation performance can be attributed to the PDMAAm network, which exhibits high compatibility with [Emim][DCA]. This consistent and superior CO_2 separation performance aligns with the requirements for CO_2 separation membranes used in capturing CO_2 emissions from coal-fired power plants [74]. Consequently, the PVA/PDMAAm DN ion gel emerges as a strong candidate material for CO_2 separation membranes suitable for CO_2 capture from coal-fired power plant emissions.

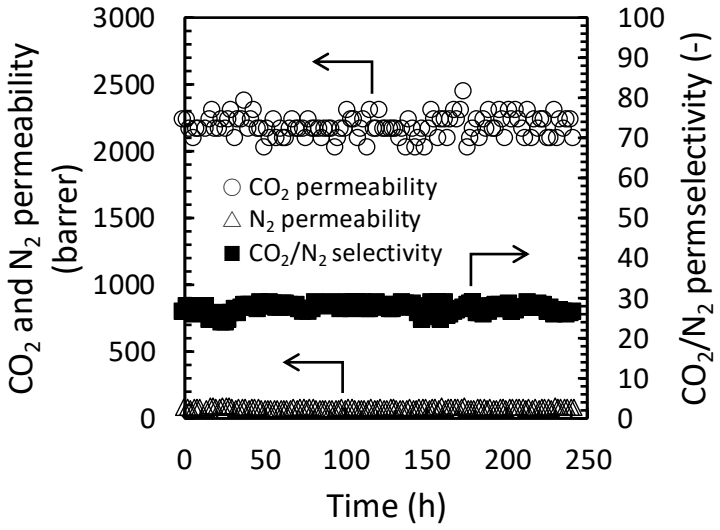

Fig. 4.13 Long-term stability of CO_2 separation performance of the PVA/PDMAAm DN ion gel membrane with 80 wt% [Emim][DCA]. The composition of CO_2/N_2 and humidity of the feed gas was 10/90 mol/mol and 80%, respectively. The long-term stability test was performed at 80 °C under atmospheric pressure condition.

4.4 Conclusion

In this study, a DN ion gel membrane consisting of CO_2-philic [Emim][DCA], semi-crystalline PVA, and loosely crosslinked PDMAAm was developed. In the DN ion gel membrane, the physically crosslinked PVA network served as a sacrificial bond, contributing to the toughness of the ion gel through an energy dissipation mechanism. The entanglement of the loosely crosslinked PDMAAm network with the PVA network significantly increased the fracture strain of the ion gel. Energy dissipation occurred even in highly deformed states, continuing until the ion gel ruptured.

Due to the high CO_2/N_2 solubility selectivity of [Emim][DCA], the DN ion gel membrane demonstrated excellent CO_2/N_2 permselectivity of 61. The robust toughness provided by the PVA/PDMAAm double network allowed the [Emim][DCA] content of the DN ion gel membrane to increase up to 93 wt%. The CO_2 permeability of the DN ion gel membrane rose exponentially with increasing [Emim][DCA] content, reaching 2920 barrer without compromising its high CO_2/N_2 permselectivity. The CO_2 separation performance of the DN ion gel membranes with over 80 wt% [Emim][DCA] surpassed the upper bound reported in 2019 [72]. Though the CO_2/N_2 permselectivity decreased slightly at elevated temperatures, a permselectivity of 28 was maintained even at 80 °C. CO_2 permeability increased with rising relative humidity without sacrificing high CO_2/N_2 permselectivity. Even with an [Emim][DCA] content of 80 wt%, the DN ion gel membrane achieved a CO_2 permeability of 2300 barrer while maintaining a CO_2/N_2 permselectivity of 30 at 80 °C and 80% relative humidity. This level of CO_2 separation performance meets the requirements for CO_2 capture from flue gases in coal-fired power plants.

References

[1] Z. Dai, R.D. Noble, D.L. Gin, et al., Combination of ionic liquids with membrane technology: A new approach for CO_2 separation, Journal of Membrane Science, 497, 2016, 1-20.

[2] L.C. Tomé, I.M. Marrucho, Ionic liquid-based materials: a platform to design engineered CO_2 separation membranes, Chemical Society Reviews, 45(10), 2016, 2785-2824.

[3] N.H. Solangi, A. Anjum, F.A. Tanjung, et al., A review of recent trends and emerging perspectives of ionic liquid membranes for CO_2 separation, Journal of Environmental Chemical Engineering, 9(5), 2021, 105860.

[4] E. Kamio, T. Yoshioka, H. Matsuyama, Recent advances in carbon dioxide separation membranes: A review, Journal of Chemical Engineering of Japan, 56(1) , 2023, 2222000.

[5] H. Weber, B. Kirchner, Complex structural and dynamical interplay of cyano-based ionic liquids, The Journal of Physical Chemistry B, 120(9), 2016, 2471-2483.

[6] K.M. Gupta, Tetracyanoborate based ionic liquids for CO_2 capture: From ab initio calculations to molecular simulations, Fluid Phase Equilibria, 415, 2016, 34-41.

[7] S.M. Mahurin, J.S. Lee, G.A. Baker, et al., Performance of nitrile-containing anions in task-specific ionic liquids for improved CO_2/N_2 separation, Journal of Membrane Science, 353(1), 2010, 177-183.

[8] S.M. Mahurin, P.C. Hillesheim, J.S. Yeary, et al., High CO_2 solubility, permeability and selectivity in ionic liquids with the tetracyanoborate anion, RSC Advances, 2(31), 2012, 11813-11819.

[9] R. Babarao, S. Dai, D.e. Jiang, Understanding the high solubility of CO_2 in an ionic liquid with the tetracyanoborate anion, The Journal of Physical Chemistry B, 115(32),

2011, 9789-9794.

[10] K.M. Gupta, J. Jiang, Systematic investigation of nitrile based ionic liquids for CO_2 capture: A combination of molecular simulation and ab initio calculation, The Journal of Physical Chemistry C, 118(6), 2014, 3110-3118.

[11] N. Amiri, H. Benyounes, Z. Lounis, et al., Design of absorption process for CO_2 capture using cyano based anion ionic liquid, Chemical Engineering Research and Design, 169, 2021, 239-249.

[12] S. Hussain, H. Dong, S. Zeng, et al., Investigation uncovered the impact of anions on CO_2 absorption by low viscous ether functionalized pyridinium ionic liquids, Journal of Molecular Liquids, 336, 2021, 116362.

[13] L.C. Tomé, M. Isik, C.S.R. Freire, et al., Novel pyrrolidinium-based polymeric ionic liquids with cyano counter-anions: High performance membrane materials for post-combustion CO_2 separation, Journal of Membrane Science, 483, 2015, 155-165.

[14] T.K. Carlisle, J.E. Bara, R.D. Noble, et al., Interpretation of CO_2 solubility and selectivity in nitrile-functionalized room-temperature ionic liquids using a group contribution approach, Industrial & Engineering Chemistry Research, 47(18), 2008, 7005-7012.

[15] A. Kodirov, D. Abduvokhidov, S. Mamatkulov, et al., The absorption mechanisms of CO_2, H_2S and CH_4 molecules in [EMIM][SCN] and [EMIM][DCA] ionic liquids: A computational insight, Fluid Phase Equilibria, 581, 2024, 114080.

[16] M. Klepić, K. Setničková, M. Lanč, et al., Permeation and sorption properties of CO_2-selective blend membranes based on polyvinyl alcohol (PVA) and 1-ethyl-3-methylimidazolium dicyanamide ([EMIM][DCA]) ionic liquid for effective CO_2/H_2 separation, Journal of Membrane Science, 597, 2020, 117623.

[17] M. Zhang, R. Semiat, X. He, Recent advances in poly(ionic liquids) membranes for CO_2 separation, Separation and Purification Technology, 299, 2022, 121784.

[18] P. Ortiz Albo, T.J. Ferreira, C.F. Martins, et al., Impact of ionic liquid structure and loading on gas sorption and permeation for ZIF-8-based composites and mixed matrix membranes, Membranes, 2022.

[19] S.N.A. Shafie, N.A.H. Md Nordin, S.M. Racha, et al., Emerging ionic liquid engineered polymeric membrane for carbon dioxide removal: A review, Journal of Molecular Liquids, 358, 2022, 119192.

[20] Y. Yu, X. Yang, C. Zhang, et al., A tough double-network ion gel membrane based on poly (ionic liquid) for efficient carbon capture, Separation and Purification Technology, 331, 2024, 125591.

[21] P. Scovazzo, Determination of the upper limits, benchmarks, and critical properties for gas separations using stabilized room temperature ionic liquid membranes (SILMs) for the purpose of guiding future research, Journal of Membrane Science, 343(1), 2009, 199-211.

[22] J. Benito, J. Sánchez Laínez, B. Zornoza, et al., Ultrathin composite polymeric membranes for CO_2/N_2 separation with minimum thickness and high CO_2 permeance, ChemSusChem, 10(20), 2017, 4014-4017.

[23] J. Liu, X. Hou, H. Lin, High-performance polymers for membrane CO_2/N_2 separation, Chemistry-A European Journal, 22(45), 2016, 15980-15990.

[24] N. Du, H.B. Park, G.P. Robertson, et al., Polymer nanosieve membranes for CO_2-capture applications, Nature Materials, 10(5), 2011, 372-375.

[25] N. Du, G.P. Robertson, L. Scoles, et al., Polymers of intrinsic microporosity (PIMs) substituted with methyl tetrazole, Polymer, 53(20), 2012, 4367-4372.

[26] H.B. Park, S.H. Han, C.H. Jung, et al., Thermally rearranged (TR) polymer membranes for CO_2 separation, Journal of Membrane Science, 359(1), 2010, 11-24.

[27] M. Askari, Y. Xiao, T.S. Chung, Natural gas purification and olefin/paraffin separation using cross-linkable 6FDA-Durene/DABA co-polyimides grafted with α, β, and γ-cyclodextrin, Journal of Membrane Science, 390-391, 2012, 141-151.

[28] H. Wang, T.S. Chung, The evolution of physicochemical and gas transport properties of thermally rearranged polyhydroxyamide (PHA), Journal of Membrane Science, 385-386, 2011, 86-95.

[29] D. Fritsch, G. Bengtson, N.B. McKeown, Synthesis and gas permeation properties of spirobischromane-based polymers of intrinsic microporosity, Macromolecular Chemistry and Physics, 212(11), 2011, 1137-1146.

[30] A. Car, C. Stropnik, K. V. Peinemann, PEG modified poly(amide-b-ethylene oxide) membranes for CO_2 separation, Journal of Membrane Science, 307(1), 2008, 88-95.

[31] K.K. Wong, Z.A. Jawad, B.L.F. Chin, A polyethylene glycol (PEG) – polyethersulfone (PES)/multi-walled carbon nanotubes (MWCNTs) polymer blend mixed matrix membrane for CO_2/N_2 separation, Journal of Polymer Research, 28(1), 2021, 6.

[32] X. Hu, J. Tang, A. Blasig, Y. Shen, M. Radosz, CO_2 permeability, diffusivity and solubility in polyethylene glycol-grafted polyionic membranes and their CO_2 selectivity relative to methane and nitrogen, Journal of Membrane Science, 281(1), 2006, 130-138.

[33] A. Kargari, S. Rezaeinia, State-of-the-art modification of polymeric membranes by PEO and PEG for carbon dioxide separation: A review of the current status and future perspectives, Journal of Industrial and Engineering Chemistry, 84, 2020, 1-22.

[34] A. Matsuoka, A. Otani, E. Kamio, H. Matsuyama, A gradient viscosity model for

estimating CO_2 permeability of amino acid ionic liquid-based facilitated transport membrane, Separation and Purification Technology, 280, 2022, 119847.

[35] F. Ranjbaran, E. Kamio, H. Matsuyama, Inorganic/organic composite ion gel membrane with high mechanical strength and high CO_2 separation performance, Journal of Membrane Science, 544, 2017, 252-260.

[36] F. Moghadam, E. Kamio, T. Yoshioka, H. Matsuyama, New approach for the fabrication of double-network ion-gel membranes with high CO_2/N_2 separation performance based on facilitated transport, Journal of Membrane Science, 530, 2017, 166-175.

[37] S. He, E. Kamio, H. Matsuyama, et al., Development of an ion gel membrane containing a CO_2-philic ionic liquid in interpenetrating semi-crystalline and crosslinkable polymer networks, Journal of Membrane Science, 685, 2023, 121912.

[38] Z. Dai, H. Aboukeila, L. Ansaloni, et al., Nafion/PEG hybrid membrane for CO_2 separation: Effect of PEG on membrane micro-structure and performance, Separation and Purification Technology, 214, 2019, 67-77.

[39] D. Nasirian, I. Salahshoori, M. Sadeghi, et al., Investigation of the gas permeability properties from polysulfone/polyethylene glycol composite membrane, Polymer Bulletin, 77(10), 2020, 5529-5552.

[40] M.R. Dilshad, A. Islam, U. Hamidullah, et al., Effect of alumina on the performance and characterization of cross-linked PVA/PEG 600 blended membranes for CO_2/N_2 separation, Separation and Purification Technology, 210, 2019, 627-635.

[41] E. Kamio, M. Minakata, H. Matsuyama, et al., Inorganic/organic double-network ion gel membrane with a high ionic liquid content for CO_2 separation, Polymer Journal, 53(1), 2021, 137-147.

[42] J. Zhang, E. Kamio, H. Matsuyama, et al., Novel tough ion-gel-based CO_2 separation membrane with interpenetrating polymer network composed of semicrystalline and cross-linkable polymers, Industrial & Engineering Chemistry Research, 61(13), 2022, 4648-4658.

[43] S. He, E. Kamio, H. Matsuyama, et al., Development of a double-network ion gel membrane composed of a CO_2-philic ionic liquid, semi-crystalline polymer network, and tetra-armed polyethylene glycol network, Journal of Membrane Science, 695, 2024, 122482.

[44] M. Gonzalez-Miquel, J. Palomar, S. Omar, et al., CO_2/N_2 Selectivity prediction in supported ionic liquid membranes (SILMs) by COSMO-RS, Industrial & Engineering Chemistry Research, 50(9), 2011, 5739-5748.

[45] A.S.L. Gouveia, E. Bumenn, K. Rohtlaid, et al., Ionic liquid-based semi-interpenetrating polymer network (sIPN) membranes for CO_2 separation, Separation and Purification Technology, 274, 2021, 118437.

[46] H.J. Min, Y.J. Kim, M. Kang, et al., Crystalline elastomeric block copolymer/ionic liquid membranes with enhanced mechanical strength and gas separation properties, Journal of Membrane Science, 66, 2022, 120837.

[47] D. Camper, J. Bara, R. Noble, Bulk-fluid solubility and membrane feasibility of rmim-based room-temperature ionic liquids, Industrial & Engineering Chemistry Research, 45(18), 2006, 6279-6283.

[48] J.E. Bara, T.K. Carlisle, C.J. Gabriel, et al., Guide to CO_2 separations in imidazolium-based room-temperature ionic liquids, Industrial & Engineering Chemistry Research, 48(6), 2009, 2739-2751.

[49] E. Kamio, J.P. Gong, H. Matsuyama, et al., Inorganic/organic double-network gels

containing ionic liquids, Advanced Materials, 29(47), 2017, 1704118.

[50] T. Yasui, E. Kamio, H. Matsuyama, Inorganic/organic double-network ion gels with partially developed silica-particle network, Langmuir, 34(36), 2018, 10622-10633.

[51] E. Kamio, M. Kinoshita, H. Matsuyama, et al., Preparation of inorganic/organic double-network ion gels using a cross-linkable polymer in an open system, Macromolecules, 53(19), 2020, 8529-8538.

[52] E. Kamio, M. Minakata, H. Matsuyama, et al., Tough ion gels composed of coordinatively crosslinked polymer networks using ZIF-8 nanoparticles as multifunctional crosslinkers, Soft Matter, 18(25), 2022, 4725-4736.

[53] J. Zhang, E. Kamio, H. Matsuyama, et al., Inorganic/organic micro-double-network ion gel-based composite membrane with enhanced mechanical strength and CO_2 permeance, Industrial & Engineering Chemistry Research, 60(34), 2021, 12698-12708.

[54] J. Zhang, E. Kamio, H. Matsuyama, et al., Development of a micro-double-network ion gel-based CO_2 separation membrane from nonvolatile network precursors, Industrial & Engineering Chemistry Research, 60(34), 2021, 12640-12649.

[55] D. Weng, F. Xu, X. Li, et al., Polymeric complex-based transparent and healable ionogels with high mechanical strength and ionic conductivity as reliable strain sensors, ACS Applied Materials & Interfaces, 12(51), 2020, 57477-57485.

[56] J.P. Gong, Y. Katsuyama, T. Kurokawa, et al., Double-network hydrogels with extremely high mechanical strength, Advanced Materials, 15(14), 2003, 1155-1158.

[57] F. Moghadam, E. Kamio, H. Matsuyama, High CO_2 separation performance of amino acid ionic liquid-based double network ion gel membranes in low CO_2 concentration gas mixtures under humid conditions, Journal of Membrane Science, 525, 2017, 290-297.

[58] Y. Huang, X. Zhao, J.L. Ke, et al., Engineering nanoscale solid networks of ionogel

for enhanced thermoelectric power output and excellent mechanical properties, Chemical Engineering Journal, 456, 2023, 141156.

[59] S. Hao, Z. Chen, H. Li, et al., Skin-inspired, highly sensitive, broad-range-response and ultra-strong gradient ionogels prepared by electron beam irradiation, Small, 2023, 2309931.

[60] T. Nakajima, T. Kurokawa, J.P. Gong, et al., Characterization of internal fracture process of double network hydrogels under uniaxial elongation, Soft Matter, 9(6), 2013, 1955-1966.

[61] J. Diani, B. Fayolle, P. Gilormini, A review on the Mullins effect, European Polymer Journal, 45(3), 2009, 601-612.

[62] A.D. Drozdov, Mullins' effect in thermoplastic elastomers: Experiments and modeling, Mechanics Research Communications, 36(4), 2009, 437-443.

[63] A. Dorfmann, R.W. Ogden, A constitutive model for the Mullins effect with permanent set in particle-reinforced rubber, International Journal of Solids and Structures, 41(7), 2004, 1855-1878.

[64] J.P. Gong, Why are double network hydrogels so tough?, Soft Matter, 6(12), 2010, 2583-2590.

[65] R. Tamate, K. Hashimoto, T. Horii, et al., Self-healing micellar ion gels based on multiple hydrogen bonding, Advanced Materials, 30(36), 2018, 1802792.

[66] M. Wang, P. Zhang, M. Shamsi, et al., Tough and stretchable ionogels by in situ phase separation, Nature Materials, 21(3), 2022, 359-365.

[67] Y.J. Wang, X.N. Zhang, Y. Song, et al., Ultrastiff and tough supramolecular hydrogels with a dense and robust hydrogen bond network, Chemistry of Materials, 31(4), 2019, 1430-1440.

[68] M. Klüppel, J. Schramm, A generalized tube model of rubber elasticity and stress softening of filler reinforced elastomer systems, Macromolecular Theory and Simulations, 9(9), 2000, 742-754.

[69] S.R. Reijerkerk, M.H. Knoef, K. Nijmeijer, et al., Poly(ethylene glycol) and poly(dimethyl siloxane): Combining their advantages into efficient CO_2 gas separation membranes, Journal of Membrane Science, 352(1), 2010, 126-135.

[70] X. Mei Wu, Q. Gen Zhang, P. Ju Lin, et al., Towards enhanced CO_2 selectivity of the PIM-1 membrane by blending with polyethylene glycol, Journal of Membrane Science, 493, 2015, 147-155.

[71] I. Akbarian, A. Fakhar, E. Ameri, Gas-separation behavior of poly(ether sulfone)–poly(ethylene glycol) blend membranes, Journal of Applied Polymer Science, 135(44), 2018, 46845.

[72] B. Comesaña Gándara, J. Chen, C.G. Bezzu, et al., Redefining the Robeson upper bounds for CO_2/CH_4 and CO_2/N_2 separations using a series of ultrapermeable benzotriptycene-based polymers of intrinsic microporosity, Energy & Environmental Science, 12(9), 2019, 2733-2740.

[73] L.M. Robeson, The upper bound revisited, Journal of Membrane Science, 320(1), 2008, 390-400.

[74] T.C. Merkel, H. Lin, R. Baker, Power plant post-combustion carbon dioxide capture: An opportunity for membranes, Journal of Membrane Scienc, 359(1), 2010, 126-139.

Chapter 5

Conclusions

Carbon dioxide emissions from the combustion of fossil fuels are a major contributor to the greenhouse effect. Although renewable energy technologies continue to advance, fossil fuels still play a crucial role in industrial processes. Therefore, capturing CO_2 emissions from fossil fuel combustion is essential for mitigating climate change and protecting the environment. In post-combustion carbon capture, membrane separation technology is gaining widespread attention for its high selectivity, low energy consumption, and environmental friendliness. Among the various CO_2 separation membranes, polymer membranes have been studied the longest and have matured to the point of industrial application. However, they face a trade-off between gas permeability and selectivity. Ionic liquids, composed of cations and anions, offer low vapor pressure, low volatility, and high CO_2 solubility selectivity, making them promising for designing CO_2 separation membranes with high gas permeability and selectivity. Ion gel membranes, which contain a significant amount of ionic liquid, provide excellent CO_2 permeability. When combined with appropriate ionic liquids, they also offer superior CO_2/N_2 selectivity due to differences in the solubility of CO_2 and N_2. Despite the high CO_2 permeability of ion gel membranes with high ionic liquid content, their lower mechanical strength can affect the stability and performance of the membranes. Therefore, this study focuses on

developing tough ion gel membranes based on toughening mechanisms of double-network. It evaluates the CO_2 separation performance of ion gel membranes to determine their potential in advancing CO_2 separation technologies.

In Chapter 2, an interpenetrating polymer network (IPN) ion gel containing a CO_2-philic IL was successfully developed by combining a semi-crystalline polymer with a cross-linkable polymer network. The resulting ion gel showed promising CO_2 permeability. In Chapter 3, the mechanical strength of IPN ion gels was enhanced by using highly ductile polymers as the second polymer network, which further improved the CO_2 permeability of the ion gels. In Chapter 4, tough double-network (DN) ion gel membranes with high CO_2 selectivity were developed using a semi-crystalline polymer and a CO_2-philic ionic liquid. These findings were detailed in Chapters 2-4.

5.1 Development of an ion gel membrane containing a CO_2-philic ionic liquid in interpenetrating semi-crystalline and cross-linkable polymer networks

A tough ion gel membrane composed of a semi-crystalline polymer, a cross-linkable polymer, and a large amount of CO_2-philic ionic liquids was successfully developed. The fracture of the crystalline region of the semi-crystalline polymer dissipates load energy and gives the ion gel high mechanical strength. The high compatibility between the cross-linkable polymer and IL gives the ion gel good IL retention. The prepared IPN ion gel has good mechanical properties and IL retention properties, and the IL content can be increased to 85 wt%. The CO_2 permeability of the IPN ion gel containing 85 wt% IL reaches 2400 barrer, and the CO_2/N_2 selectivity is 40. Therefore, the developed PVDF-HFP/poly(EA-*co*-NSA) IPN ion gel is promising as a CO_2 separation membrane material for carbon capture.

5.2 Development of a double-network ion gel membrane composed of a CO_2-philic ionic liquid, semi-crystalline polymer network, and tetra-armed polyethylene glycol network

In this chapter, we utilized a highly ductile tetra-PEG network as the second polymer network, interpenetrating with a semi-crystalline polymer network, to fabricate tough ion gel membranes. The developed IPN ion gel adheres to the toughening principle of double-network gels: the semi-crystalline polymer network forms a cross-linked structure, serving as sacrificial bonds to dissipate loading energy, while the highly ductile tetra-PEG network prevents macro-destruction of the ion gel under large elongation and enhancing its mechanical strength. Consequently, the developed ion gel exhibits exceptional mechanical properties, enabling an increase in the [Emim][$C(CN)_3$] content to 92.5 wt%. The ion gel membrane containing 92.5 wt% IL demonstrates a CO_2 permeability of 3100 barrer and a CO_2/N_2 selectivity of 43, surpassing the CO_2 separation performance of previously reported ionic liquid-based membranes. In a long-term stability test exceeding 10 days, conducted at high temperatures of 80°C and relative humidity of 80%, the ion gel membrane containing 80 wt% [Emim][$C(CN)_3$] maintained a CO_2 permeability exceeding 2000 barrer and a CO_2/N_2 selectivity of 25. Such remarkable CO_2 separation performance positions it ideally for processing flue gas emissions from coal-fired power plants.

5.3 Highly selective CO_2 permeable double-network ion gel membrane containing 1-ethyl-3-methylimidazolium dicyanamide

In this chapter, a DN ion gel membrane composed of a CO_2-philic ionic liquid ([Emim][DCA]), semi-crystalline polymer (PVA), and loosely crosslinked PDMAAm

was developed. In the DN ion gel, the physically crosslinked PVA network acted as a sacrificial bond to toughen the ion gel by dissipating energy. The entanglement of the loosely crosslinked PDMAAm network with the PVA network significantly increased the fracture strain of the ion gel. Thanks to the excellent toughness given by the PVA/PDMAAm double-network, the [Emim][DCA] content in the ion gel was able to up to 93 wt%, and the CO_2 permeability reached 2920 barrer. Due to the high CO_2/N_2 solubility selectivity of [Emim][DCA], the DN ion gel exhibited excellent CO_2/N_2 permselectivity of 61. The good CO_2 separation performance was beyond the upper bound reported in 2019. Even if the IL content was 80 wt%, the CO_2 permeability was stable under a high transmembrane pressure difference, and the CO_2 permeability reached 2300 barrer with keeping the CO_2/N_2 perselectivity of 30 at 80 °C and 80% relative humidity. The CO_2 separation performance meets the demand for CO_2 capture from the flue gases from coal-fired power plants.

Publication list

Chapter 2:

S He, E Kamio, J Zhang, et al. Development of an ion gel membrane containing a CO_2-philic ionic liquid in interpenetrating semi-crystalline and crosslinkable polymer networks[J]. Journal of Membrane Science, 2023, 685: 121912.

Chapter 3:

S He, E Kamio, et al. Development of a double-network ion gel membrane composed of a CO_2-philic ionic liquid, semi-crystalline polymer network, and tetra-armed polyethylene glycol network[J]. Journal of Membrane Science, 2024, 695: 122482.

Chapter 4:

S He, E Kamio, et al. Highly selective CO_2 permeable double-network ion gel membrane containing 1-ethyl-3-methylimidazolium dicyanamide. (Submitted)

Doctoral Dissertation, Kobe University
“Development of tough ion gel membranes composed of CO_2-philic ionic liquids and semi-crystalline polymer network (高 CO_2 親和性イオン液体と半結晶性高分子から構成される高強度イオンゲル膜の創製)”, 155 pages
Submitted on July 01, 2024
When published on the Kobe University institutional repository */Kernel/*, the publication date shall appear on the cover of the repository version.